United States Patent [19]

Hornbeck

[11] **Patent Number: 5,061,049**

[45] **Date of Patent: Oct. 29, 1991**

[54] **SPATIAL LIGHT MODULATOR AND METHOD**

[75] Inventor: **Larry J. Hornbeck**, Van Alstyne, Tex.

[73] Assignee: **Texas Instruments Incorporated**, Dallas, Tex.

[21] Appl. No.: **582,804**

[22] Filed: **Sep. 13, 1990**

Related U.S. Application Data

[63] Continuation of Ser. No. 355,049, May 15, 1989, abandoned, which is a continuation of Ser. No. 168,724, Mar. 16, 1988, abandoned, which is a continuation-in-part of Ser. No. 159,466, Feb. 19, 1988, abandoned, which is a continuation of Ser. No. 636,180, Jul. 31, 1984, abandoned, and Ser. No. 43,740, Apr. 29, 1987, abandoned, which is a continuation-in-part of Ser. No. 792,947, Oct. 30, 1985, Pat. No. 4,662,746, and Ser. No. 129,353, Nov. 30, 1987, abandoned, which is a continuation of Ser. No. 877,654, Jun. 23, 1986, abandoned, which is a continuation-in-part of Ser. No. 646,399, Aug. 31, 1984, Pat. No. 4,596,992.

[51] **Int. Cl.**[5] **G02F 1/27**; B44C 1/22; H04N 5/74; G02B 26/08

[52] **U.S. Cl.** **359/224**; 358/206; 359/213; 359/298; 359/847

[58] **Field of Search** 350/6.9

[56] **References Cited**

U.S. PATENT DOCUMENTS

2,993,403	7/1961	Harries	350/6.5
3,896,338	7/1975	Nathanson et al.	315/373
4,317,611	3/1982	Petersen	350/6.6
4,441,791	4/1984	Hornbeck	350/360
4,592,628	6/1986	Altman et al.	350/486
4,596,992	6/1986	Hornbeck	350/360
4,638,309	1/1987	Ott	350/360
4,662,746	5/1987	Hornbeck	332/7.51
4,698,602	10/1987	Armtage	332/7.51
4,710,732	12/1987	Hornbeck	332/7.51
4,793,699	12/1988	Tokuhara	350/6.6
4,831,614	5/1989	Duerig et al.	369/101

FOREIGN PATENT DOCUMENTS

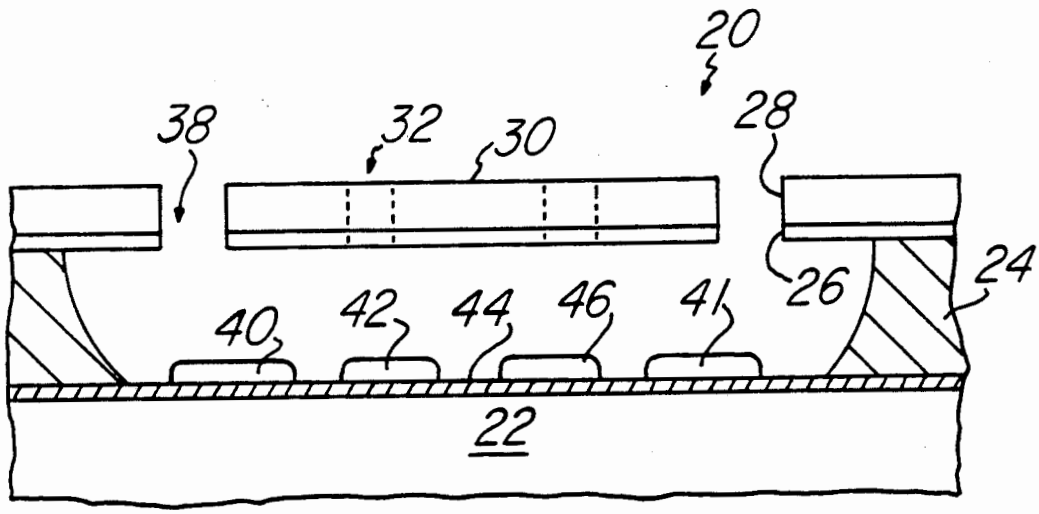
0232413	10/1986	Japan	350/6.5
0021115	1/1987	Japan	350/6.5
0035321	2/1987	Japan	350/486
0035322	2/1987	Japan	350/6.5
0100417	5/1988	Japan	350/6.5
1441840	3/1974	United Kingdom	350/487

Primary Examiner—Nelson Moskowitz
Attorney, Agent, or Firm—James C. Kesterson; James T. Comfort; Melvin Sharp

[57] **ABSTRACT**

An electrostatically deflectable beam spatial light modulator with the beams (**30**), address electrodes (**42, 46**), and landing electrodes (**40, 41**) to provide soft-landing of the beams on the landing electrodes (**40, 41**) which gives uniform large-angle deflection plus high reliability.

28 Claims, 34 Drawing Sheets



PCNA Ex. 1039
U.S. Patent No. 9,955,551

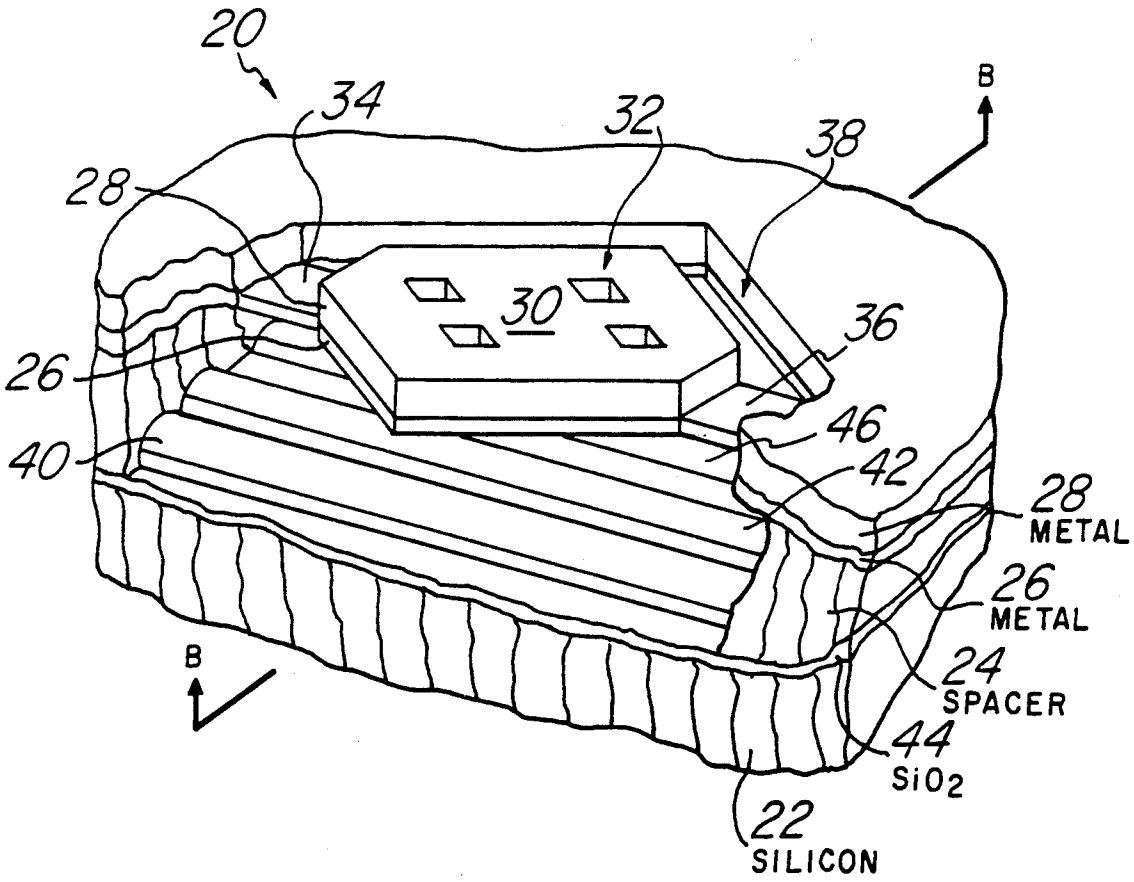

20
34
32
38
B
28
30
36
26
46
40
42
28
METAL
26
METAL
B
24
SPACER
44
SiO2
22
SILICON

Fig. 1a

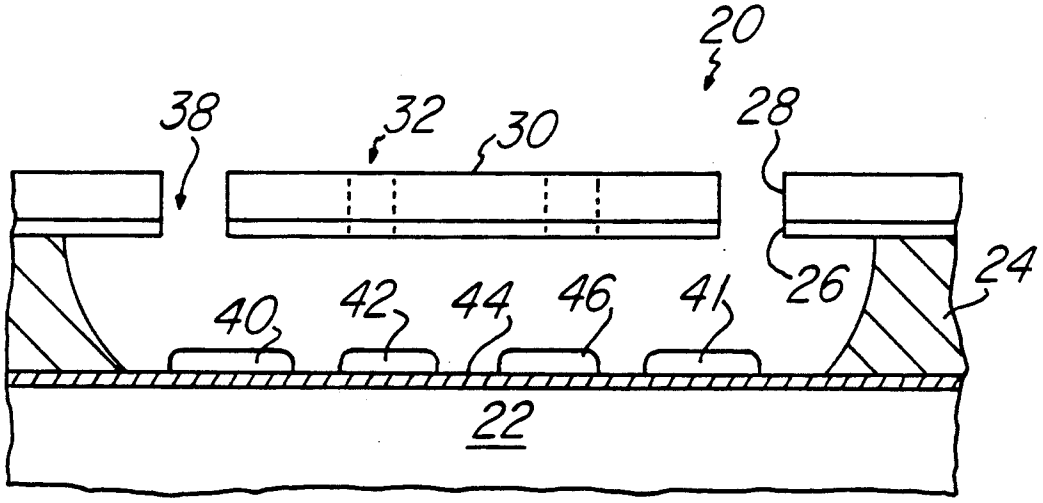

20
38
32
30
28
26
24
40
42
44
46
41
22

Fig. 1b

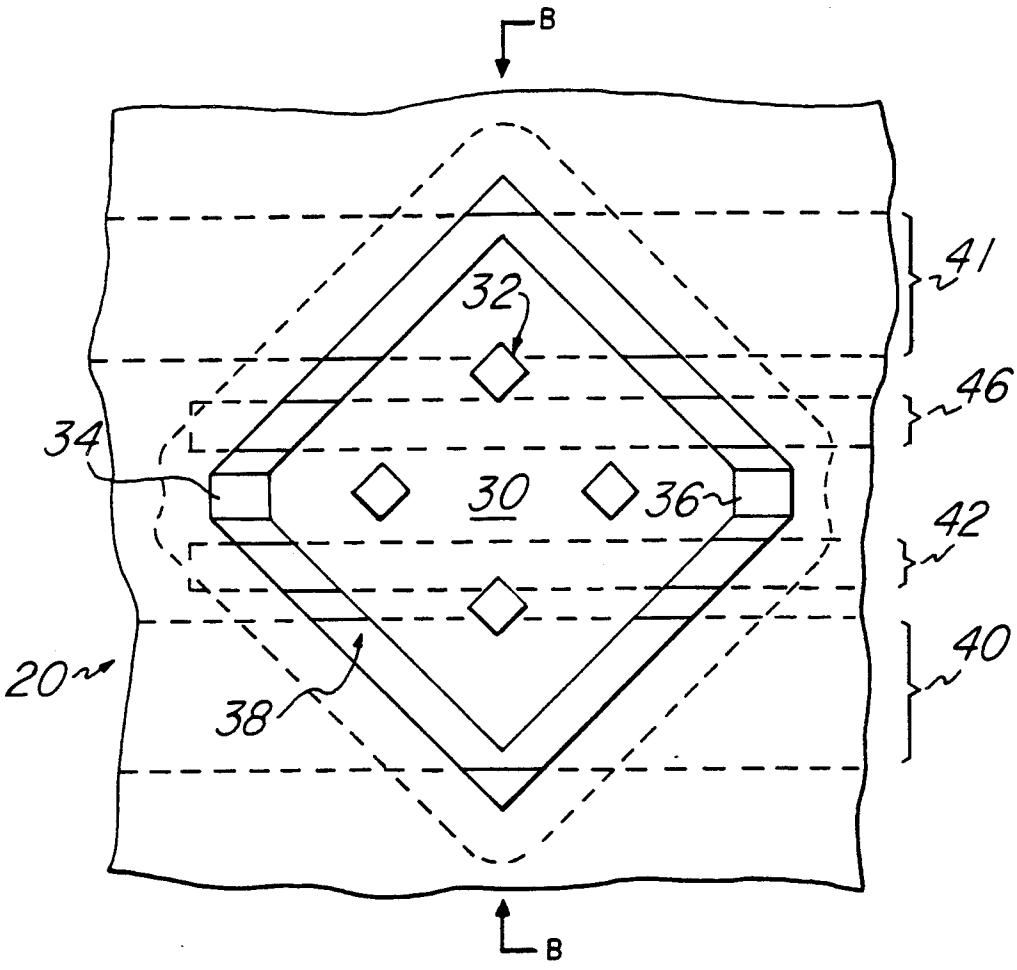

B
41
32
46
34
30
36
42
40
20
38
B

Fig. 1c

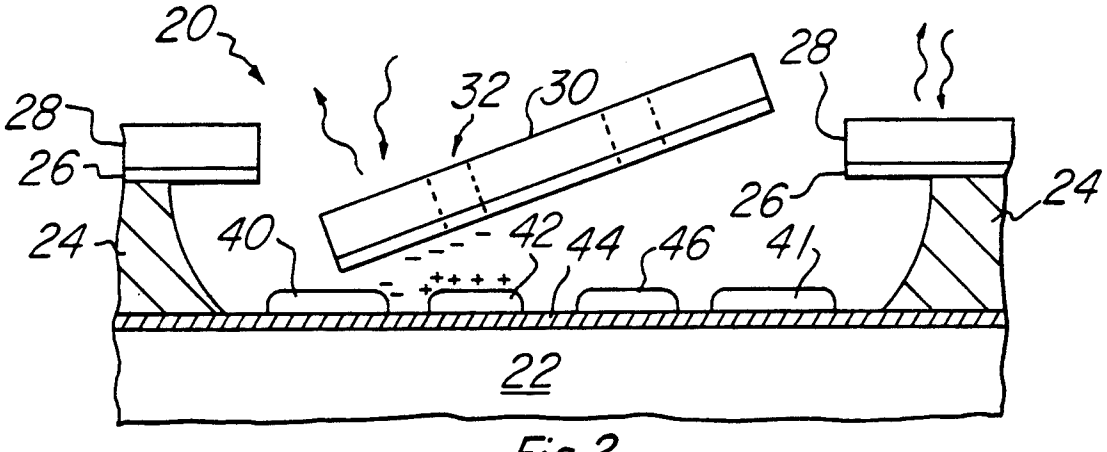

20
28
32
30
28
26
26
24
24
40
42
44
46
41
22

Fig. 2

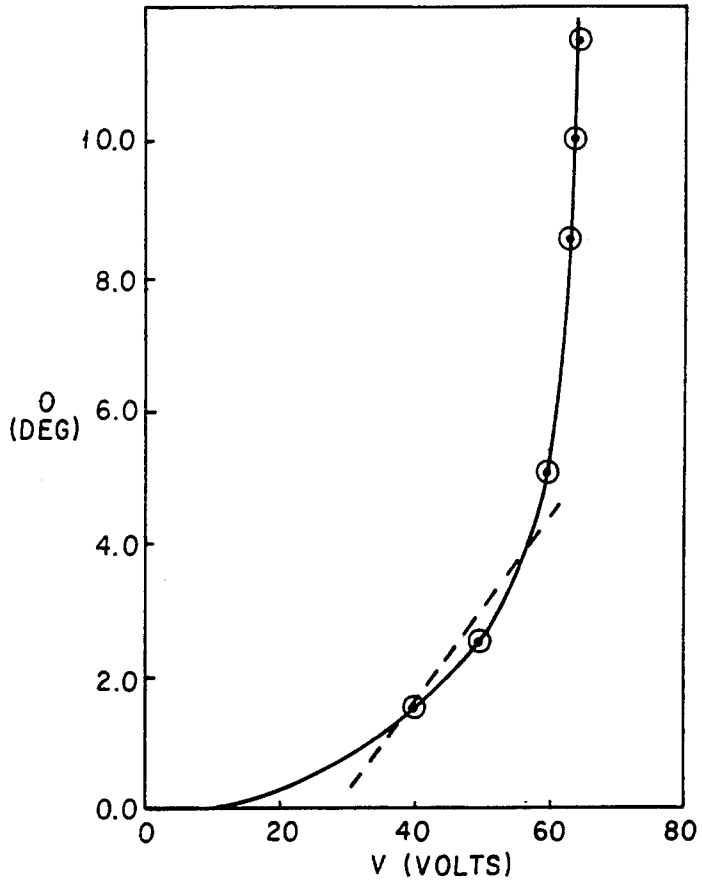

10.0
8.0
6.0
4.0
2.0
0.0
θ (DEG)
0
20
40
60
80
V (VOLTS)

Fig.3a

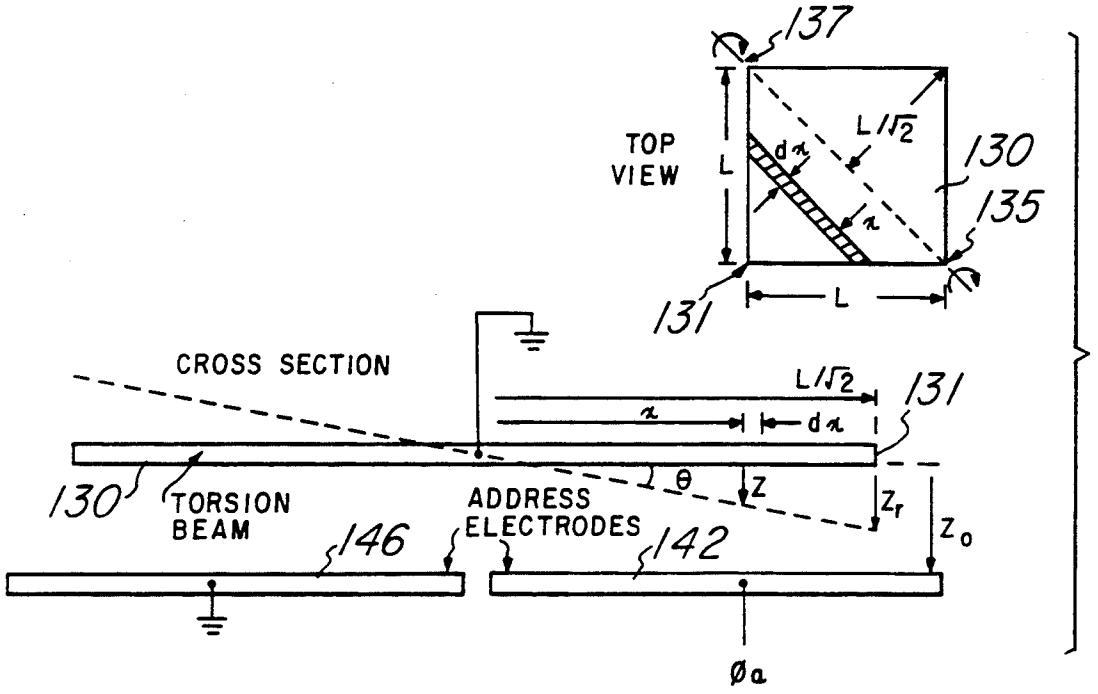

137
TOP VIEW
L
L/√2
dx
x
130
135
131
L
CROSS SECTION
L/√2
131
x
dx
130
TORSION BEAM
θ
Z
Zr
Z0
ADDRESS ELECTRODES
146
142
Øa

Fig.4

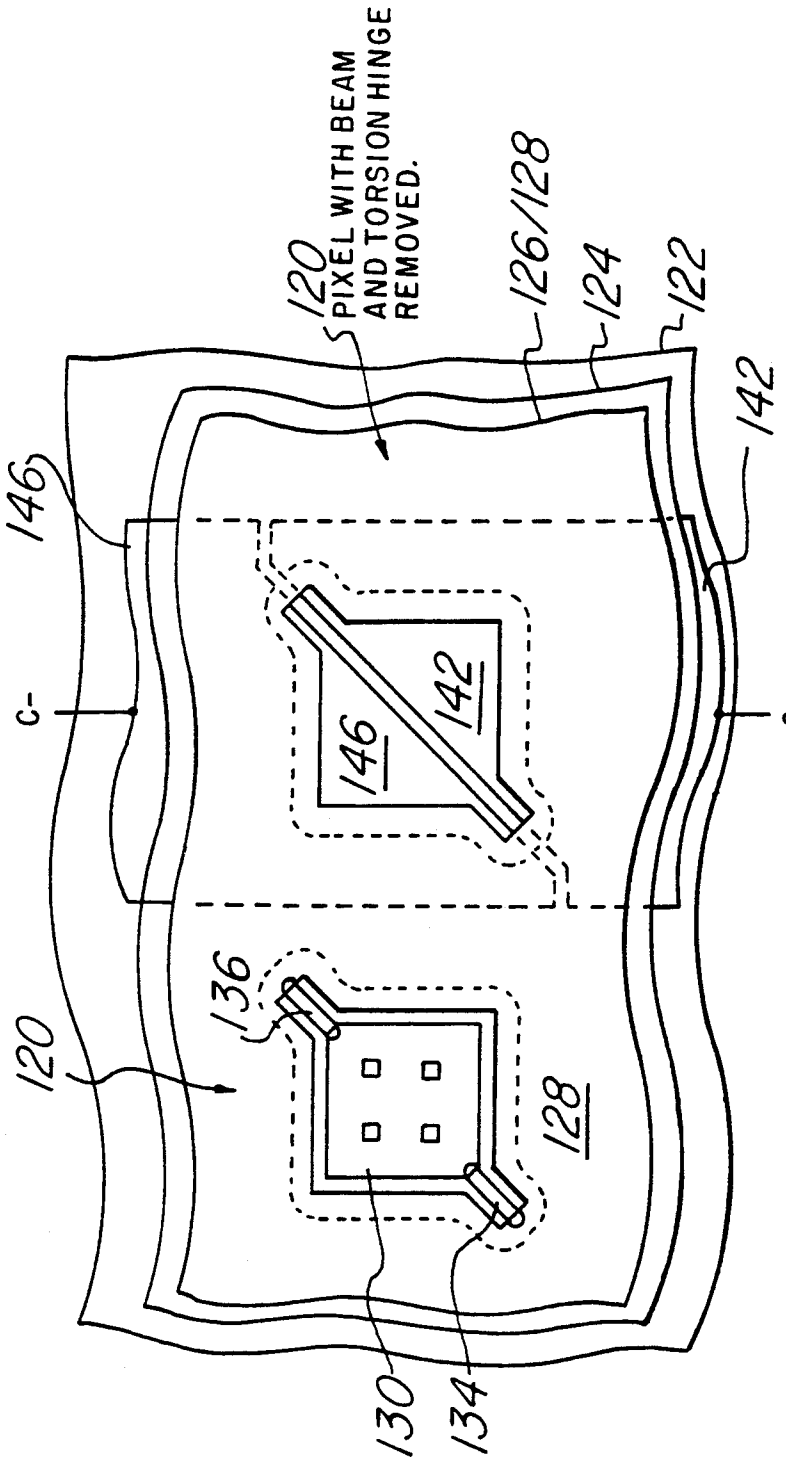

120
PIXEL WITH BEAM AND TORSION HINGE REMOVED.
126/128
124
122
142
146
C-
C+
146
142
136
120
128
130
134

Fig. 3b

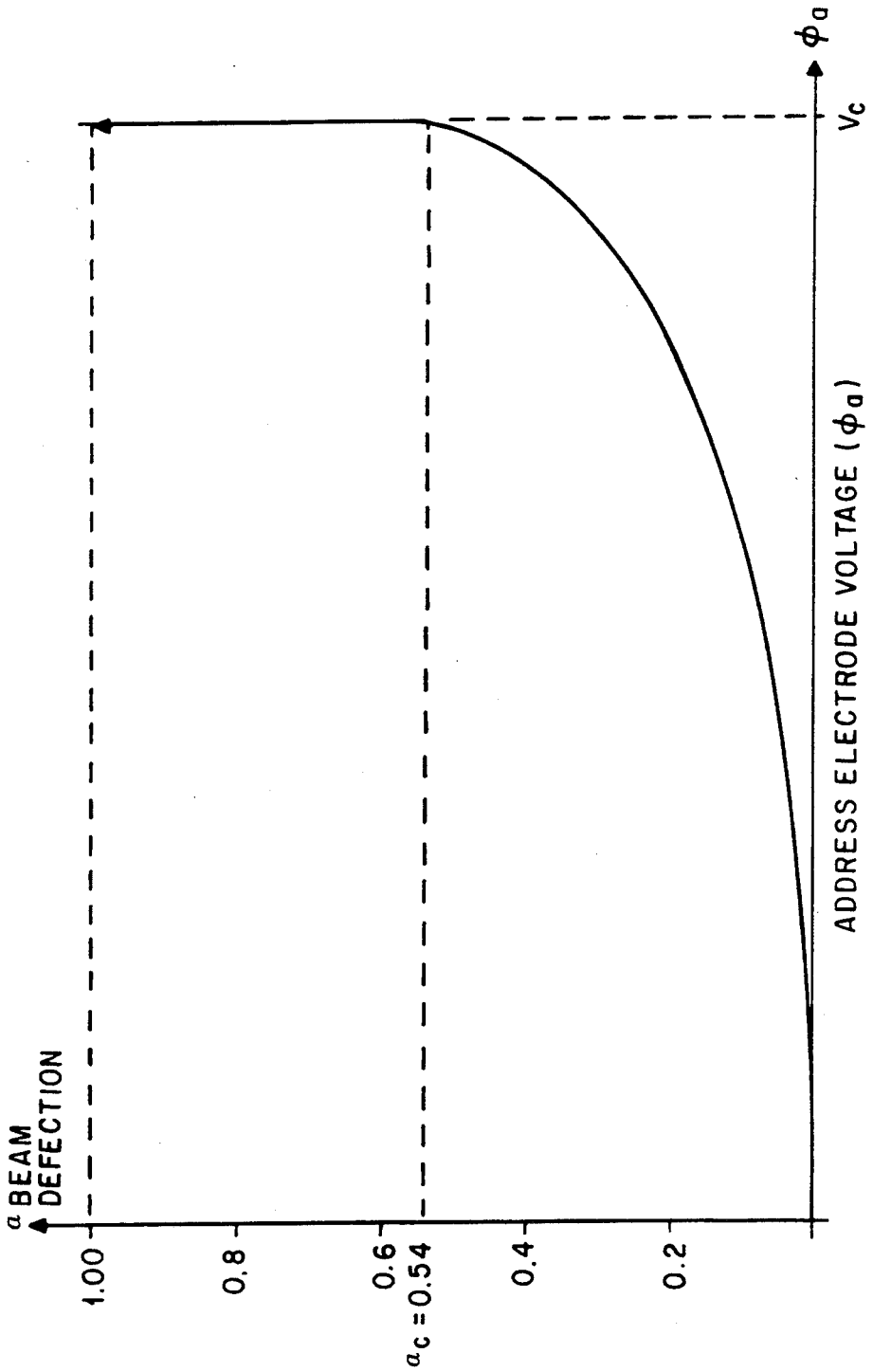

ϕ_a
V_c
ADDRESS ELECTRODE VOLTAGE (ϕ_a)
α BEAM DEFECTION
1.00
0.8
0.6
$\alpha_c = 0.54$
0.4
0.2

Fig. 6

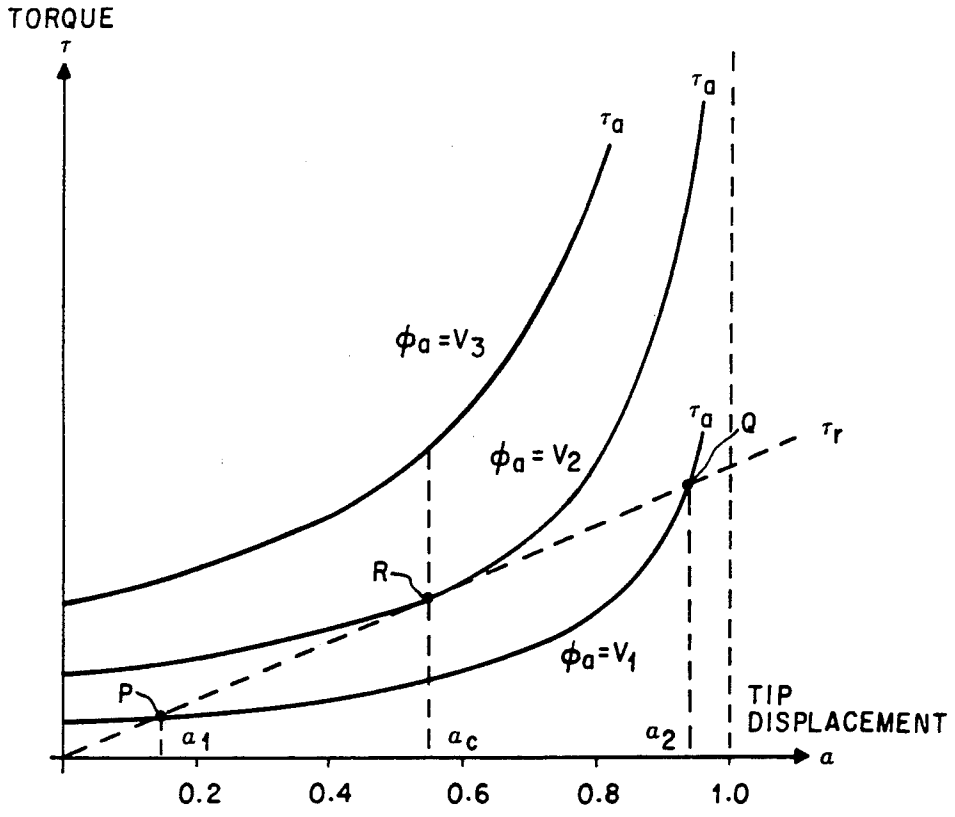

TORQUE
τ
τa
τa
τa
Q
τr
φa = V3
φa = V2
φa = V1
R
P
a1
ac
a2
TIP
DISPLACEMENT
a
0.2
0.4
0.6
0.8
1.0

Fig.5

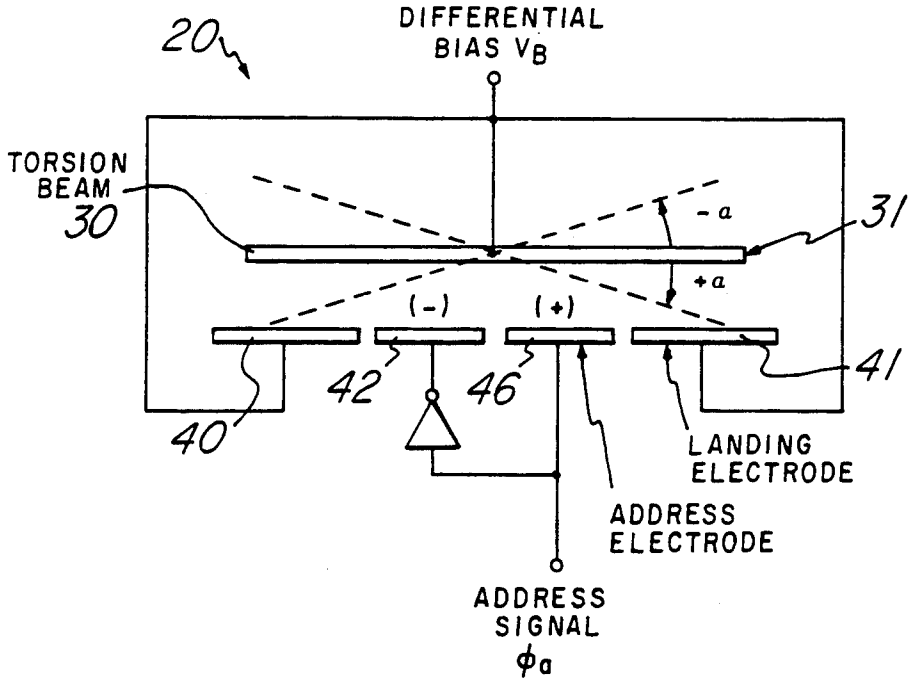

20
DIFFERENTIAL
BIAS VB
TORSION
BEAM
30
-a
31
+a
(-)
(+)
42
46
41
40
LANDING
ELECTRODE
ADDRESS
ELECTRODE
ADDRESS
SIGNAL
φa

Fig.7

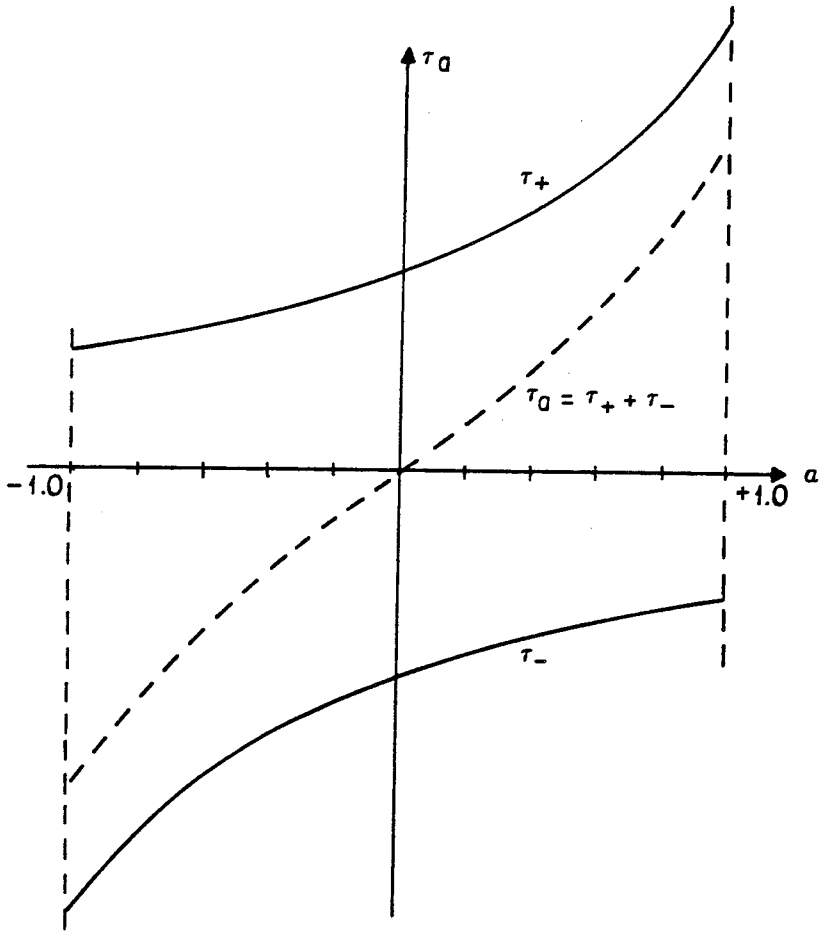


Fig. 8

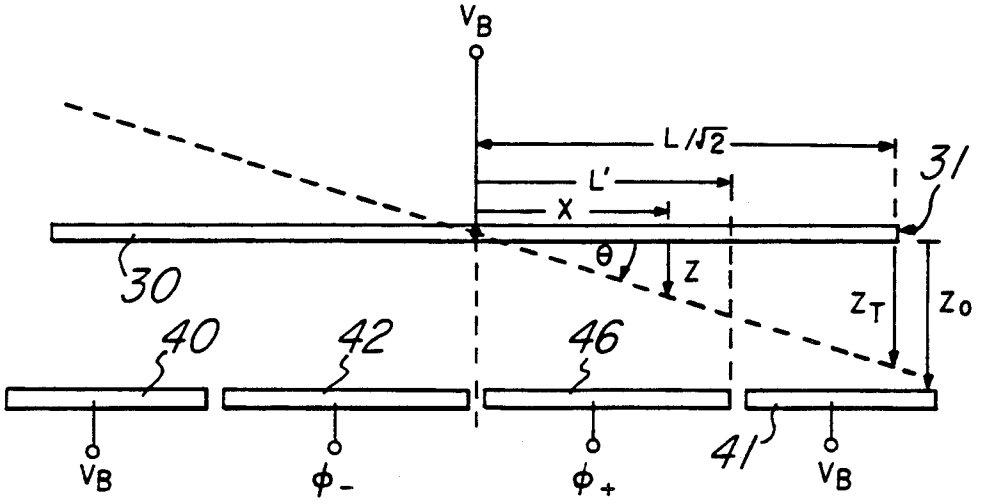


Fig. 9

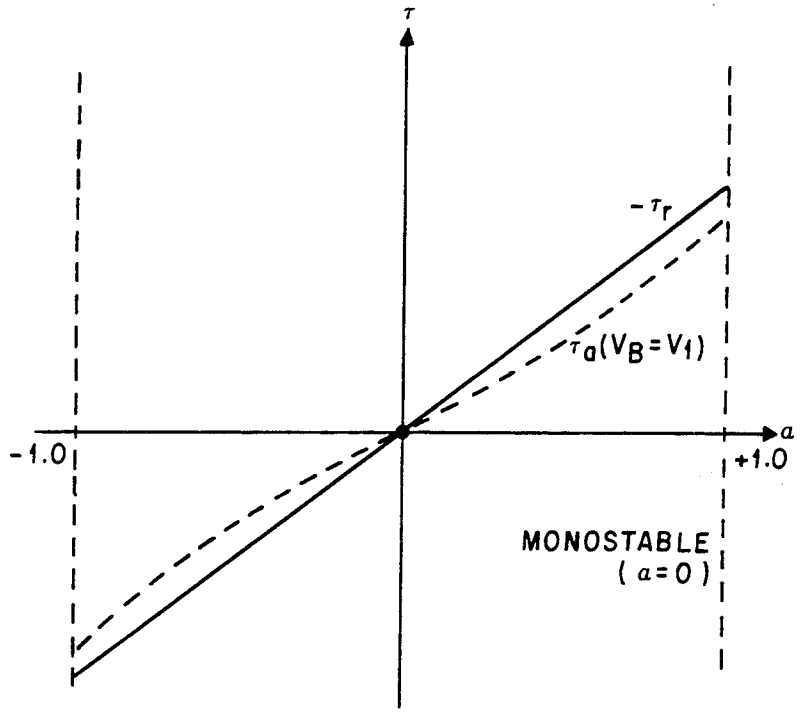

τ
$-\tau_r$
$\tau_a(V_B=V_1)$
a
-1.0
+1.0
MONOSTABLE
(a=0)

Fig. 10

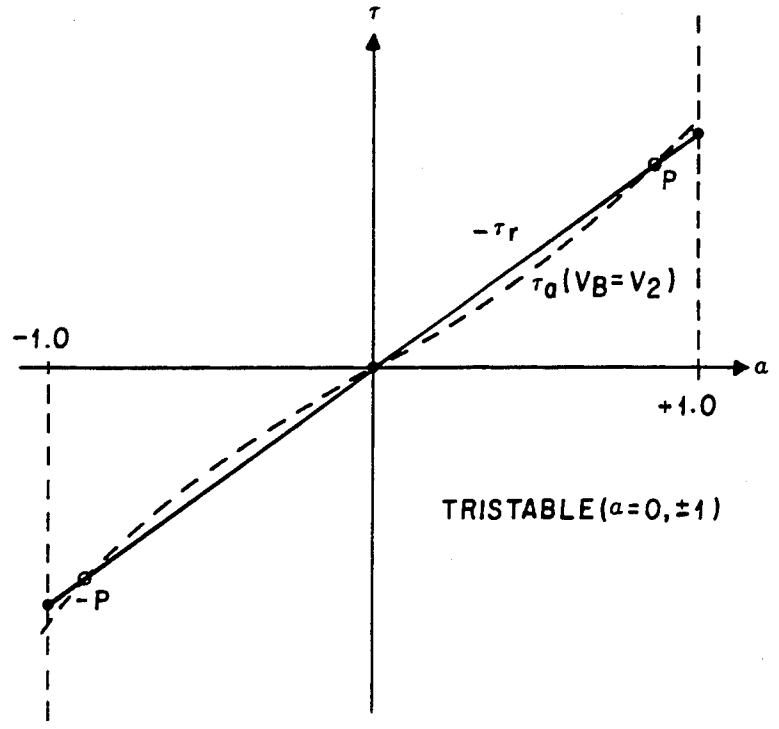

τ
P
$-\tau_r$
$\tau_a(V_B=V_2)$
-1.0
a
+1.0
TRISTABLE(a=0,±1)
-P

Fig. 11

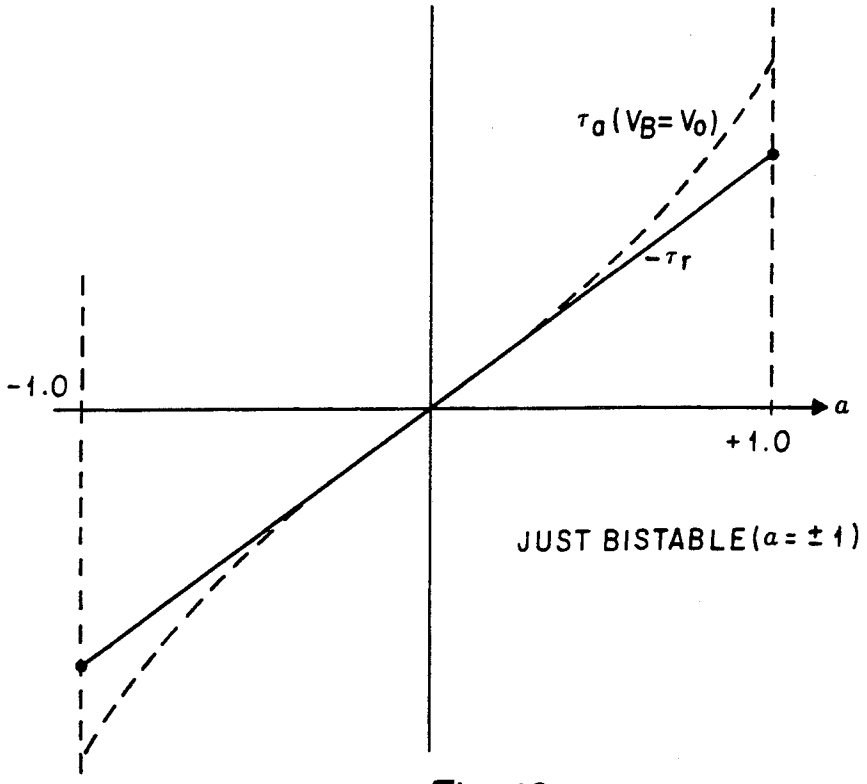

$\tau_a (V_B = V_0)$
$-\tau_r$
-1.0
+1.0
a
JUST BISTABLE ($a = \pm 1$)

Fig. 12

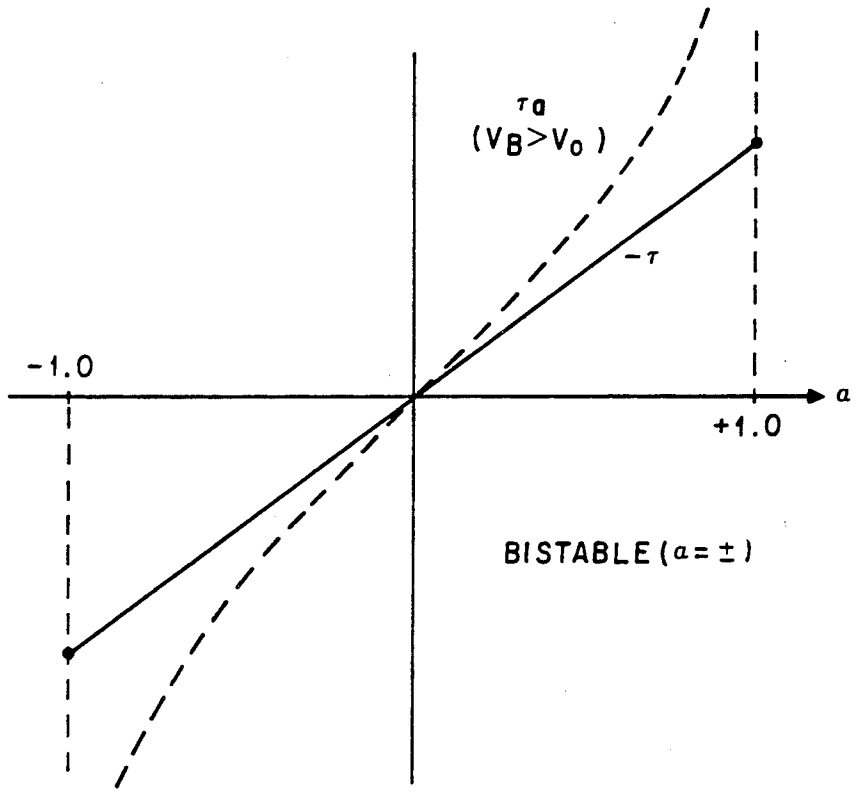

τ_a
$(V_B > V_0)$
$-\tau$
-1.0
+1.0
a
BISTABLE ($a = \pm$)

Fig. 13

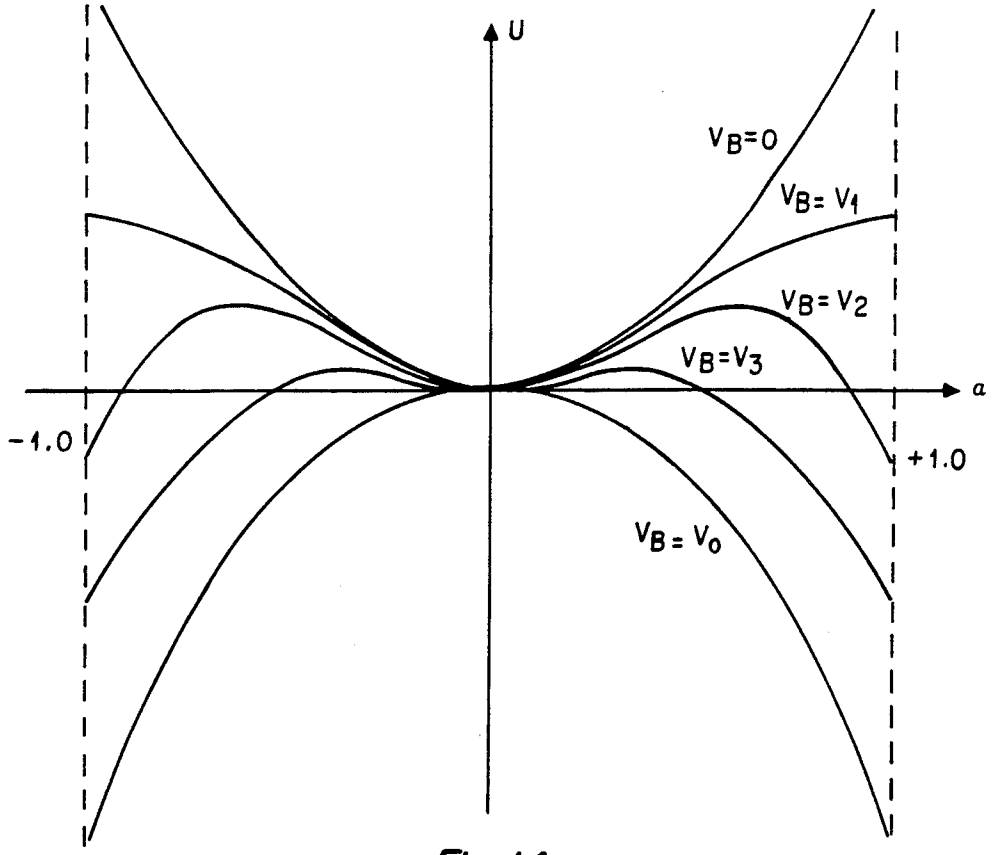

U
$V_B=0$
$V_B=V_1$
$V_B=V_2$
$V_B=V_3$
$V_B=V_0$
a
-1.0
+1.0

Fig. 14

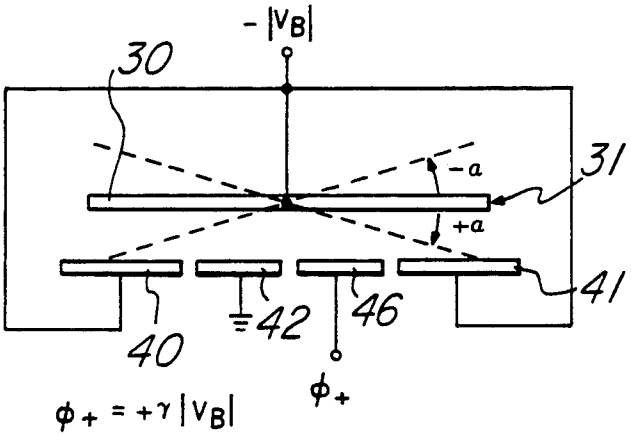

$-|V_B|$
30
31
-a
+a
41
40
42
46
ϕ_+
$\phi_+ = +\gamma|V_B|$

Fig. 15

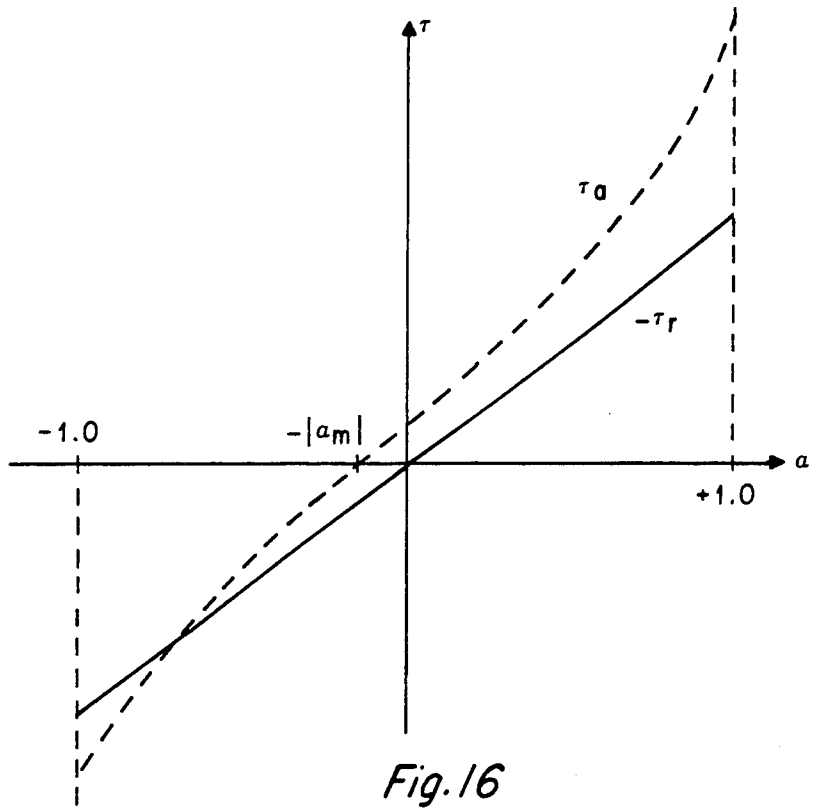


Fig. 16

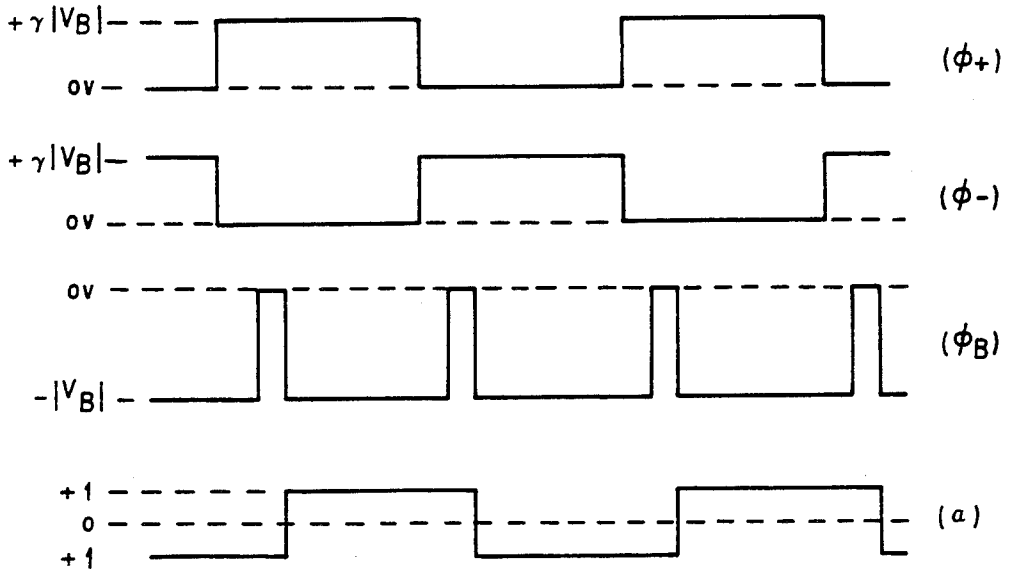


Fig. 17

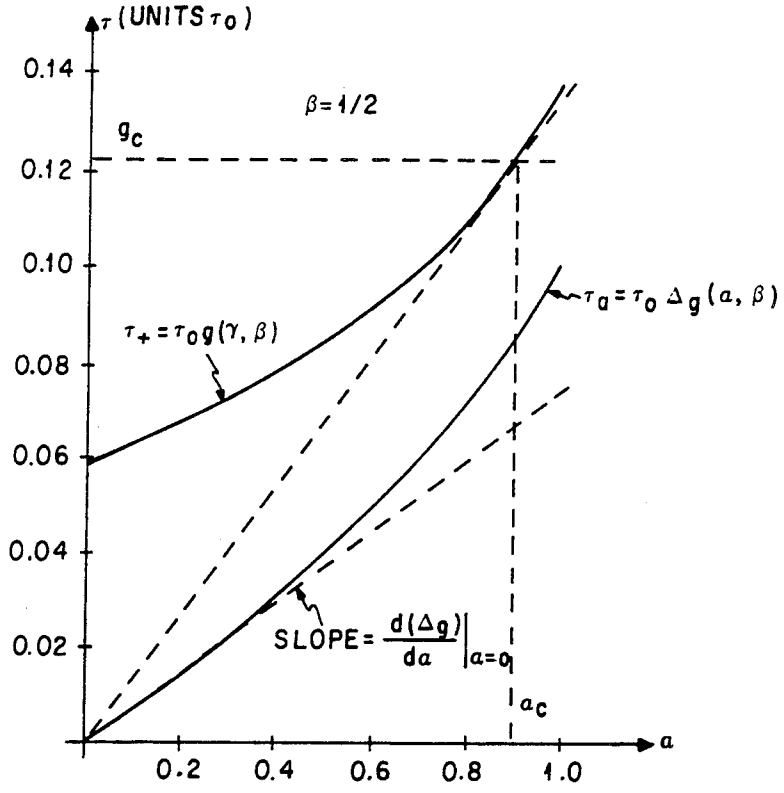

τ (UNITS τ0)
0.14
0.12
0.10
0.08
0.06
0.04
0.02
β=1/2
gc
τ+ = τ0 g(γ, β)
τa = τ0 Δg(a, β)
SLOPE = d(Δg)/da |a=0
ac
a
0.2
0.4
0.6
0.8
1.0

Fig. 18

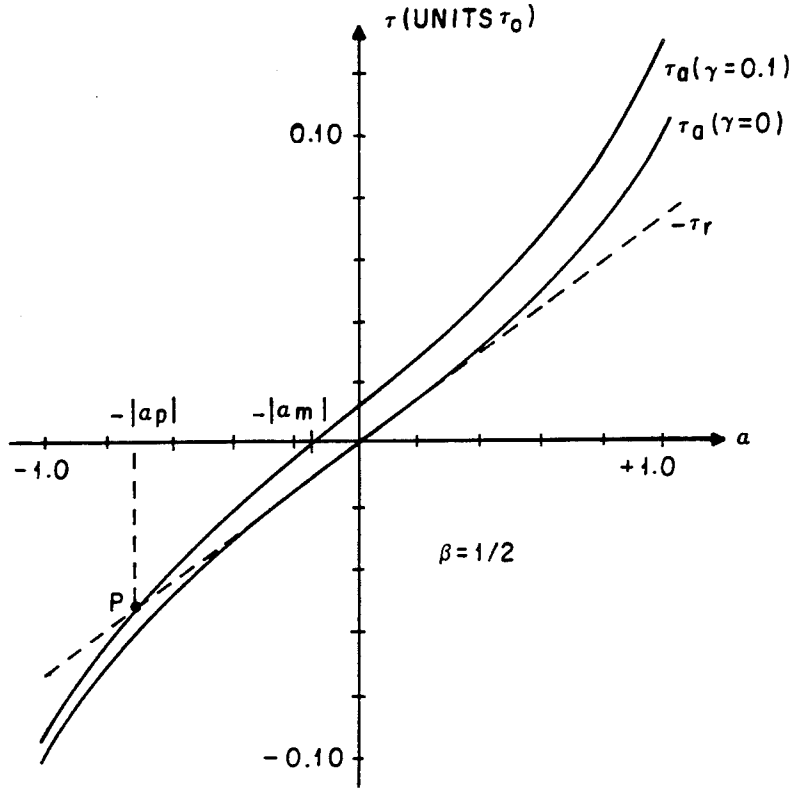

τ (UNITS τ0)
τa(γ=0.1)
τa(γ=0)
−τr
0.10
−|ap|
−|am|
a
-1.0
+1.0
β=1/2
P
-0.10

Fig. 19

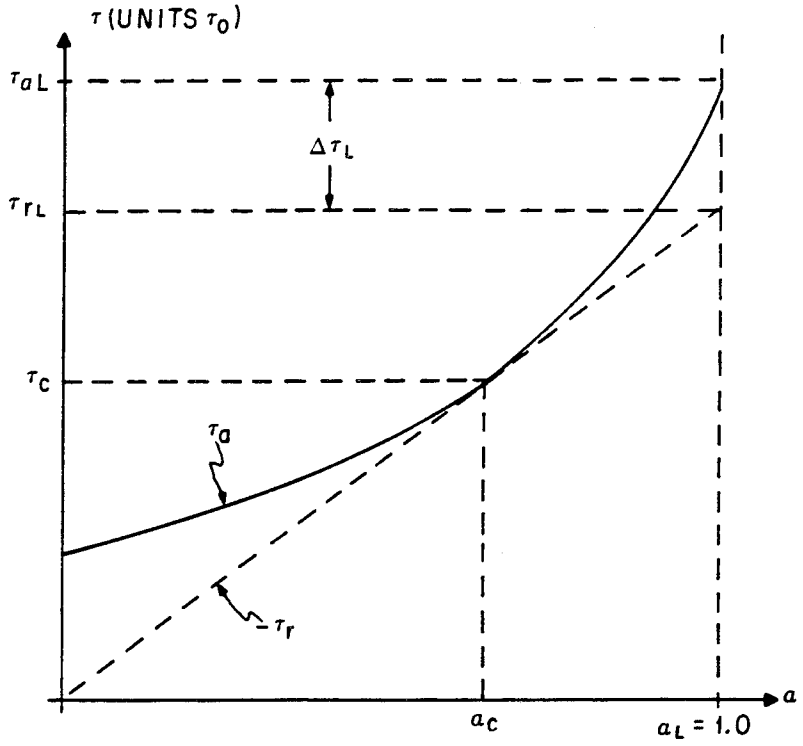

τ (UNITS τ0)
τaL
ΔτL
τrL
τc
τa
τr
a
ac
aL = 1.0

Fig. 20

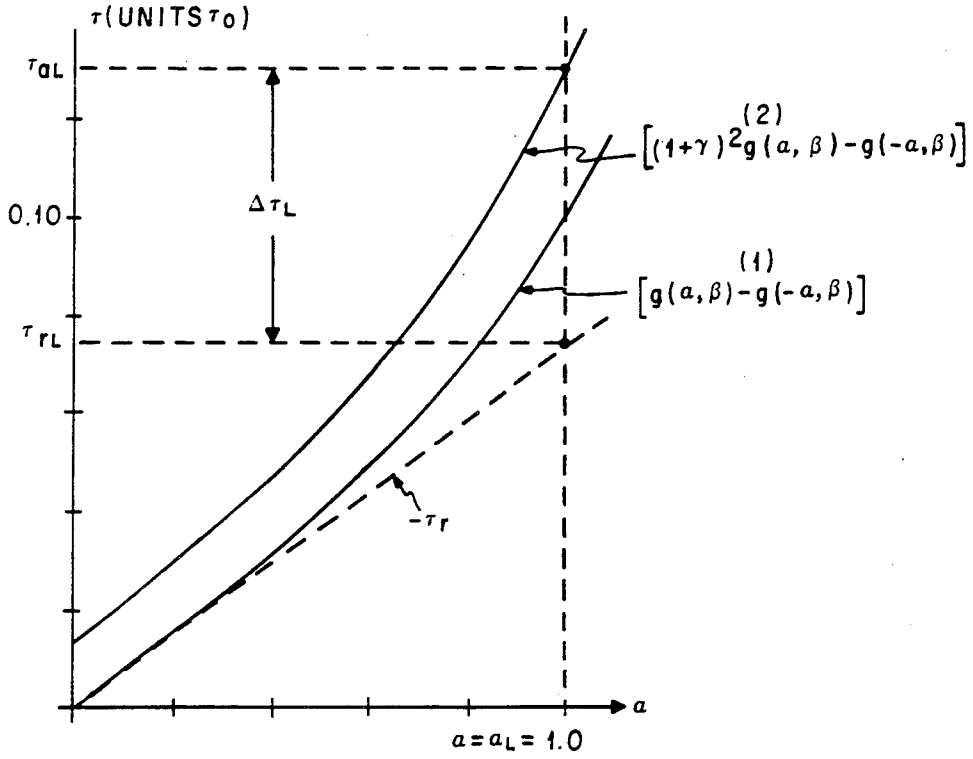

τ(UNITS τ0)
τaL
0.10
ΔτL
τrL
τr
a
a=aL= 1.0
(2)
[(1+γ)2g(a, β)-g(-a,β)]
(1)
[g(a,β)-g(-a,β)]

Fig. 21

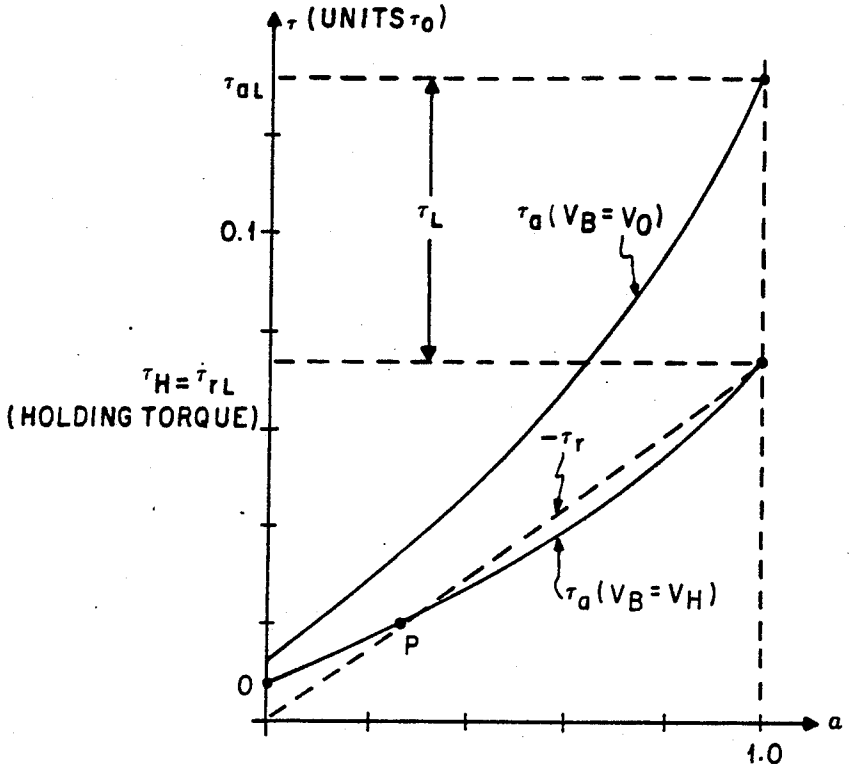

τ (UNITS τ0)
τaL
0.1
τL
τa (VB = V0)
τH = τrL
(HOLDING TORQUE)
τr
τa (VB = VH)
P
0
a
1.0

Fig. 22

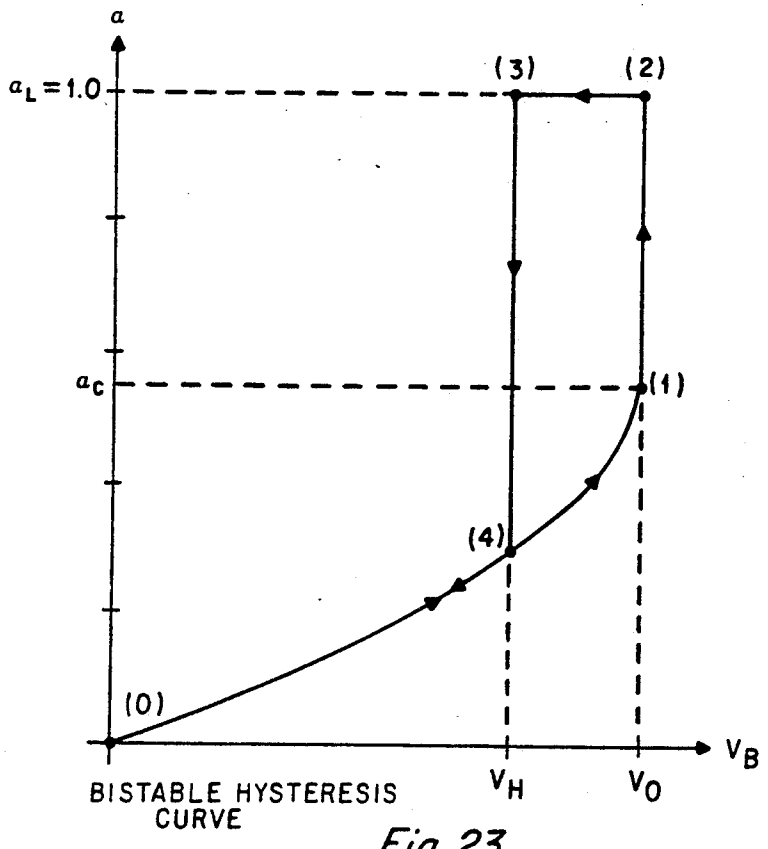

a
aL = 1.0
(3)
(2)
aC
(1)
(4)
(0)
VB
BISTABLE HYSTERESIS CURVE
VH
V0

Fig. 23

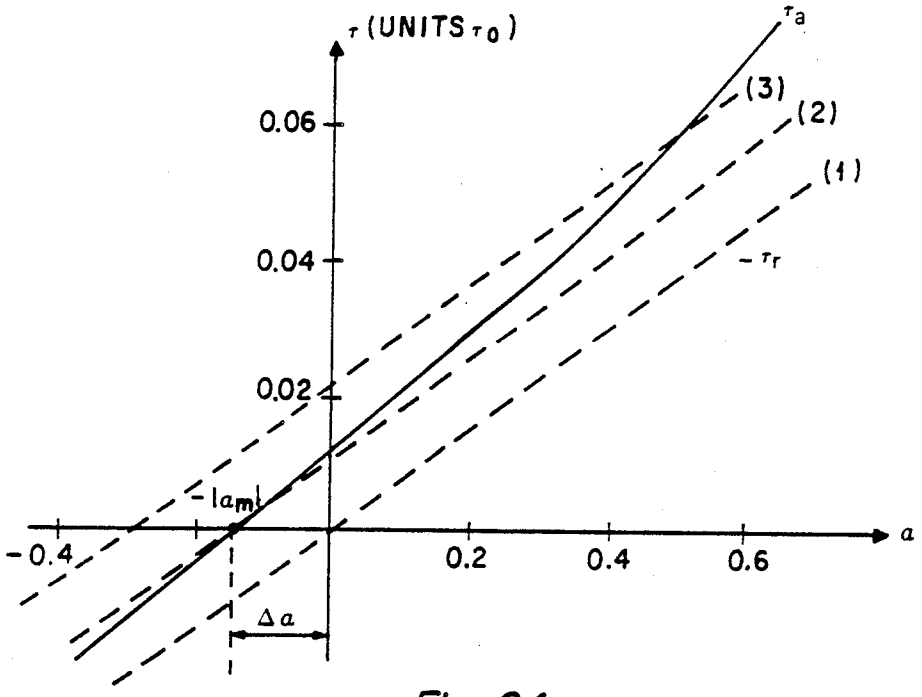

τ (UNITS τ0)
τa
(3)
(2)
(1)
-τr
0.06
0.04
0.02
-|am|
-0.4
0.2
0.4
0.6
a
Δa

Fig. 24

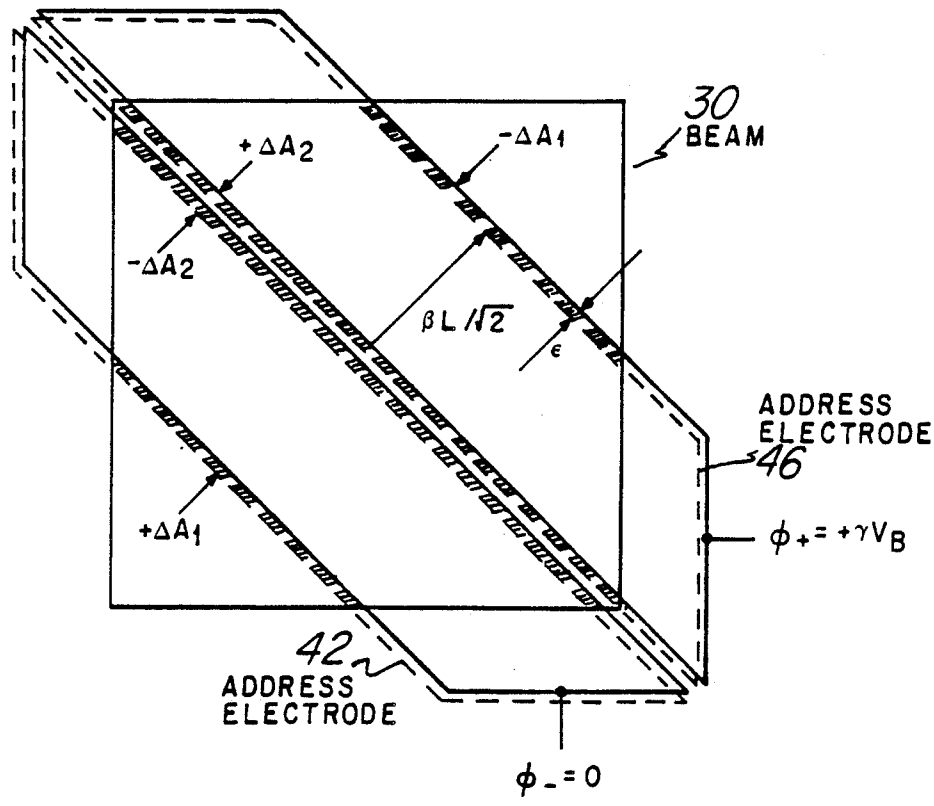

30
BEAM
+ΔA2
-ΔA1
-ΔA2
βL√2
ε
ADDRESS
ELECTRODE
46
+ΔA1
φ+ = +γVB
42
ADDRESS
ELECTRODE
φ- = 0

Fig. 25

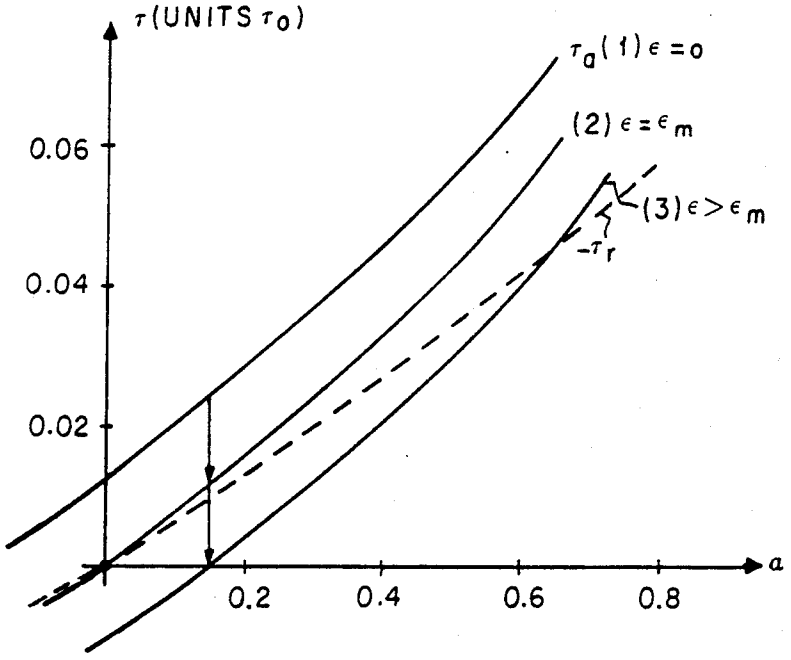

τ(UNITS τ0)
τa(1) ε=0
(2) ε=εm
(3) ε>εm
-τr
0.06
0.04
0.02
0.2
0.4
0.6
0.8
a

Fig.26

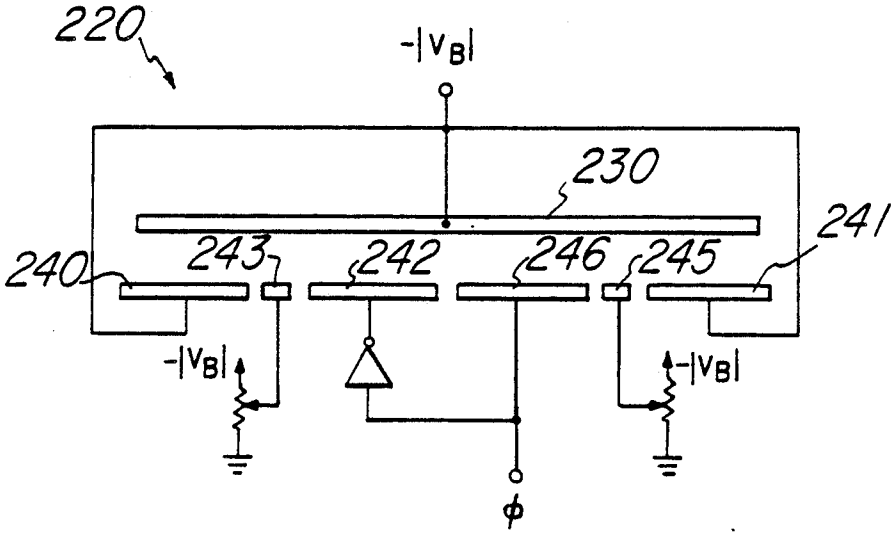

220
-|VB|
230
241
240
243
242
246
245
-|VB|
-|VB|
φ

Fig.27

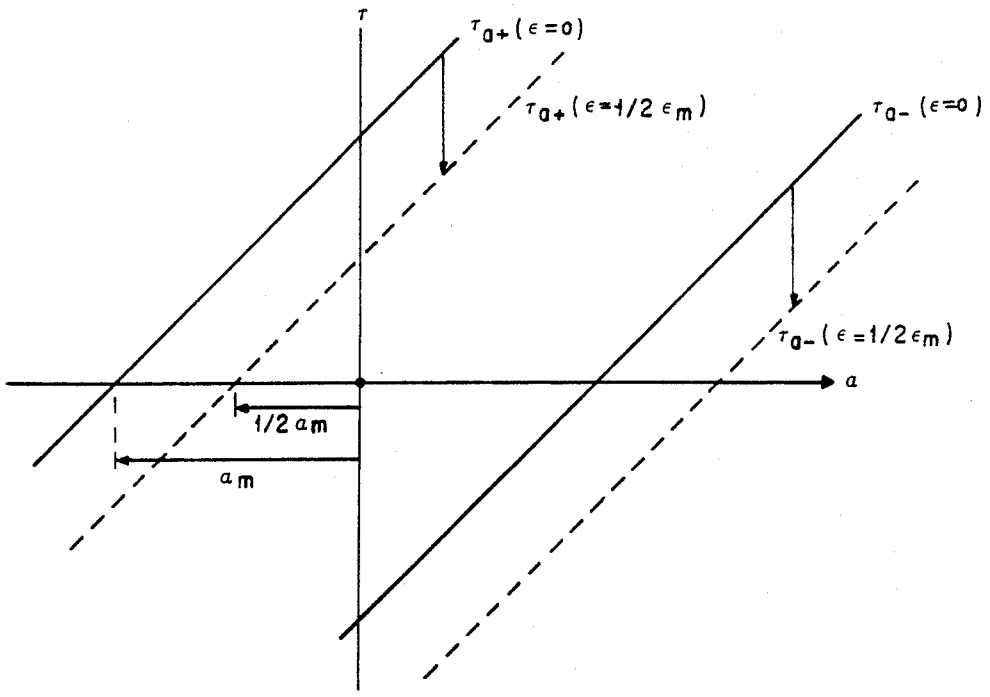

τ
τa+ (ε=0)
τa+ (ε=1/2 εm)
τa- (ε=0)
τa- (ε=1/2 εm)
a
1/2 am
am

Fig. 28

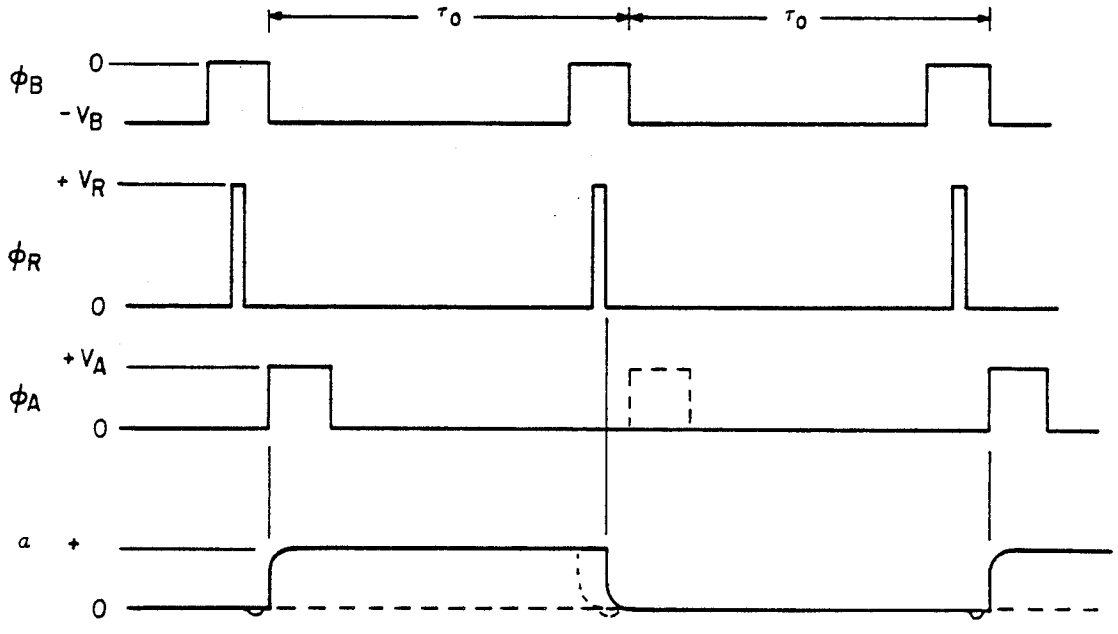

τo
τo
φB
0
-VB
+VR
φR
0
+VA
φA
0
a
+
0

Fig. 29

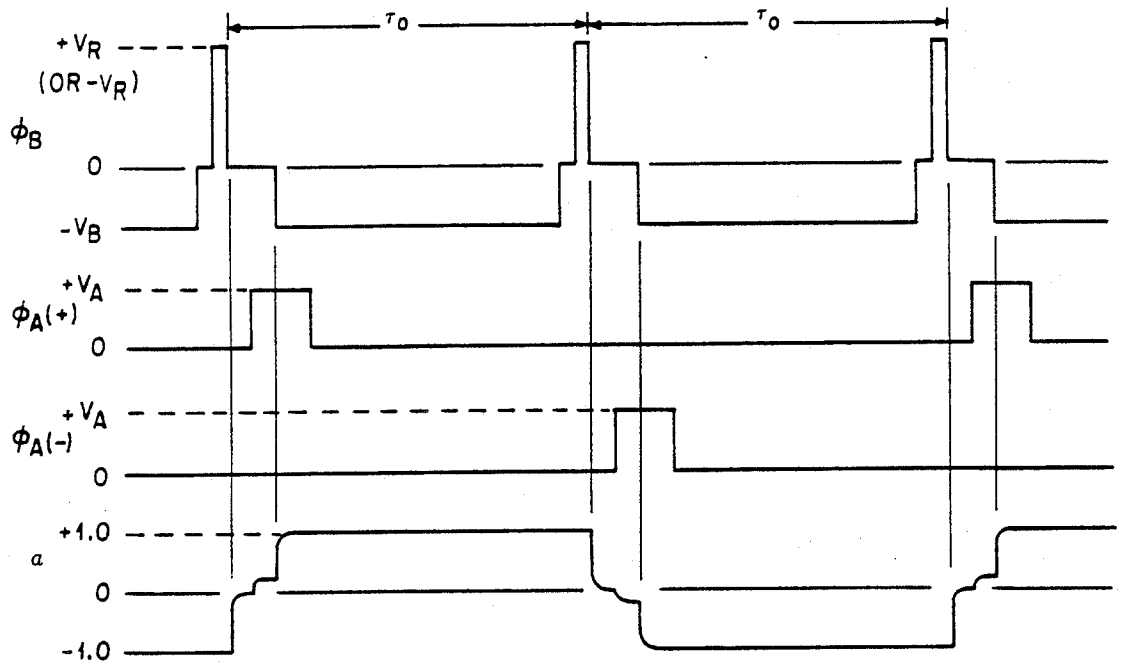


Fig. 30a

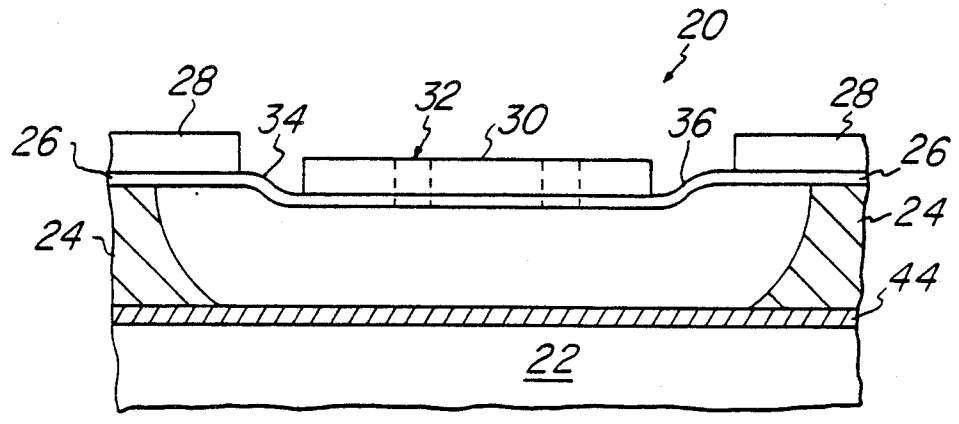


Fig. 30b

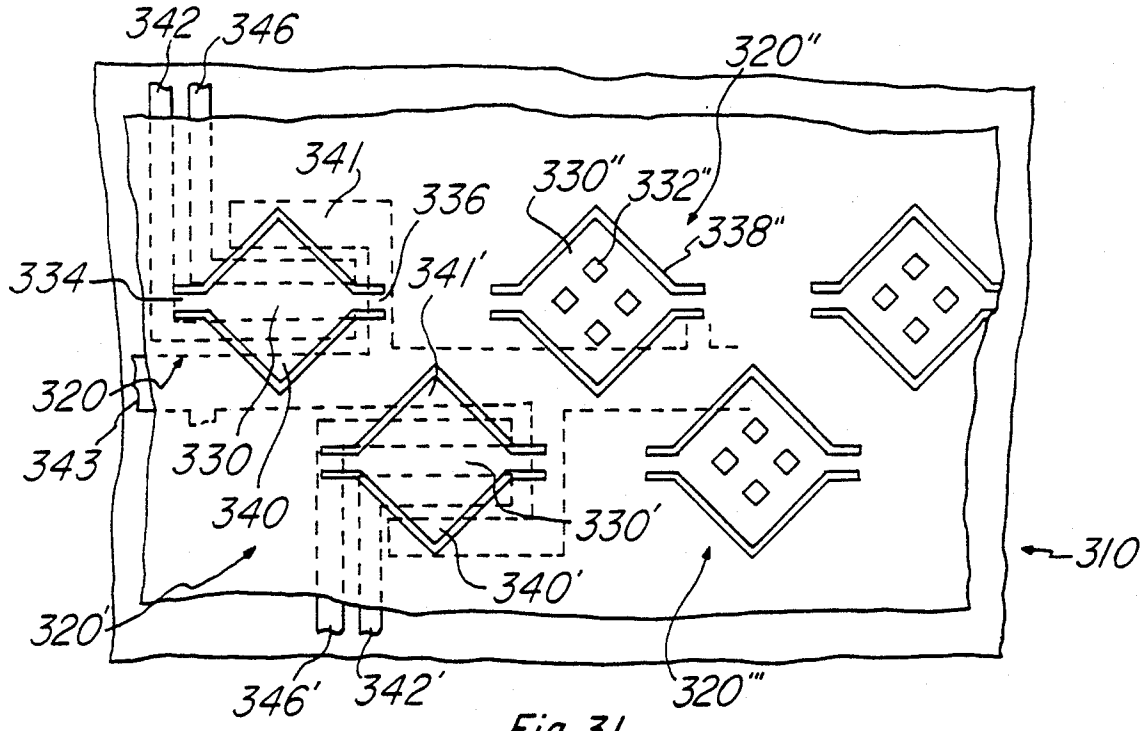


Fig. 31

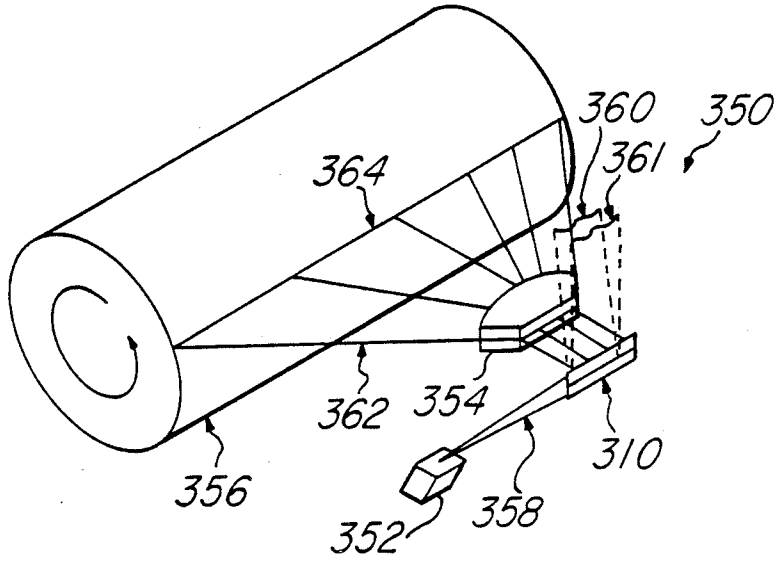


Fig. 32a

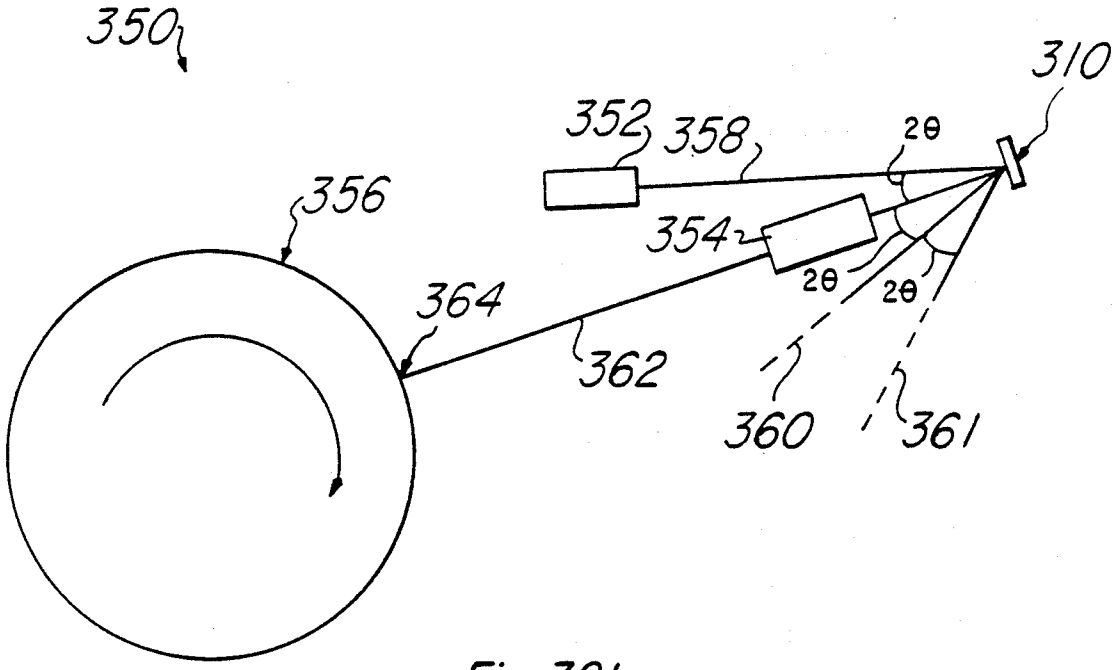


Fig. 32b

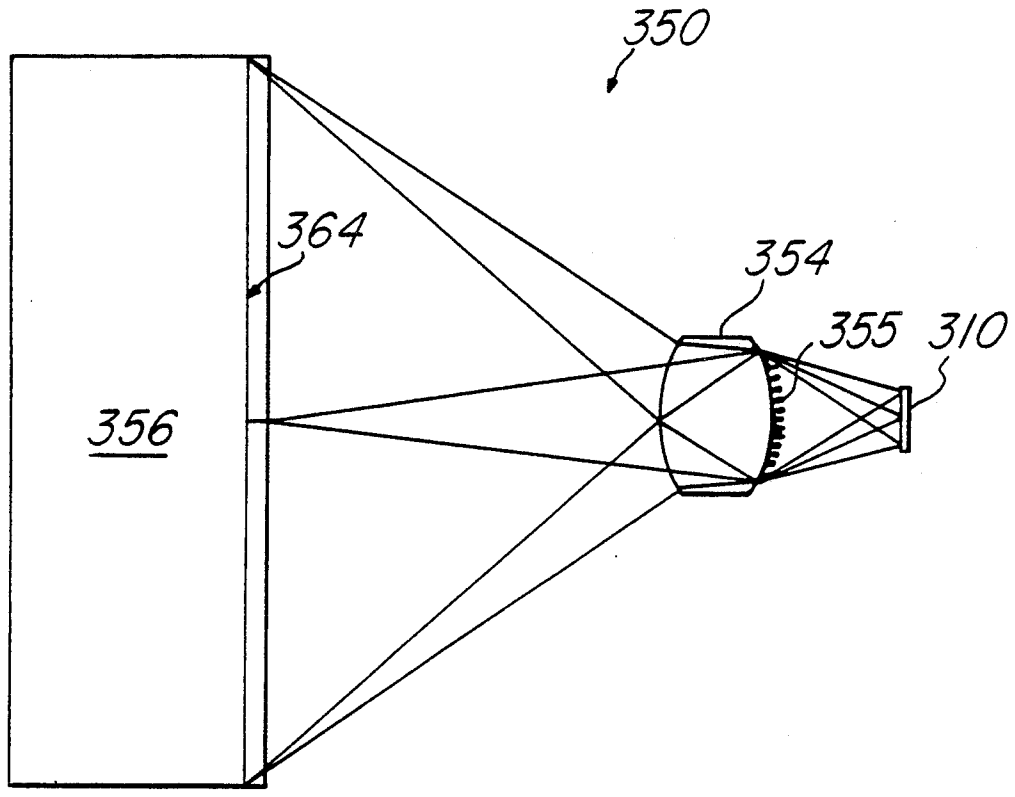


Fig. 32c

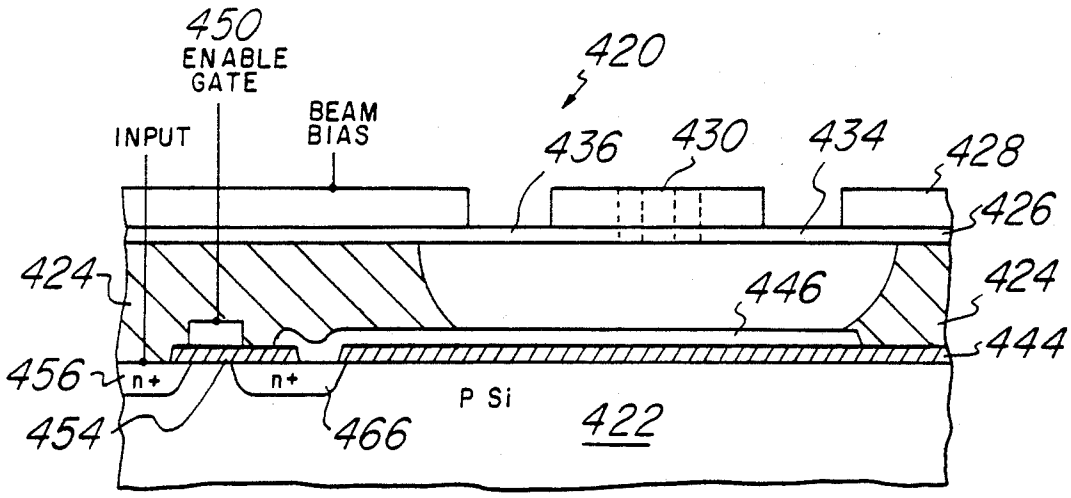

450
ENABLE GATE
INPUT
BEAM BIAS
420
436
430
434
428
426
424
446
424
444
456
n+
n+
P Si
454
466
422

Fig. 33

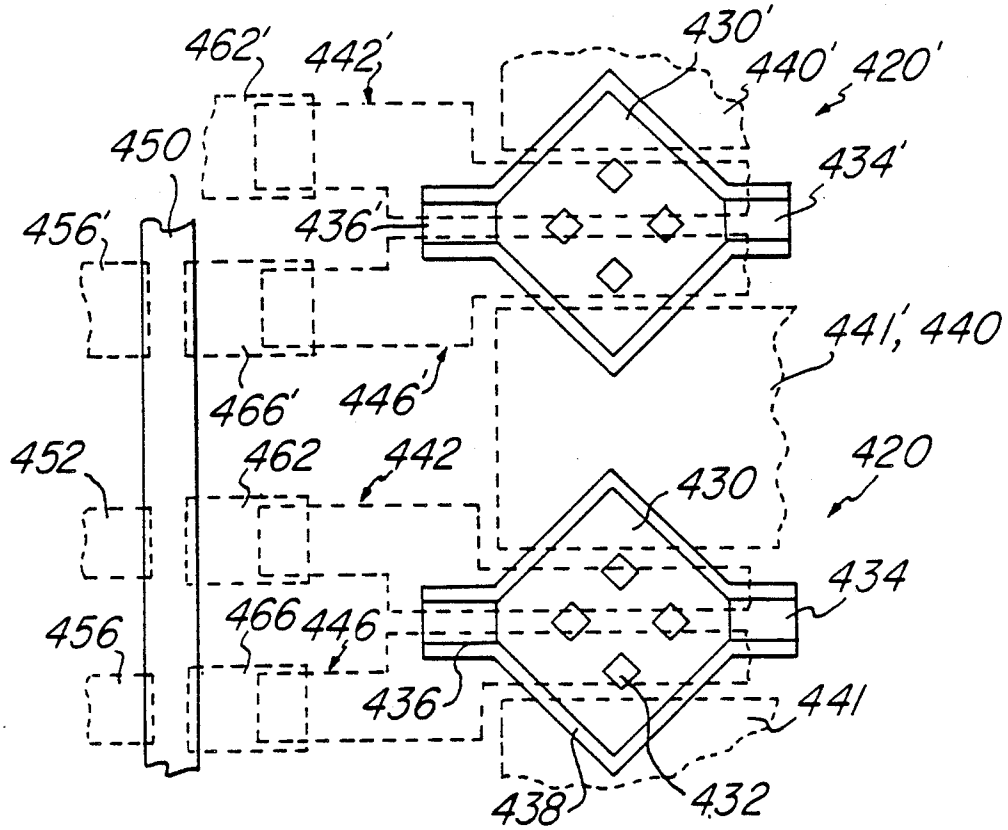

462'
442'
430'
440'
420'
450
434'
456'
436'
441', 440
466'
446'
452
462
442
420
430
434
456
466
446
436
441
438
432

Fig. 34

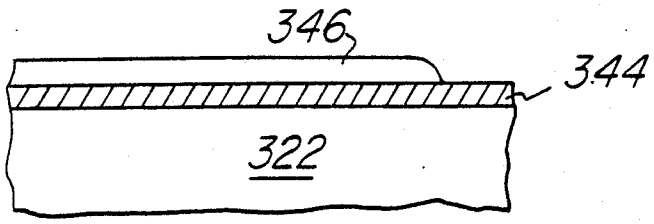


Fig. 35a

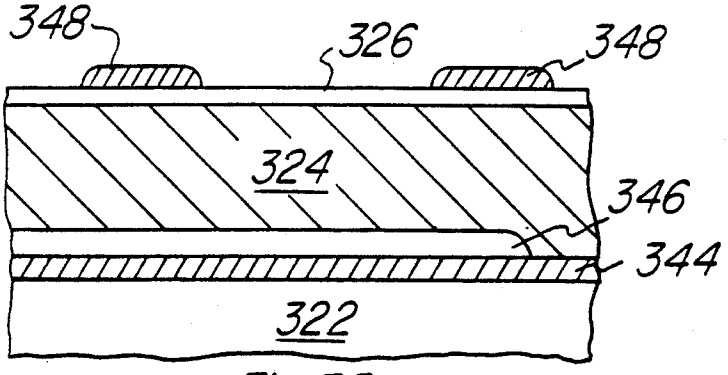


Fig. 35b

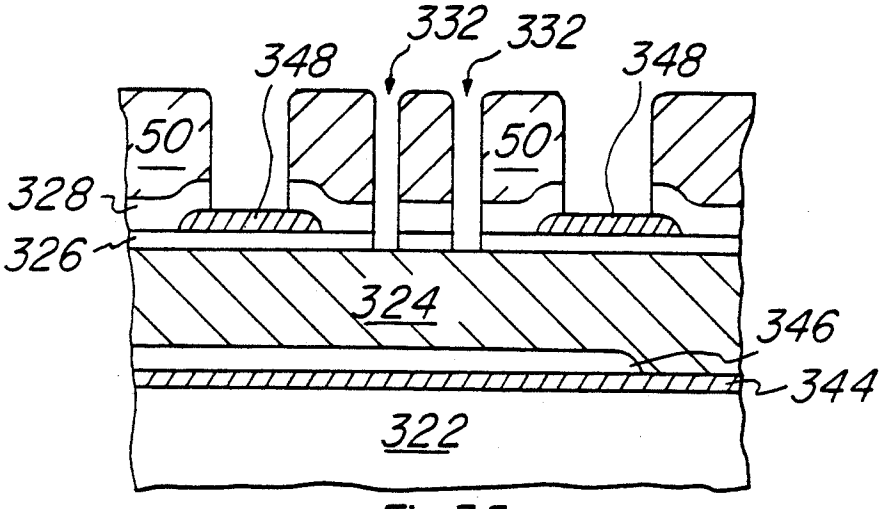


Fig. 35c

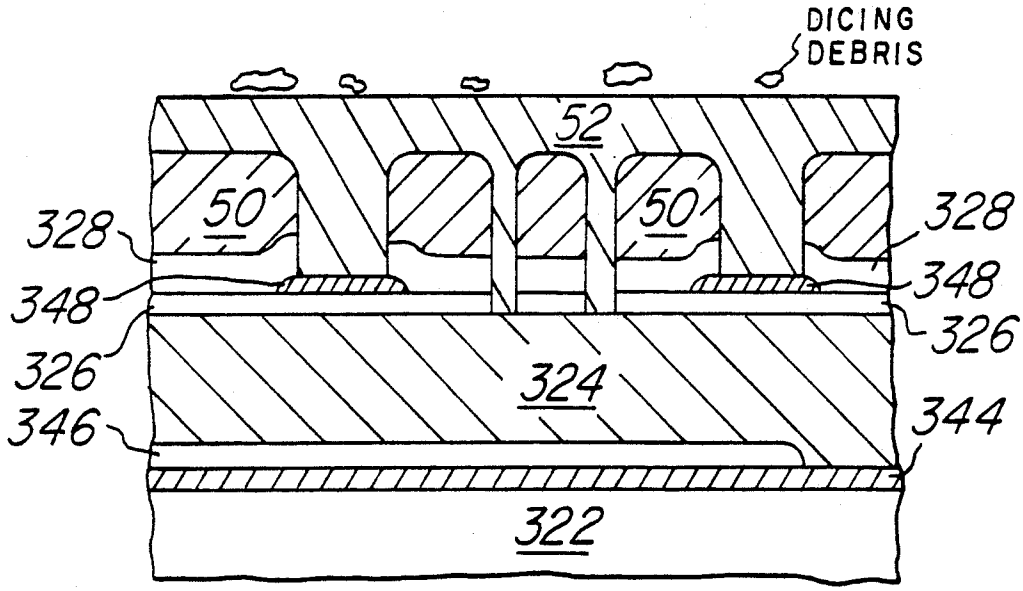


Fig. 35d

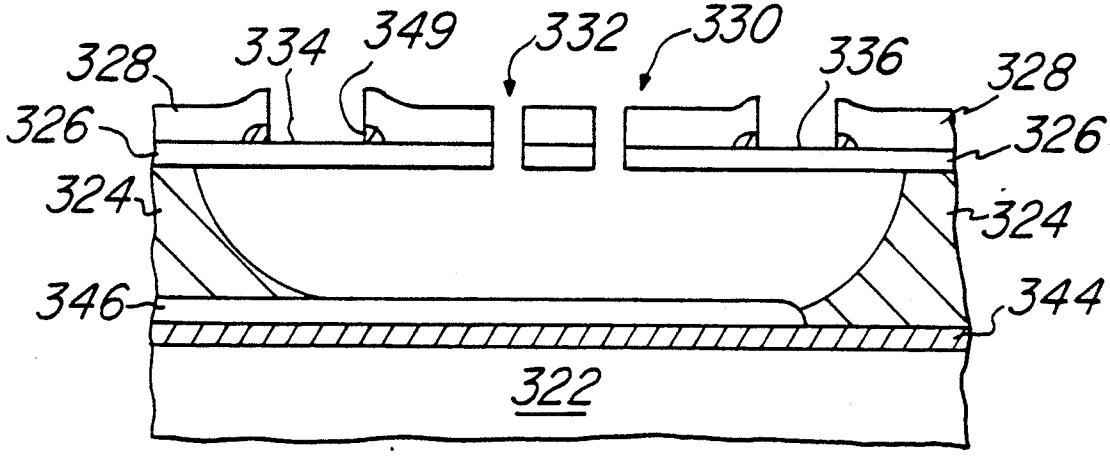


Fig. 35e

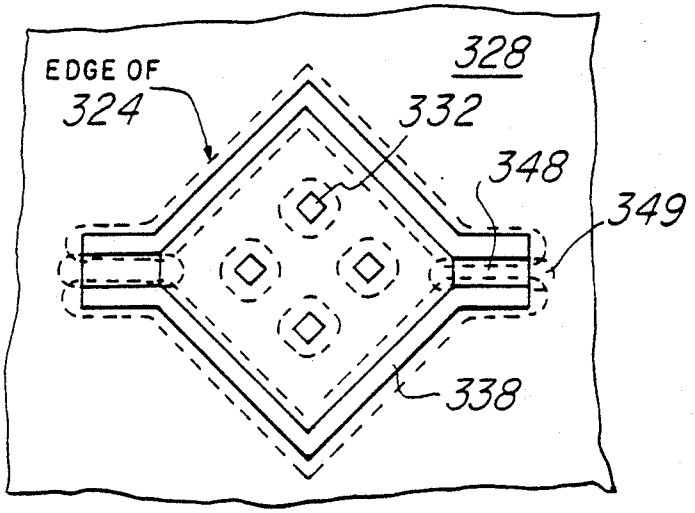


Fig. 36a

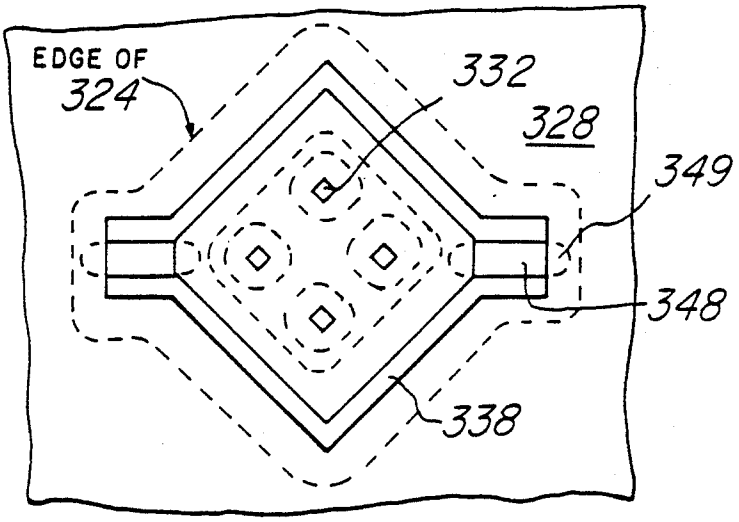


Fig. 36b

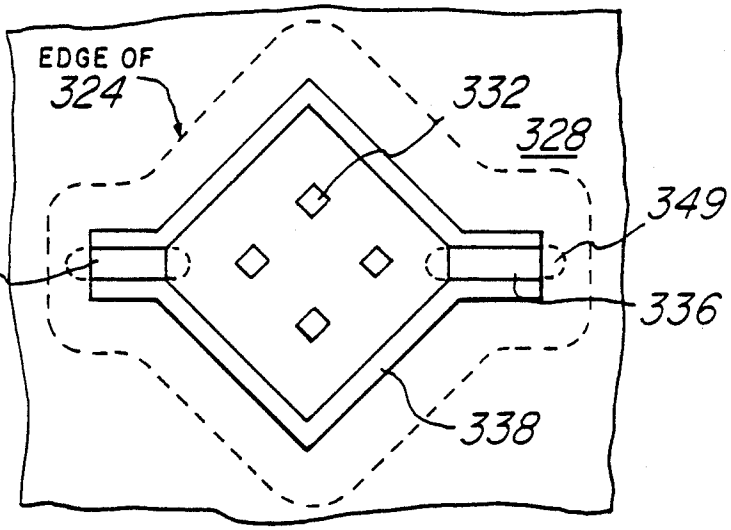


Fig. 36c

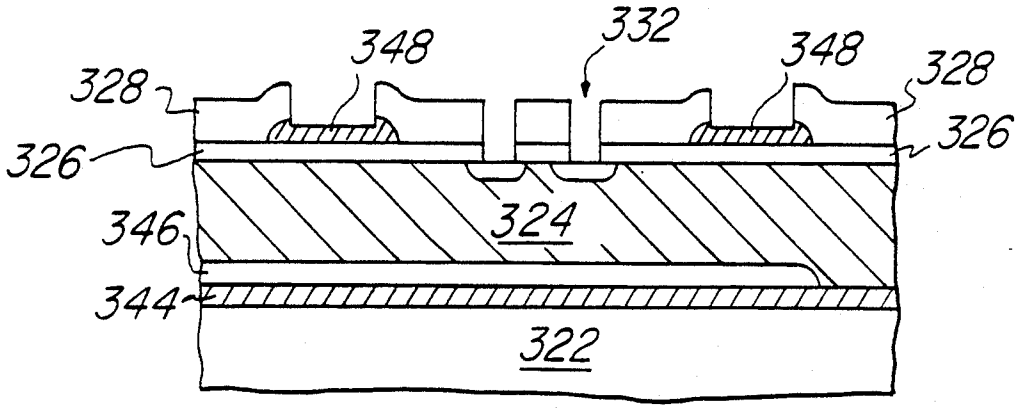


Fig. 37a

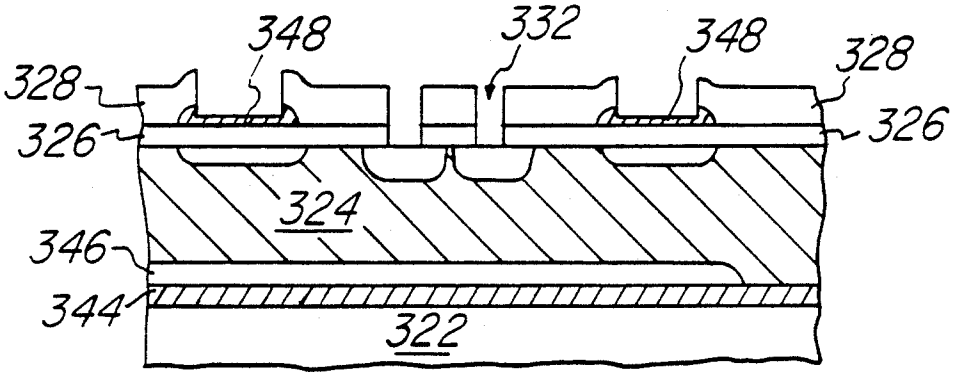


Fig. 37b

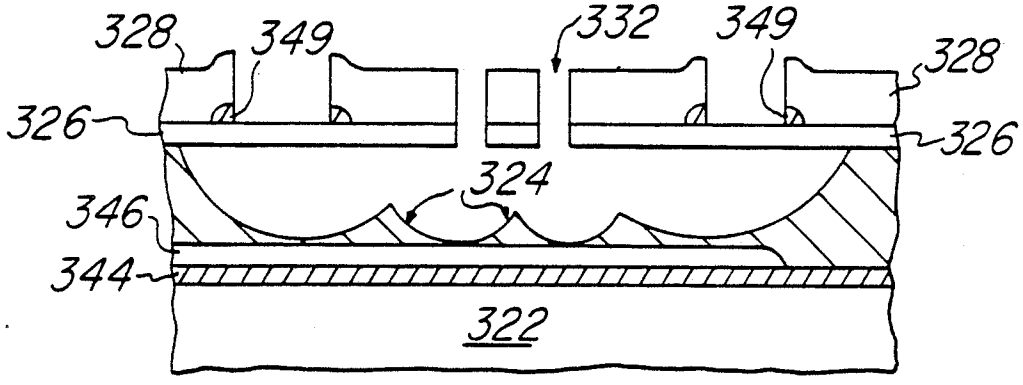


Fig. 37c

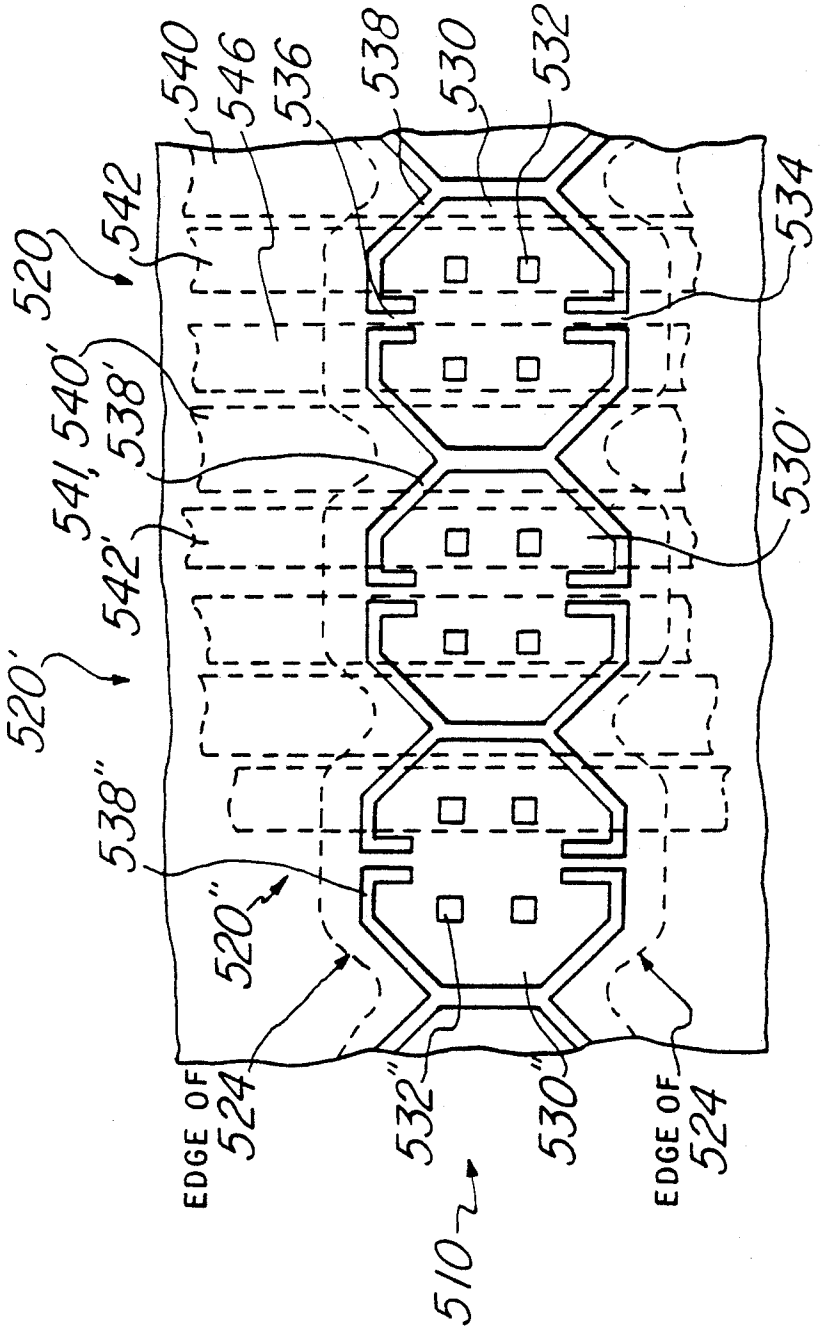

540
546
536
538
530
532
542
534
520
541, 540'
538'
530'
542'
520'
538"
520"
EDGE OF 524
532"
530"
EDGE OF 524
510

Fig. 38

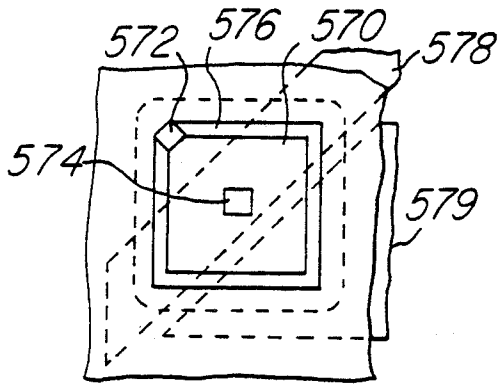


Fig. 39a

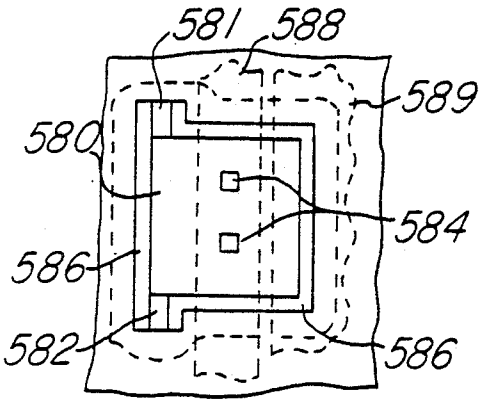


Fig. 39b

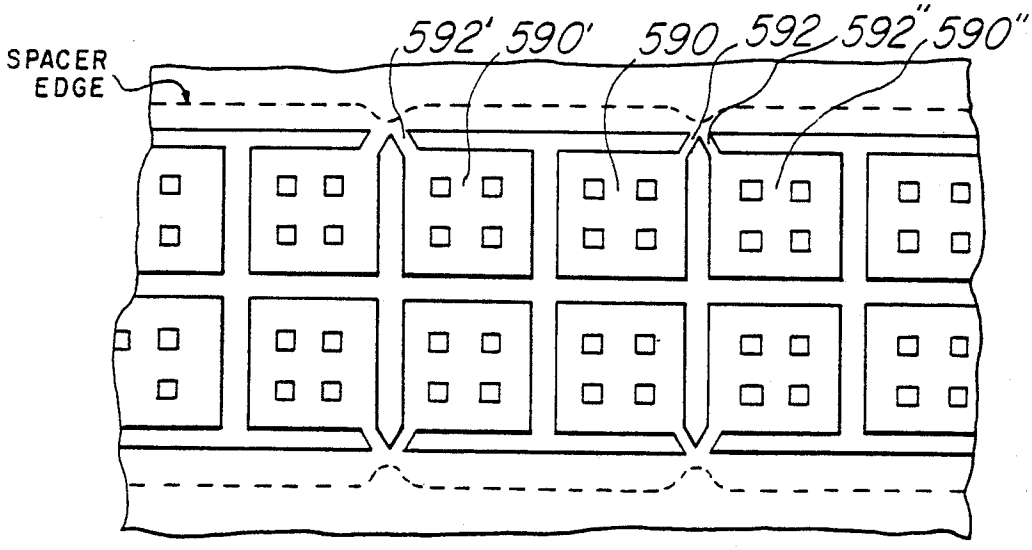


Fig. 39c

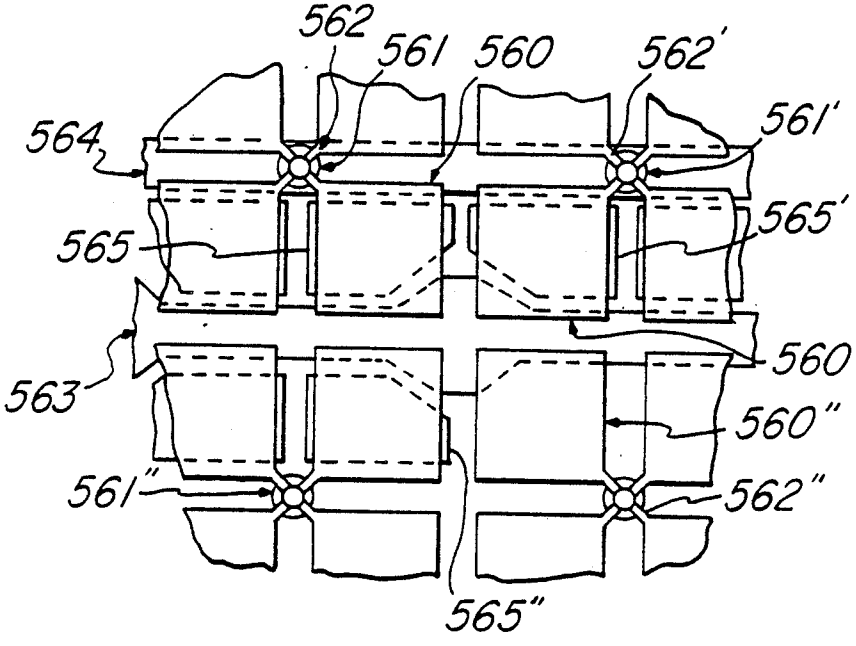


Fig. 39d

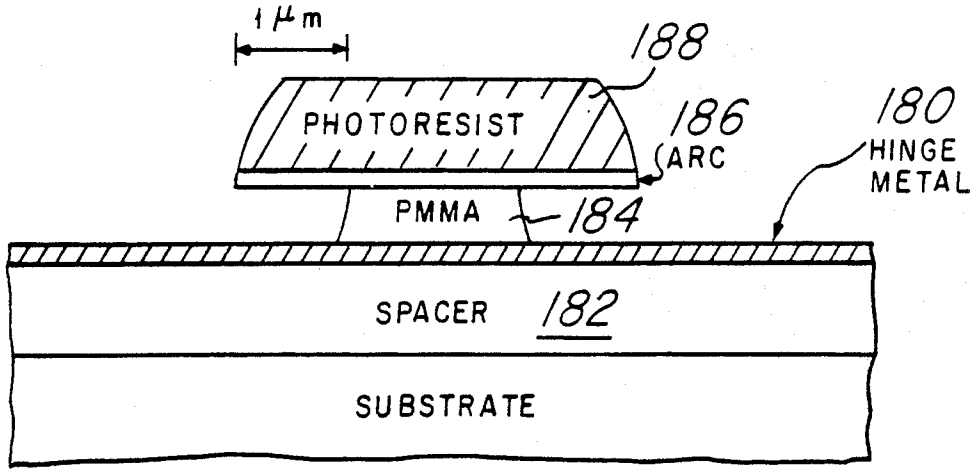


Fig.40a

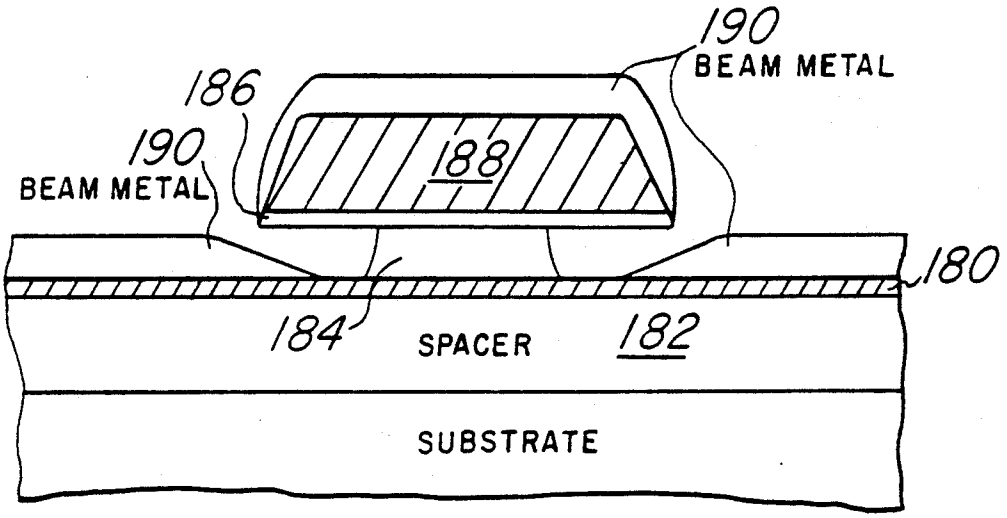


Fig.40b

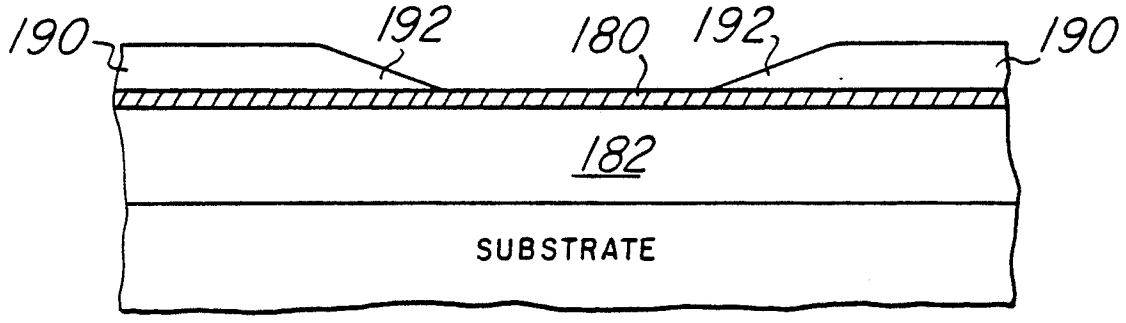


Fig.40c

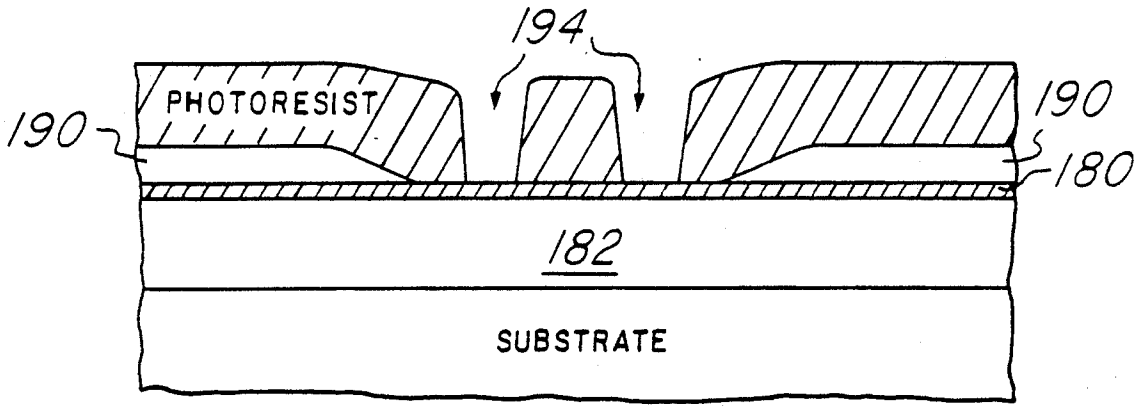


Fig. 40d

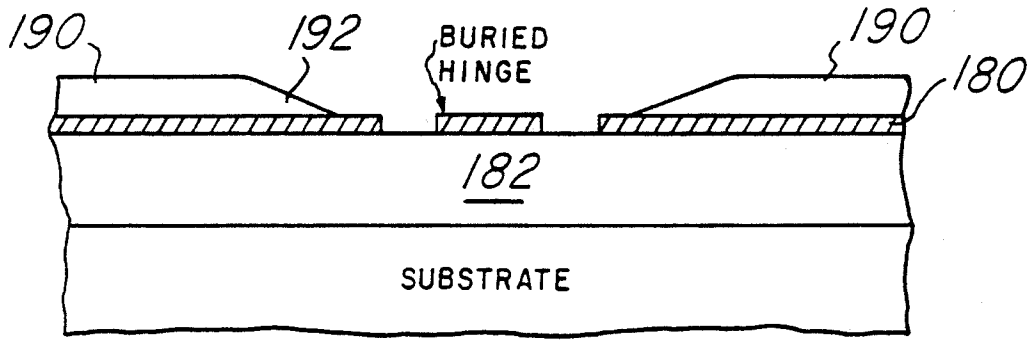


Fig. 40e

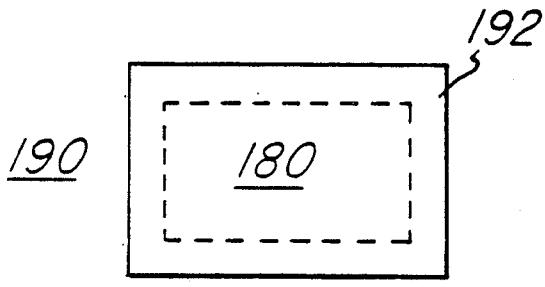


Fig. 41a

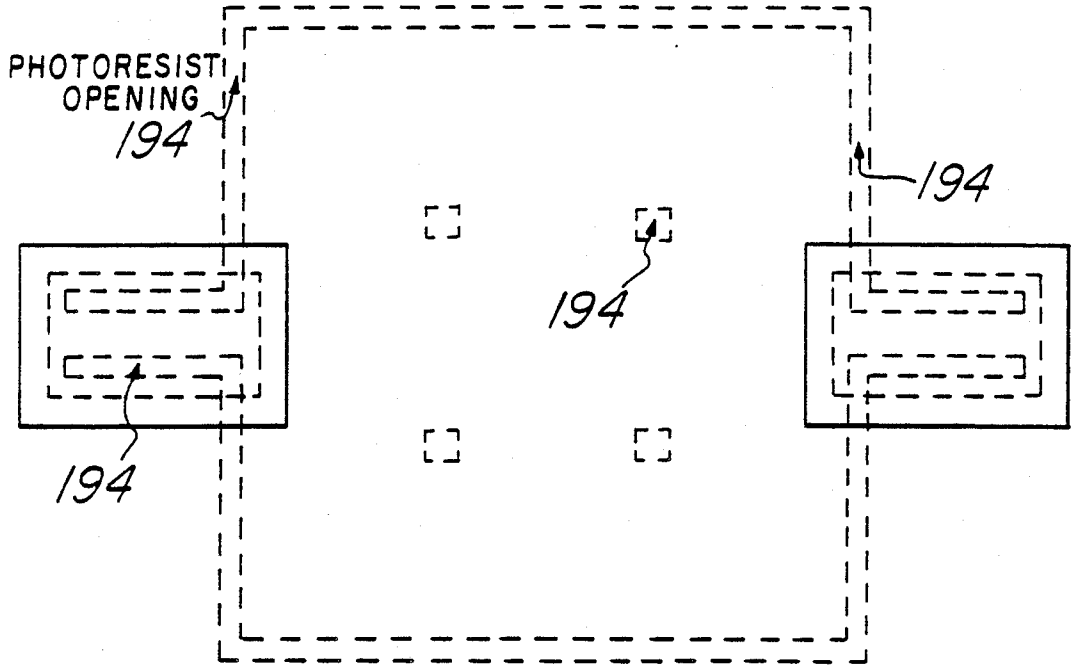


Fig. 41b

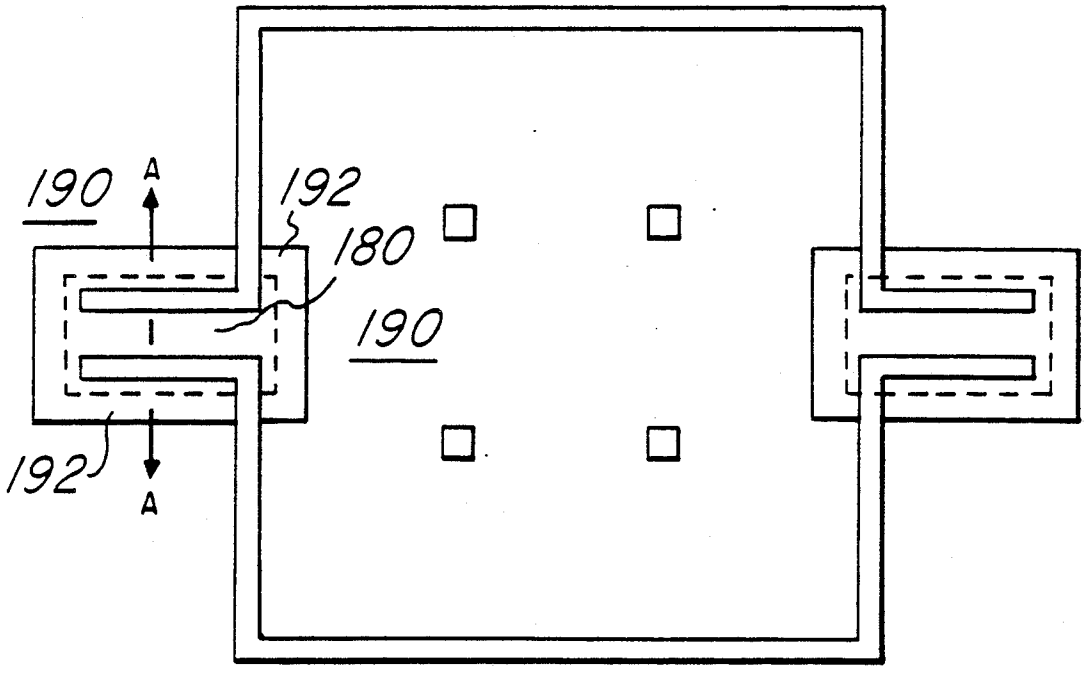


Fig. 41c

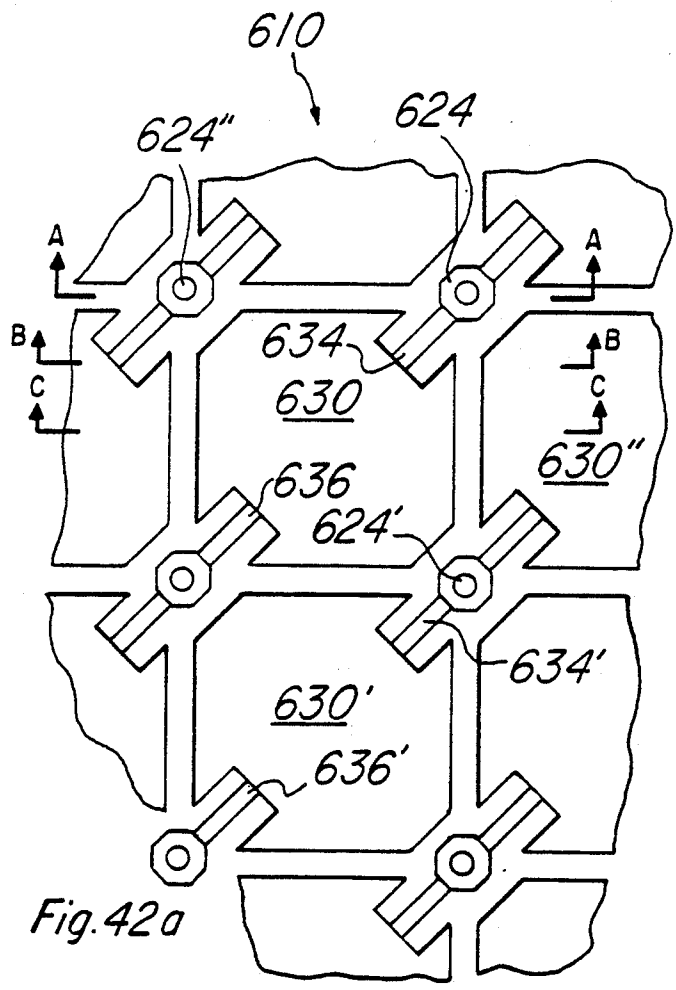


Fig. 42a

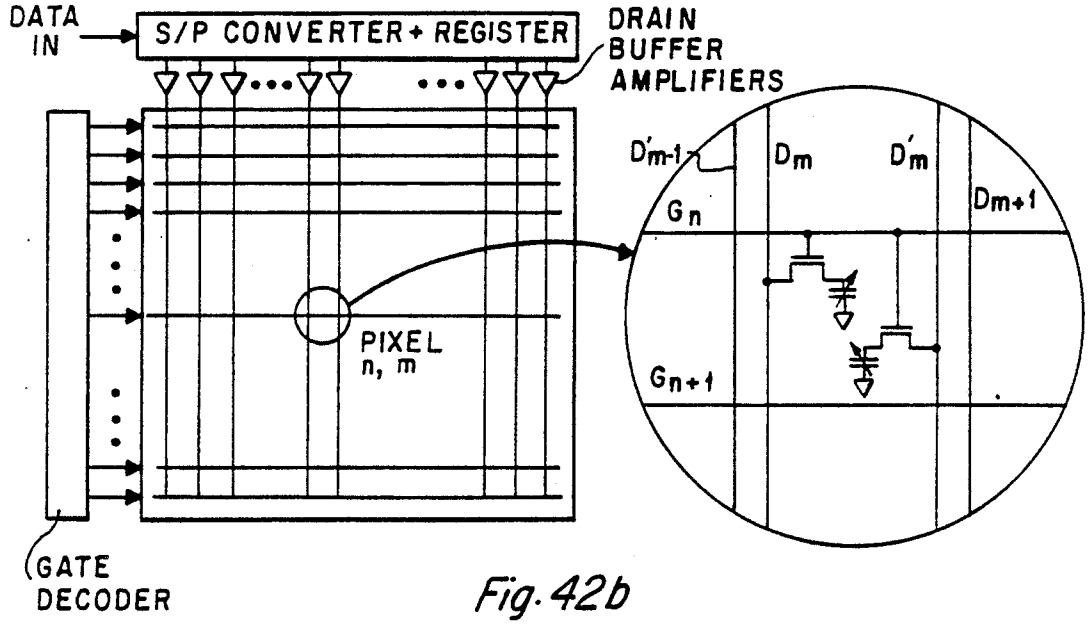


Fig. 42b

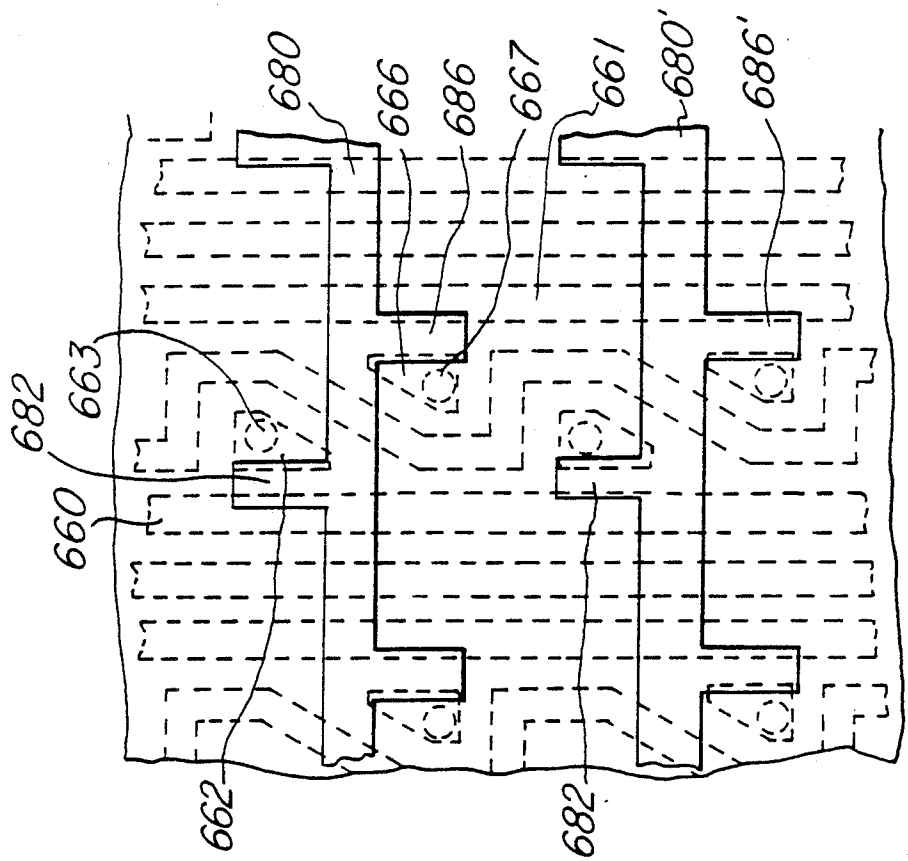


Fig. 43b

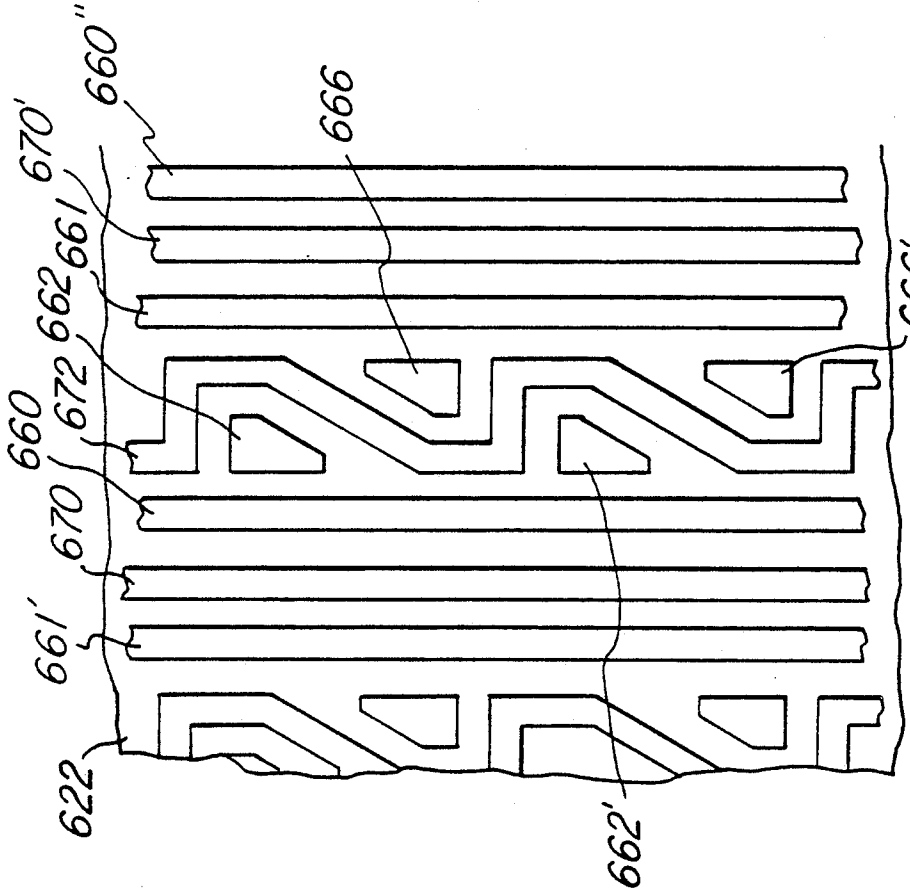


Fig. 43a

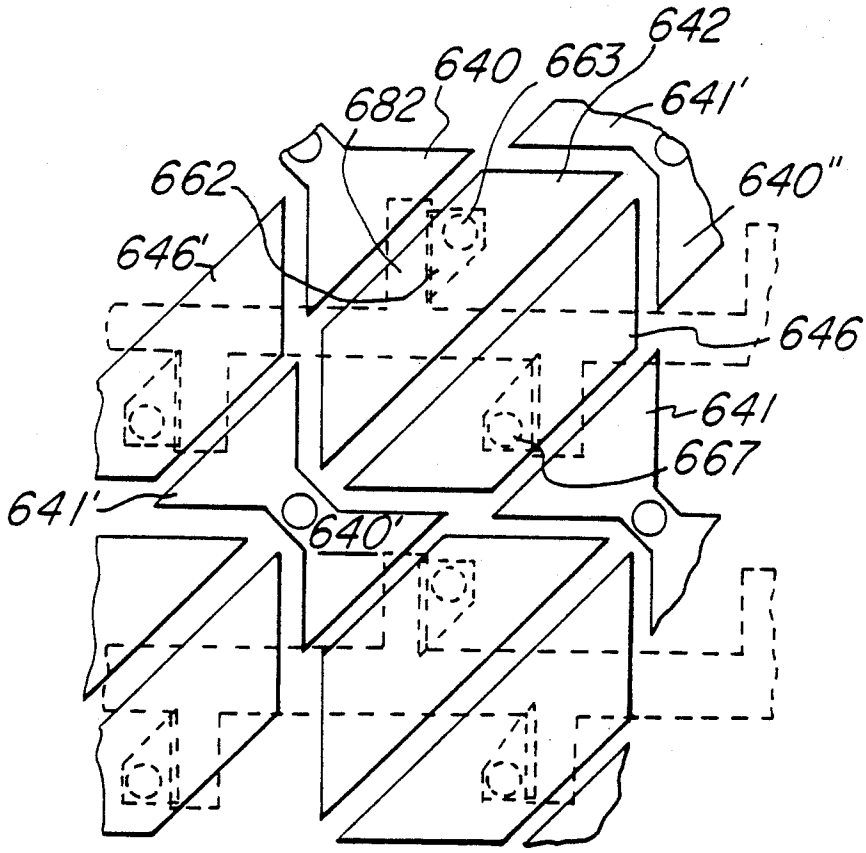


Fig.43c

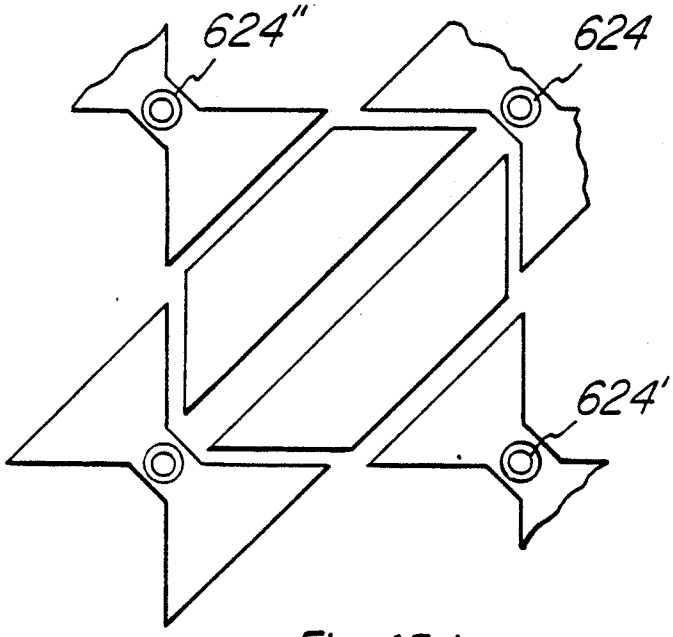


Fig. 43d

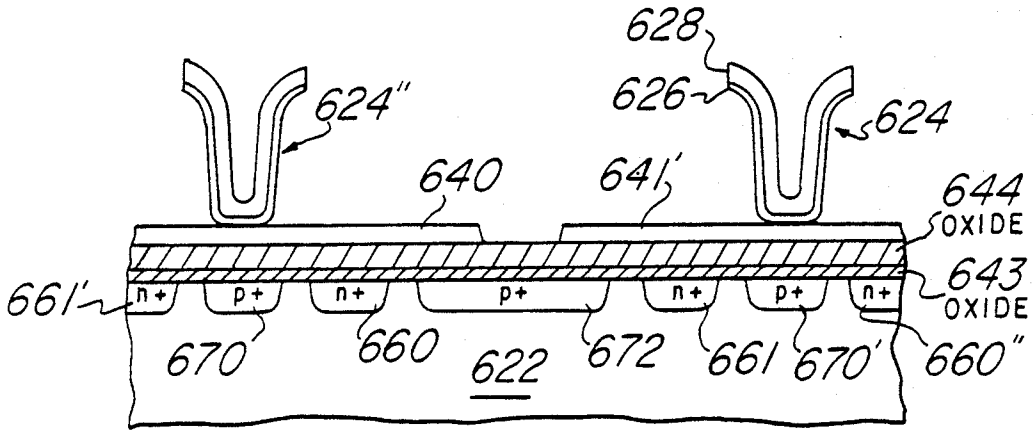


Fig.44a

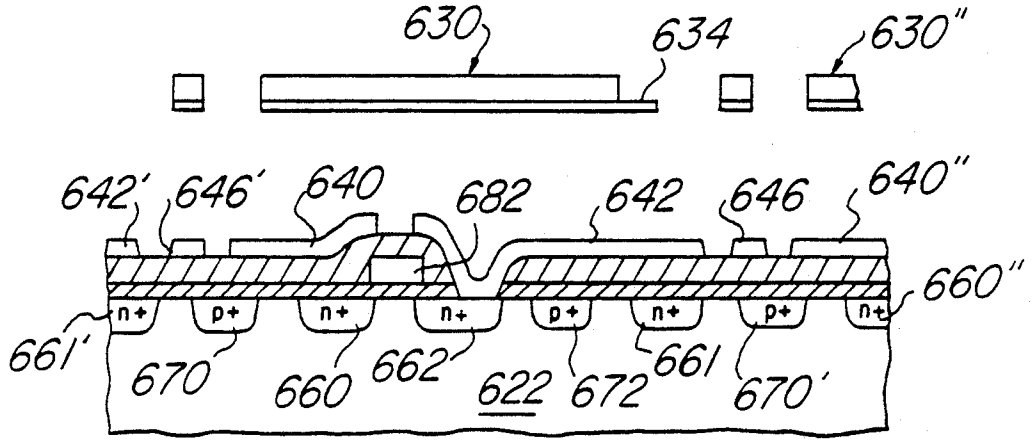


Fig.44b

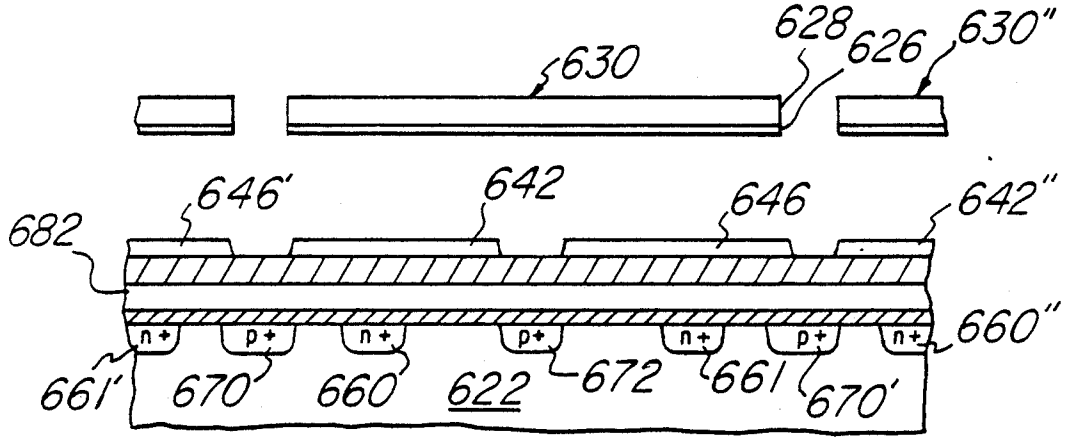


Fig.44c

SPATIAL LIGHT MODULATOR AND METHOD

RELATED APPLICATIONS

This application is a continuation of application Ser. No. 07/355,049, filed May 15, 1989 now abandoned which is a continuation of Ser. No. 07/168,724, filed Mar. 16, 1988, abandoned; which is a continuation in part of Ser. No. 07/159,466, filed Feb. 19, 1988, abandoned; which is a continuation of Ser. No. 06/636,180, filed Jul. 31, 1984, abandoned; and a continuation of Ser. No. 07/043,740, filed Apr. 29, 1987, abandoned; which is a continuation in part of Ser. No. 06/792,947, filed Oct. 30, 1985, now U.S. Pat. No. 4,662,746; and a continuation in part of Ser. No. 07/129,353 filed Nov. 30, 1987, abandoned; which is a continuation of Ser. No. 06/877,654 filed June 23, 1986, abandoned; which is a continuation in part of Ser. No. 06/646,399 filed Aug. 31, 1984, now U.S. Pat. No. 4,596,992.

BACKGROUND OF THE INVENTION

The present invention relates to spatial light modulators (light valves), and, more particularly, to spatial light modulators with pixels formed of electronically addressable deflectable beams.

Spatial light modulators (SLM) are transducers that modulate incident light in a spatial pattern corresponding to an electrical or optical input. The incident light may be modulated in its phase, intensity, polarization, or direction, and the light modulation may achieved by a variety of materials exhibiting various electrooptic or magnetoopotic effects and by materials that modulate light by surface deformation. SLMs have found numerous applications in the areas of optical information processing, projection displays, and electrostatic printing. See references cited in L. Hornbeck, 128 X 128 Deformable Mirror Device, 30 IEEE Tran. Elec. Dev. 539 (1983).

A well known SLM used for large bright electronic displays is the Eidophor, a system which uses an electrostatically dimpled oil film as the active optical element. See, E. Baumann, The Fischer large-screen projection system (Eidophor), 20 J. SMPTE 351 (1953). In this system a continuous oil film is scanned in raster fashion with an electron beam that is modulated so as to create a spatially periodic distribution of deposited charge within each resolvable pixel area on the oil film. This charge distribution results in the creation of a phase grating within each pixel by virtue of the electrostatic attraction between the oil film surface and the supporting substrate, which is maintained at constant potential. This attractive force causes the surface of the film to deform by an amount proportional to the quantity of deposited charge. The modulated oil film is illuminated with spatially coherent light from a xenon arc lamp. Light incident to modulated pixels on the oil film is diffracted by the local phase gratings into a discrete set of regularly spaced orders which are made to fall on a schlieren stop consisting of a periodic array of alternating clear and opaque bars by part of the optical system. The spacing of the schlieren stop bars is chosen to match the spacing of the diffracted signal orders at the stop plane so that high optical throughput efficiency is achieved. Light that is incident to unmodulated regions of the light valve is blocked from reaching the projection lens by the opaque bars of the schlieren stop. Images formed of unmodulated areas on the light valve by the schlieren imaging system on the projection screen are therefore dark, while the phase perturbations introduced by the modulated electron beam are converted into bright spots of light at the screen by the schlieren projector. In spite of numerous technical difficulties associated with oil polymerization by electron bombardment and organic vapor contamination of the cathode, this type of oil-film system has been successfully developed to the point that it is the almost universally used system for a total light requirement of thousands of lumens at the screen. However, such systems are expensive, bulky, and have short-lived components.

A number of non-oil-film SLMs have also been developed and include deflectable element types, rotation of plane of polarization types, and light scattering types. These SLM types employ various effects such as deformation of reflective layers of metal, elastomer, or elastomer-photoconductor, and polarization and scattering of ferroelectrics, PLZT ceramics, and liquid crystals. For example, R. Sprague et al, Linear total internal reflection spatial light modulator for laser printing, 299 Proc. SPIE 68 (1981) and W. Turner and R. Sprague, Integrated total internal reflection (TIR) spatial light modulator for laser printing, 299 Proc. SPIE 76 (1982) and U.S. Pat. No. 4,380,373 describe a system for non-impact printing on a photosensitive medium in which laser light is formed into a line of illumination and passed through a linear array of light modulators and then imaged onto the photosensitive medium. The arra is implemented as a total internal reflection spatial light modulator with the electrodes and drive electronics fabricated on an integrated drive element which is placed against the total internal reflection surface of an electrooptic crystal such as lithium niobate. The localized change in index of refraction produced by the fringing field between each two electrodes is read out with schlieren readout optics which image the TIR interface onto the photosensitive medium. This is a one dimensional image, and the photosensitive medium is rotated on a drum beneath the image of the linear array to generate the two dimensional image (e.g., a page of text) for printing applications. However, the SLM (light valve) is highly susceptible to fabrication problems due to its hybrid nature. The fringing field strength, and hence the amount of light diffracted from modulated pixels, is sensitive to changes in the air gap thickness between the address electrodes and the electrooptic crystal surface of less than one tenth micron. Thus, even very small particles trapped between the crystal and electrode structure could cause illumination nonuniformity problems at the photosensitive medium. The system optical response for pixels located at the boundary between modulated and unmodulated areas of the light valve is also significantly lower than the response for pixels near the middle of a modulated region due to the nature of the addressing technique. A commercially available printer based on this technology has not been introduced to date.

M. Little et al., CCD-Addressed Liquid Crystal Light Valve, Proc. SID Symp. 250 (April 1982) describes a SLM with a CCD area array on the front side of a silicon chip and a liquid crystal array on the backside of the chip. Charge is input into the CCD until a complete frame of analog charge data has been loaded; the charge is then dumped to the backside of the chip where it modulates the liquid crystal. This device suffers from severe fixed pattern noise as well as resolution degradation due to the charge spreading from the front-to-back transfer.

Another SLM type which may be fabricated in both one and two dimensional arrays is the deformable mirror. Deformable mirrors may be subdivided into three classes: elastomers, membranes, and cantilever beams. In the elastomer approach a metallized elastomer is addressed by a spatially varying voltage that produces surface deformation through compression of the elastomer. Because of the address voltage requirements in the order of one or two hundred volts, the elastomer is not a good candidate for integration with a high-density silicon address circuit. See, generally, A. Lakatos and R. Bergen, TV projection display using an amorphous Se-type RUTICON light valve, 24 IEEE Tran. Elec. Dev. 930 (1977).

Membrane deformable mirrors come in a variety of types. One type is essentially a substitute for the oil film of the Eidophor system discussed above. In this system a thin reflective membrane is mounted to the faceplate of a cathode ray tube (CRT) by means of a support grid structure. Addressing is by a raster scanned electron beam as with the Eidophor. The charge deposited on the glass faceplate of the CRT by the electron beam electrostatically attracts the membrane which is held at a constant voltage. This attractive force causes the membrane to sag into the well formed by the grid structure, thereby forming a miniature spherical mirror at each modulated pixel location. The light diffracted from this type of modulated pixel is concentrated into a relatively narrow cone that is rotationally symmetric about the specularly reflected beam. This type of light valve is thus used with a schlieren stop that consists of a single central obscuration positioned and sized so as to block the image of the light source that is formed by the optical system after specular reflection from unmodulated areas of the light valve. Modulated pixels give rise to a circular patch of light at the schlieren stop plane that is larger than the central obscuration, but centered on it. The stop efficency, or fraction of the modulated pixel energy that clears the schlieren stop, is generally somewhat lower for projectors based on deformable membranes than it is for the oil film Eidophor projector. Further, such membrane deformable mirror systems have at least two major problems. High voltages are required for addressing the relatively stiff reflective membrane, and slight misalignments between the electron beam raster and the pixel support grid structure lead to addressing problems. Such misalignments would cause image blurring and nonuniformity in display brightness.

Another type of membrane deformable mirror is described in L. Hornbeck, 30 IEEE Tran. Elec. Dev. 539 (1983) and U.S. Pat. No. 4,441,791 and is a hybrid integrated circuit consisting of an array of metallized polymer mirrors bonded to a silicon address circuit. The underlying analog address circuit, which is separated by an air gap from the mirror elements, causes the array of mirrors to be displaced in selected pixels by electrostatic attraction. The resultant two-dimensional displacement pattern yields a corresponding phase modulation pattern for reflected light. This pattern may be converted into analog intensity variations by schlieren projection techniques or used as the input transducer for an optical information processor. However, the membrane deformable mirror has manufacturability problems due to the susceptibility to defects that result when even small, micron sized particles are trapped between the membrane and the underlying support structure. The membrane would form a tent over these trapped particles, and the lateral extent of such tents is much larger than the size of the particle itself, and these tents would in turn be imaged as bright spots by a schlieren imaging system.

A cantilever beam deformable mirror is a micromechanical array of deformable cantilever beams which can be electrostatically and individually deformed by some address means to modulate incident light in a linear or areal pattern. Used in conjunction with the proper projection optics, a cantilever beam deformable mirror can be employed for displays, optical information processing, and electrophotographic printing. An early version with metal cantilever beams fabricated on glass by vacuum evaporation appears in U.S. Pat. No. 3,600,798. This device has fabrication problems which include the alignment of the front and back glass substrates arising from the device's nonintegrated architecture.

A cantilever beam deformable mirror device is described in R. Thomas et al, The Mirror-Matrix Tube: A Novel Light Valve for Projection Displays, 22 IEEE Tran. Elec. Dev. 765 (1975) and U.S. Pat. Nos. 3,886,310 and 3,896,338. This device is fabricated as follows: a thermal silicon dioxide layer is grown on a silicon on sapphire substrate; the oxide is patterned in a cloverleaf array of four cantilever beams joined in the middle. The silicon is isotropically wet etched until the oxide is undercut, leaving within each pixel four oxide cantilever beams supported by a central silicon support post. The cloverleaf array is then metallized with aluminum for reflectivity. The aluminum which is deposited on the sapphire substrate forms a reference grid electrode which is held at a DC bias. The device is addressed by a scanning electron beam which deposits a charge pattern on the cloverleaf beams causing the beams to be deformed by electrostatic attraction towards the reference grid. Erasure is achieved by negatively biasing a closely spaced external grid and flooding the device with low-energy electrons. A schlieren projector is used to convert the beam deformation into brightness variations at the projection screen. A significant feature of this device is the cloverleaf geometry which leads to beam deflection in a direction rotated forty-five degrees from the openings between the beams; this permits use of a simple cross shaped schlieren stop to block out the fixed diffraction background signal without attenuating the modulated diffraction signal. The device was fabricated with a pixel density of five hundred pixels per inch with beams deflectable up to four degrees. The optics employed a 150 watt xenon arc lamp, reflective schlieren optics and a 2.5 by 3.5 foot screen with a gain of five. Four hundred TV lines of resolution were demonstrated with a screen brightness of thirty-five foot-lumens, a contrast ratio of fifteen to one, and a beam diffraction efficiency of forty-eight percent. Write times of less than 1/30 second were achieved and erase times were as short as 1/10 of the write time. However, the device has problems, including degradation of resolution from scanning errors, poor manufacturing yield, and no advantage over conventional projection cathode ray tubes. That is, the scan-to-scan positioning accuracy is not high enough to reproducibly write on individual pixels. The resulting loss of resolution forces at least a four fold increase in the number of pixels required to maintain the same resolution compared to comparably written phosphor. Also, the device yield is limited by the lack of an etch stop for the cloverleaf support post, the wet etching of

the beams leading to beam breakage, and the need to evaporate normally tensile aluminum in a state of zero stress on the oxide beams. Further, the device offers no apparent cost or performance advantage over conventional projection CRTs.

Cantilever beam deformable mirrors integrated on silicon with addressing circuitry, thus eliminating the electron beam addressing with its high voltage circuitry and vacuum envelopes of the previously described cantilever device, appear in K. Petersen, Micromechanical Light Modulator Array Fabricated on Silicon, 31 Appl. Phys. Lett. 521 (1977) and U.S. Pat. No. 4,229,732. The first of these references describes a 16 by 1 array of diving board-shaped cantilever beams fabricated as follows: an epitaxial layer of (100)-oriented silicon (either p or n) of thickness of about 12 microns is grown on a p+substrate (or buried layer); the epilayer is oxidized to a thickness of about 0.5 micron and covered with a Cr-Au film of thickness about 500 A. The Cr-Au is etched away to form contact pads and address lines and to define the diving board metallization. The oxide is etched away in a comb pattern around the metallization in a second masking step. Finally, the silicon itself is etched in a solution of ethylenediamine and pyrocatechol at 120 degrees C. If the proper orientation of the mask with respect to the crystalline axes is maintained, the metal-coated oxide diving boards will be undercut by the etch and freed from the silicon. Since the etch is anisotropic, further lateral etching will be stopped by the (111) planes defining the rectangular envelope of the comb pattern. In addition, the etchant is inhibited by p+material, so the depth of the well beneath the diving boards is defined by the thickness of the epilayer. When a dc voltage is applied between the substrate and the diving board metallization, the thin oxide diving board will be electrostatically deflected downward into the etched well. Diving boards of length 106 microns and width 25 microns showed a threshold voltage of about 66 volts.

The second reference (Hartstein and Petersen, U.S. Pat. No. 4,229,732) describes devices fabricated in a manner similar to the diving board device (a buried p+layer as an etch stop for forming the wells underneath metallized silicon dioxide cantilever beams) but has a different architecture; namely, the cantilever beams are in the shape of square flaps hinged at one corner, the flaps form a two dimensional array instead of the one dimensional row of diving boards, and the wells underneath the flaps are not connected so that addressing lines for the flaps may be formed on the top surface of the silicon between the rows and columns of flaps. Of course, the corner hinging of the flaps derives from the cloverleaf architecture of U.S. Pat. Nos. 3,886,310 and 3,896,338, but the full cloverleaf architecture could not be used because this would preclude the surface addressing lines since cloverleaf flaps are hinged to a central post isolated from the silicon surface. Further, these devices have problems including poor resolution and low efficiency due to density limitations and the small fractional active area, low manufacturing yield, degradation of contrast ratio due to diffraction effects from the address circuitry, and residual image due to the charging effects of the oxide flap. More particularly, the addressing circuitry is squeezed around the active area (flaps) because no option exists for placing the address circuitry under the active area due to the wells being formed by etching away the epilayer down to the p+etch stop. Thus the active area is reduced substantially together with the diffraction efficiency. This means more lamp power is required for the same screen brightness. Because the address circuitry requires additional area, the pixel size is increased far beyond the flap area with a resulting decrease in achievable resolution. The wet etching required to form the wells leads to low electrical and mechanical yield; indeed, wet cleanups, such as after dicing into chips, destroy flaps and diving boards because during the spin-rinse/dry cycle the water trapped under the beam breaks the beam as it is spun from the surface. If the water is instead evaporated from the surface it leaves behind surface residues which can increase surface leakage currents contributing to erratic device operation. Also, the addressing circuitry being on the silicon surface is exposed to the incident light to be modulated and creates unwanted diffraction effects from the transistor gates plus lowers the contrast ratio. In addition, light leakage into the address structure produces photogenerated charge and reduces storage time. Lastly, the oxide/metal flap has the insulating side facing the well and will charge up due to the intense electric fields which exist across the well; this produces a residual ("burn-in") image. The AC drive required to eliminate this residual image problem cannot be supplied by the NMOS drive circuitry described. Further, if the flap is deflected past the maximum stable deflection, then it will collapse and stick to the bottom of the well. Thus, voltages over the collapse voltage must be absolutely avoided.

A variation of the cantilever beam approach appears in K. Petersen, Silicon Torsional Scanning Mirror, 24 IBM J. Res. Devp. 631 (1980) and M. Cadman et al, New Micromechanical Display Using Thin Metallic Films, 4 IEEE Elec. Dev. Lett. 3 (1983). This approach forms metallic-coated silicon flaps or metallic flaps which are connected to the surrounding reflective surface at two hinges and operate by twisting the flaps along the axes formed by the hinges. The flaps are not formed monolithically with the underlying addressing substrate, but are glued to it in a manner analogous to the deformable membrane devices mentioned above.

Cade, U.S. Pat. No. 4,356,730 combines aspects of the foregoing and has a silicon substrate with metal coated silicon dioxide cantilever diving boards, corner-hinged flaps, and torsion hinged flaps. The addressing electrodes (two per diving board or flap for x-y addressing as in a memory array) are on the surface, and the diving board or flap may be operated as a switch or memory bit and collapsed to the bottom of the pit etched in the silicon substrate by application of a threshold voltage. The diving board or flap can then be held at the bottom of the pit by a smaller standby voltage.

The cantilever beam references discussed above suggest that schlieren projection optical systems be used with the cantilever beam devices. But such systems have limitations in terms of attainable optical performance. First, the aperture diameter of the imaging lens must be larger than is necessary to pass the signal energy alone. Hence the speed of the lens must be relatively high (or, equivalently, its f-number must be relatively low) to pass all the signal energy around the central schlieren stop obscuration. In addition, the signal passes through the outer portion of the lens pupil in this imaging configuration. Rays of light emanating from any given point on the SLM and passing through the outermost areas of an imager lens pupil are the most difficult ones to bring to a well-corrected focus during

the optical design of any imaging lens. When the outer rays are brought under good control, the rays passing through the center of the imager lens are automatically well-corrected. Hence, a greater level of optical design complexity is required of the imagining lens. Second, the field angle over which the imaging lens can form well-corrected images of off-axis pixels on a cantilever beam SLM is also restricted. Any lens design task involves a compromise between the speed of the lens and the field angle it can cover with good image quality. Fast lenses tend to work over small fields, while wide angle lenses tend to be relatively slow. Since the schlieren imager must be well-corrected over its entire aperture, and since this aperture is larger in diameter than is required to pass the image forming light, the field angle that can be covered by the lens is smaller than it could be if a different imaging configuration could be devised in which the signal was passed through the center of an unobscured, smaller diameter lens. Lastly, for an imager lens having a given finite speed, the use of the schlieren stop configuration also limits the size of the light source that can be utilized. This in turn limits the irradiance level that can be delivered to a projection screen or a photoreceptor at the image of a deflected pixel. This irradiance level, or the delivered power per unit area, depends on the product of the radiance of the light source, the transmittance of the optical system, and the solid angle of the cone of image forming rays of light. The source radiance is determined only by the particular lamp that is used. The optics transmittance depends on the stop efficiency for the particular SLM/schlieren stop configuration and surface transmission losses. But the solid angle of the image forming cone of light is directly proportional to the area of the imager lens pupil that is filled with signal energy. The use of a schlieren stop that obscures the central area of the imager lens pupil limits the usable pupil area and thus the image plane irradiance level that can be obtained for a lens of a given speed and a source of a given radiance; this is in addition to the fundamental irradiance limitation that the maximum usable cone of light has an opening angle equal to the beam deflection angle.

The known beam SLMs have problems including beam insulator charging effects, lack of overvoltage protection against beam collapse, small-angle and nonuniform beam deflection leading to optical inefficiency and nonuniformity, and high voltage addressing of the pixels.

SUMMARY OF THE INVENTION

The present invention provides deflectable beam spatial light modulators with both addressing and landing electrodes for each beam, permitting soft-landing of the beams to a precise, architecturally determined angle without destructive collapse. This solves the problems of small-angle and nonuniform beam deflection and overvoltage collapse plus provides increased deflection cycle lifetime and optical contrast.

The preferred embodiments also provide the technique of differential biasing which permits low voltage addressing without contrast degradation of a conventional bias, as well as introducing two modes of operation having two or three statically stable states of beam deflection that do not require a continuous address voltage for their maintenance.

BRIEF DESCRIPTION OF THE DRAWINGS

FIGS. **1A–C** illustrate in perspective, cross sectional elevation, and plan views a first preferred embodiment pixel;

FIG. **2** illustrates deflection of the pixel beam of the first preferred embodiment;

FIGS. **3A–B** show the dependence of beam deflection on applied voltage for a simplified version of the first preferred embodiment pixel and a plan view of the simplified version pixel;

FIG. **4** is a cross sectional elevation schematic view of the simplified version pixel defining analysis terms;

FIG. **5** illustrates the torques on the beam in the simplified version pixel;

FIG. **6** illustrates the beam deflection as a function of control voltage for the simiplified version pixel;

FIG. **7** is a schematic cross sectional elevation view of the first preferred embodiment;

FIG. **8** illustrates the torques on the beam in the first preferred embodiment;

FIG. **9** shows definition of terms in the analysis of the first preferred embodiment;

FIGS. **10–13** illustrate the torques on the beam for different modes of operation of the first preferred embodiment;

FIG. **14** illustrates the potential energy functions involved in the different modes of operation of the first preferred embodiment;

FIG. **15** shows the differential bias on the first preferred embodiment;

FIG. **16** illustrates the torques for applied differential bias in the first preferred embodiment;

FIG. **17** is a timing diagram for bistable operation of the first preferred embodiment;

FIGS. **18–23** show the torques and deflection for analysis of the operation of the first preferred embodiment;

FIGS. **24–26** illustrate noise margin analysis for the first preferred embodiment;

FIG. **27** is a schematic cross sectional elevation view of balance electrodes added to the first preferred embodiment;

FIG. **28** illustrates noise margin interaction;

FIG. **29** is a timing diagram for a first method of reset for the first preferred embodiment;

FIGS. **30A–B** are a timing diagram and cross sectional elevation view of a second method of reset for the first preferred embodiment;

FIG. **31** is a plan view of a linear array second preferred embodiment;

FIGS. **32A–C** schematically illustrate use of the second preferred embodiment for electrophotographic printing;

FIG. **33** illustrates the addressing of a second preferred embodiment pixel in cross sectional elevation view along a control electrode;

FIG. **34** illustrates the addressing of the second preferred embodiment pixel in plan view;

FIGS. **35A–E** illustrate in cross sectional view the steps of the first preferred embodiment method of fabrication;

FIGS. **36A–C** and **37A–C** further illustrate the last step of the first preferred embodiment method of fabrication.

FIG. **38** illustrates in plan view a third preferred embodiment;

FIGS. 39A–D show alternative beam geometries and layouts in plan views;

FIGS. 40A–E illustrate in cross sectional view the steps of the second preferred embodiment method of fabrication;

FIGS. 41A–C illustrate in plan view the steps of the second preferred embodiment method of fabrication;

FIGS. 42A–B are plan and schematic views of an array of fourth preferred embodiment pixels;

FIGS. 43A–D and 44A–C are plan views of levels of and cross sectional elevation views of fourth preferred embodiment pixels.

DESCRIPTION OF THE PREFERRED EMBODIMENTS

The preferred embodiment deflectable beam spatial light modulators (SLM) are typically formed of linear or area arrays of pixels, each pixel individually addressable and containing at least one deflectable reflecting beam; the pixels are organized in the form of monolithic silicon based chips. The chips are fabricated by processing silicon wafers, dicing the wafers into chips, followed by further processing of the individual chips. The chips will vary in size depending upon the application; for example, a 2400 by 1 linear array of pixels (which could be a component of a 300 dots per inch printer) may be fabricated on a chip about 1300 mils by 250 mils with pixels about 12 microns (one-half mil) square. The SLMs operate by reflecting light off of the pixels, and the reflected light is modulated by varying the deflection of the deflectable beams. Such SLMs are consequently also called deformable mirror devices (DMDs) and the deflectable beams are also called mirror elements. The following descriptions are primarily of the individual pixels for a DMD, and all of the drawings are schematic for clarity of explanation.

A first preferred embodiment single pixel of a DMD fabricated by a first preferred embodiment method is illustrated in perspective view in FIG. 1A, in cross sectional elevation in FIG. 1B, and in plan view in FIG. 1C. The pixel, generally denoted **20**, is basically a beam (flap) covering a shallow well and includes silicon substrate **22**, insulating spacer **24**, metal hinge layer **26**, metal beam layer **28**, beam **30** formed in layers **26–28**, and plasma etch access holes **32** in beam **30**. The portions **34**, **36** of hinge layer **26** that are not covered by beam layer **28** form torsion hinges (torsion rods) attaching beam **30** to the portion of layers **26–28** supported by spacer **24**. Electrodes **40**, **42**, **46** and **41** run between spacer **24** and substrate **22** and are isolated from substrate **22** by silicon dioxide layer **44**. FIG. 1B is a cross section along line B-B as indicated in FIGS. 1A and 1C.

Typical dimensions for pixel **20** would be as follows: beam **30** is a square with sides 12.5 microns long, spacer **24** is 4.0 microns thick (vertical in FIG. 1B), hinge layer **26** is 800 Å thick, beam layer **28** is 3,600 Å thick, hinges **34** and **36** are each 4.6 microns long and 1.8 microns wide, plasma etch access holes **32** are 2.0 microns square, and plasma etch access gap **38** (the space between beam **30** and the remainder of beam layer **28**) is 2.0 microns wide.

Another set of typical dimensions for pixel **20** that yield a maximum beam deflection angle of about ten degrees would be as follows: beam **30** is a square with sides 19 microns long, spacer **24** is 2.3 microns thick (vertical in FIG. 1B), hinge layer **26** is 750 Å thick, beam layer **28** is 3,000 Å thick, torsion hinges **34** and **36** are each 4.6 microns long and 1.0 microns wide, plasma etch access holes **32** are 1.5 microns square, and plasma etch access gap **38** (the space between beam **30** and the remainder of beam layer **28**) is 1.0 micron wide.

Substrate **22** is (100) silicon with resistivity about 10 ohm-cm and typically will have addressing circuitry formed on its surface, including peripheral devices in addition to electrodes **40**, **41**, **42**, and **46**. Spacer **24** is positive photoresist which is an insulator; hinge layer **26** and beam layer **28** are both an aluminum, titanium, and silicon alloy (Ti:Si:Al) with 0.2% Ti and 1% Si. This alloy has a coefficient of thermal expansion not drastically different from spacer **24** and thus minimizes the stress between the metal layers and spacer **24** generated during the fabrication process described in the following; also, the two layers **26** and **28** being the same metal minimizes stress. Note that any stress between layers in the beam or hinge would cause warping or curling of the beam or hinge, and any stress between the metal and the spacer can cause buckling or warping of the free portion of the metal over the well.

The architecture of FIGS. 1A–C simultaneously satisfies two criteria: (1) it is possible to make the beam metal as thick and the hinge metal as thin as desired without the problems of step coverage of the hinge metal over the beam metal and (2) the spacer surface under the beam metal is not exposed to processing side effects which would arise if the hinge were formed as a rectangular piece on the spacer prior to deposition of the beam metal.

Pixel **20** is operated by applying a voltage between metal layers **26–28** and electrodes **42** or **46** on substrate **22**: beam **30** and the electrodes form the two plates of an air gap capacitor and the opposite charges induced on the two plates by the applied voltage exert electrostatic force attracting beam **30** to substrate **22**, whereas electrodes **40** and **41** are held at the same voltage as beam **30**. This attractive force causes beam **30** to twist at hinges **34** and **36** and be deflected towards substrate **22**; see FIG. 2 for a schematic view of this deflection together with an indication of the charges concentrated at the regions of smallest gap for a positive voltage applied to electrode **42**. For voltages in the range of 20 to 30 volts, the deflection is in the range of 2 degrees. Of course, if hinge **34** were made longer or thinner or narrower, the deflection would increase as the compliance of hinge **34** varies linearly with the inverse of its width and directly with the square of its length and inversely with the cube of its thickness. Note that the thickness of beam **30** prevents significant warping of beam **30** due to surface stress generated during processing, but that the thinness of hinge **34** allows for large compliance. FIG. 2 also indicates the reflection of light from deflected beam **30** as may occur during operation of a DMD.

The deflection of beam **30** is a highly nonlinear function of the applied voltage because the restoring force generated by the twisting of hinge **34** is approximately a linear function of the deflection but the electrostatic force of attraction increases as a function of the reciprocal of the distance between the closest corner of beam **30** and substrate **22** (recall that the capacitance increases as the distance decreases so the induced charges both increase in quantity and get closer together). FIG. 3A illustrates the approximate dependence of deflection on voltage for pixel **120** which is a simplified version of pixel **20** with electrodes **42** and **40** joined together as address electrode **142** (and electrodes **41** and **46** joined together as address electrode **146**). See FIG. 3B for a

plan view with the elements of pixel **120** referenced numbered **100** higher than the corresponding elements of pixel **20**. The voltage at which torsion beam **130** of pixel **120** becomes unstable and bends all the way to touch substrate **122** is called the collapse voltage. For voltages somewhat less than the collapse voltage the deflection is approximately a linear function of the voltage (see the dotted line in FIG. **3**) and this is the analog operating region. Note that the voltages involved (40–50 volts) for analog operation are much larger than the usual for integrated circuits.

Prior to analysis of the operation of pixel **20**, a qualitative analysis of the simplified pixel **120** will be presented. FIG. **4** is a schematic cross sectional elevation view (analogous to FIGS. **1B** and **2**) of pixel **120** showing definitions of the variables involved; and FIG. **3B** is a plan view to two adjacent pixels **120**.

As indicated in FIG. **4**, address electrode **146** and torsion beam **130** are grounded and a voltage ϕ_α is applied to address electrode **142** which causes torsion beam **130** to rotate through an angle θ. The rotation of the torsion beam may be expressed in terms of the distance that tip **131** of torsion beam **130** is deflected, z_T, or as a distance α normalized to the distance between the undeflected torsion beam tip **131** and address electrode **142**, z_O; that is

$$\alpha = \frac{z_T}{z_0}$$

For small angles of rotation and with θ expressed in radians, θ and α are related by

$$\theta = \frac{z_T}{L/\sqrt{2}} = \frac{\alpha z_0 \sqrt{2}}{L}$$

where L is the length of the side of square torsion beam **130** which is torsion hinged at opposite corners **135** and **137**.

The torque exerted on torsion beam **130** about the axis through corners **135** and **137** by application of voltage ϕ_α to address electrode **142** is computed as follows. First consider the small (infinitesimal) area of torsion beam **130** located a distance x from the axis of rotation and of width dx (see the top view in FIG. **4**). The electrostatic energy in the small vertical volume between the small area on torsion beam **130** and address electrode **142** is approximately (assuming a uniform electric field ignoring fringing fields) equal to

$$dU = \frac{1}{2} D \cdot E(z_0 - z)2(L/\sqrt{2} - x)dx$$

where $\vec{E}$ is the electric field and $\vec{D}$ is the electric displacement in the small vertical volume. Note that $z_O - z$ is the height of the small vertical volume and that $2(L/\sqrt{2} - x)$ is the length of the small area on torsion beam **130**. Of course, electrostatic $\vec{D}$ and $\vec{E}$ are related by the permittivity of the medium: $\vec{D} = \epsilon_0 \vec{E}$; and the electric field magnitude is just the voltage difference divided by the separation:

$$|E| = \frac{\phi_a}{z_0 - z}$$

The small force in the vertical (z) direction on the small area by the electric field is just the partial derivative of dU in the z direction:

$$dF_z = \frac{\partial(dU)}{\partial z}$$

so

$$dF_z = \frac{1}{2} \epsilon_o \frac{\phi_a^2}{(z_0 - z)^2} 2(L/\sqrt{2} - x)dx$$

and the small torque exerted on torsion beam **130** by this small force is just xdF_z because the force has moment arm equal to x. Thus the total attracting torque, τ_α, exerted on torsion beam **130** by ϕ_α applied to address electrode **142** is given by

$$\tau_a = \int x dF_z = \frac{1}{2} \epsilon_o \phi_a^2 \int_0^{L/\sqrt{2}} \frac{2x(L/\sqrt{2} - x)}{(z_0 - x\theta)^2} dx$$

where the small angle approximation $\theta = \tan(\theta)$ was used to set $z = x\theta$.

Evaluation of the integral yields:

$$\tau_a = \frac{\frac{1}{2} \epsilon_o \phi_a^2 L^3}{z_0^2} \frac{1}{\alpha^3 \sqrt{2}} [(\alpha - 2)\log(1 - \alpha) - 2\alpha]$$

where θ has been expressed in terms of α, the normalized deflection. FIG. **5** illustrates the dependence of τ_α on α for three different address voltages ($V_1 < V_2 < V_3$). The restoring torque produced by the twisting of the torsion hinges is given by

$$\tau_r = \frac{-\theta}{C} = -\alpha \left(\frac{z_0 \sqrt{2}}{CL} \right)$$

where C is the torsion hinge compliance. The magnitude of the restoring torque is indicated by the dashed line in FIG. **5**.

Points of stable equilibrium for torsion beam **130** may be found by analyzing points of zero net torque. In FIG. **5** for $\phi_\alpha = V_1$ there is zero net torque at the points labelled "P" and "Q". Point "P" (for $\alpha = \alpha_1$) represents a stable equilibrium because for small excursions of α in either direction the net torque restores α towards α_1. Contrarily, for point "Q" the net torque for small excursions of α away from α_2 acts to increase the excursion; either back to α_1 or to collapse with tip **131** landing on electrode **142** ($\alpha = 1$). Similar behavior obtains for any ϕ_α between 0 and V_2.

For $\phi_\alpha = V_2$ the points "P" and "Q" coalesce to a single point "R" at the tangency of the τ_α and τ_r curves. Point "R" (with $\alpha = \alpha_c$) represents a quasi-stable equilibrium: for excursions of α below α_c the net torque restores α towards α_c, but for excursions of α above α_c the net torque leads to collapse of tip **131** to address electrode **142** ($\alpha = 1$). For ϕ_α greater than V_2, such as V_3 illustrated in FIG. **5**, there are no points of zero net torque. Thus V_2 is the collapse voltage and denoted V_c. FIG. **6** summarizes the foregoing: increasing ϕ_α from 0 to V_c leads to an increasing stable deflection equilibrium α_1, and at $\phi_\alpha = V_c$ the stable equilibrium has reached α_c

where it disappears. If the collapsed deflection ($\alpha=1$) is included, then pixel **120** can be considered as having two stable equilibria for $\phi_\alpha<V_c$ with one an analog equilibrium (deflection depends upon ϕ_α) and another digital ($\alpha=1$) independent of ϕ_α. For $\phi_\alpha \geqq V_c$ the analog equilibrium disappears and pixel **120** is only digital.

Note that at collapse, torsion beam tip **131** touches address electrode **142** and a large current passes through tip **131** to electrode **142** and tip **131** is welded to electrode **142**. Therefore collapse is a destructive phenomenon for this particular architecture. For very thin torsion hinges, the hinges act as fusible links and are blown away when the torsion beam collapses.

Pixel **20** overcomes the problems of pixel **120** of high voltage operation and destructive collapse of the torsion beam to the underlying electrodes. Pixel **20** has the addition of landing electrodes **40** and **41** which are electrically connected to torsion beam **30** and the connection of address electrode **42** with address electrode **46** but with a logical inversion of the address signal ϕ_α. See schematic FIG. **7**. The operation of pixel **20** is described in the following paragraphs.

First for a fixed address signal voltage ϕ consider the torque τ_+ produced between beam **30** and address electrode **46** as a function of the normalized deflection α of beam **30**. Initially presume that beam **30** and landing electrodes **40** and **41** are grounded ($V_B=0$) and that voltage ϕ is also applied to address electrode **42**. Unlike the torque for the simplified pixel **120**, the torque τ_+ does not tend to ∞ as α tends to 1 because tip **31** of beam **30** hits landing electrode **41** and keeps beam **30** separated from address electrode **46**. In contrast to the destructive nature of tip **131** in pixel **120** hitting electrode **142**, the hitting of landing electrode **41** by tip **31** does not lead to a large current pulse and the welding of tip **31** to landing electrode **41** because beam **30** and landing electrode **41** are electrically connected. Further, as beam **30** is deflected in the opposite direction towards landing electrode **40**, α tends to -1 and τ_+ decreases because the separation between beam **30** and address electrode **46** is increasing; see FIG. **7**.

The torque τ_- produced on beam **30** by address electrode **42** is easily seen to be related to τ_+ by symmetry: $\tau_-(\alpha)=-\tau_+(-\alpha)$. Thus for a fixed voltage ϕ applied to both address electrodes **42** and **46** and a normalized deflection of α, the net attractive torque τ_α is just the sum $\tau_++\tau_-$ with positive torque attracting to electrode **46** and negative torque attracting to electrode **42**. The net attractive torque as a function of α is illustrated in FIG. **8**; the curves for $\tau_+(\alpha)$ and $\tau_-(\alpha)$ will be derived in a manner analogous to the derivation of τ_α in connection with the discussion of pixel **120**. FIG. **9** illustrates the variables used; these are the same variables as in FIG. **4** with the addition of L′ to measure the extent of address electrodes **42** and **46** under torsion beam **30**. It is convenient to express L′ as a normalized distance β defined by

$$\beta = \frac{L'}{L/\sqrt{2}}$$

Thus for pixel **120** L′ would equal $L/\sqrt{2}$ and β would equal 1. With this definition and a change of integration variables, the computation for τ_+ is:

$$\tau_+ = \int x dF_z = \frac{1}{2}\epsilon_o\phi^2 \int_0^{L'} \frac{2x(L/\sqrt{2}-x)}{(z_0-x\theta)^2}\,dx$$

$$= \frac{\frac{1}{2}\epsilon_o\phi^2 L^3}{z_0^2}\,\frac{1}{\alpha^3\sqrt{2}} \int_0^{\alpha\beta} \frac{w(\alpha-w)}{(1-w)^2}\,dw$$

This is immediately integrated by partial fractions to yield:

$$\tau_+ = \frac{\frac{1}{2}\epsilon_o\phi^2 L^3}{z_0^2}\,\frac{1}{\alpha^3\sqrt{2}}\left[(\alpha-2)\log(1-\alpha\beta)+\frac{\alpha\beta(\alpha\beta+\alpha-2)}{1-\alpha\beta}\right]$$

$$= \frac{\frac{1}{2}\epsilon_o\phi^2 L^3}{z_0^2}\,g(\alpha,\beta)$$

where $g(\alpha,\beta)$ is a dimensionless function defined by the equation. Putting $\beta=\frac{1}{2}$ leads to the curves in FIG. **8**.

To analyze the operation of pixel **20**, preliminarily consider the effect of increasing the positive differential bias V_B applied to beam **30** and landing electrodes **40** and **41** while address electrodes **42** and **46** are both held at ground potential. (Of course, this generates the same torque as applying V_B to both address electrodes and grounding beam **30** and both landing electrodes; also negative V_Bs give symmetric results but only positive V_Bs will be considred for notational simplicity.) As with the analysis of pixel **120**, the computation of points with zero net torque (attractive torque τ_α plus restoring torque τ_r) determines equilibrium points. Now τ_r is the same as for pixel **120** because τ_r just depends upon the torsion beam deflection and the torsion hinge compliance; however, the attractive torque τ_α for pixel **20** is bounded, symmetric and passes through zero at $\alpha=0$ (see FIG. **8**) in contrast to the unbounded torque at $\alpha=1$ and the positive torque at $\alpha=0$ for pixel **120** (see FIG. **5**). This leads to a qualitative difference from the previously discussed operation of pixel **120** as follows.

FIG. **10** shows τ_α and τ_r for pixel **20** with small V_B and grounded address electrodes **42** and **46**. The net torque vanishes at $\alpha=0$ and beam **30** remains undeflected. Note that for any nonzero α (including $\alpha=\pm1$ where beam **30** is collapsed to one of the landing elctrodes **40** or **41**) the net torque restores beam **30** to the undeflected state ($\alpha=0$) and this is the only stable equilibrium. Thus this is a monostable mode of operation.

As the differential bias is increased from $V_B=V_1$ (FIG. **10**) to $V_B=V_2$ (FIG. **11**), two additional points of zero net torque appear: $\alpha=0$ and points "P" and "−P" near $\alpha=\pm1$. Again $\alpha=0$ is a stable equilibrium, but the points "P" and "−P" are unstable analogous to the point "Q" in FIG. **5** for pixel **120**; small excursions about "P" or "−P" to smaller $|\alpha|$ provide a net torque to return beam **30** to the undeflected state $\alpha=0$, and small excursions about "P" or "−P" to larger $|\alpha|$ provide a net torque to collapse beam **30** to either landing electrode **40** or **41** ($\alpha=\pm1$). Thus with this differential

bias beam **30** has three stable equilibria: $\alpha=0,\pm1$. Thus this is a tristable mode of operation.

Further increase of the differential bias from $V_B=V_2$ to $V_B=V_o$ (see FIG. **12**) makes the τ_α and τ_r curves tangent at $\alpha=0$, and $\alpha=0$ disappears as a stable equilibrium. Indeed, any small excursion in α about 0 will have $|\tau_\alpha|>|\tau_r|$ and beam **30** will collapse to one of the landing electrodes ($\alpha=\pm1$). For the differential bias V_B greater than V_o, pixel **20** continues to have two stable points: $\alpha=\pm1$; thus this is a bistable mode of operation. See FIG. **13**.

In summary, for both address electrodes tied to the same potential, pixel **20** is monostable ($\alpha=0$) for small differential bias, becomes tristable ($\alpha=0,\pm1$) for increasing differential bias, and settles at bistable ($\alpha=\pm1$) for all differential biases greater than or equal to V_o. This progression in behavior with increasing differential bias may be graphically illustrated by plotting the potential energy of torsion beam **30** as a function of beam deflection for various values of the differential bias V_B; FIG. **14**. For low values of the differential bias ($V_B=0$ in FIG. **14**) the potential increases in both directions from $\alpha=0$, and beam **30** is monostable with zero deflection the only stable point. As V_B increases to V_1, the slope of the potential energy curve becomes 0 at $\alpha=\pm1$ and the net torque is zero at these points. For $V_B>V_1$ the potential energy is lowered at $\alpha=\pm1$ and barriers develop between $\alpha=0$ and $\alpha=\pm1$; beam **30** is now tristable. Further increase of V_B to V_o leads to a coalescing and disappearance of the barriers at $\alpha=0$ and beam **30** becomes bistable for $V_B\geqq V_o$.

The minimal differential bias V_o required to make pixel **20** bistable is derived as follows. With V_B applied to beam **30** and landing electrodes **40** and **41** and address electrodes **42** and **46** grounded, the net torque produced by the address electrodes on beam **30** is:

$$\tau_a=\tau_+ + \tau_- = \frac{\frac{1}{2}\epsilon_o V_B^2 L^3}{z_0^2}\left(g(\alpha,\beta)-g(-\alpha,\beta)\right) = \tau_0\Delta g(\alpha,\beta)$$

where $\Delta g(\alpha,\beta)=g(\alpha,\beta)-g(-\alpha,\beta)$,$g(\alpha,\beta)$ is the dimensionless function previously defined in connection with analysis of pixel **120**, and τ_0 is the dimensional quantity

$$\frac{\frac{1}{2}\epsilon_o V_B^2 L^3}{z_0^2}.$$

FIG. **18** illustrates the functions. Then V_o is the value of V_B that makes τ_α and τ_r tangent at $\alpha=0$:

$$\left.\frac{\partial\tau_a}{\partial\alpha}\right|_{\alpha=0}=\left.\frac{\partial\tau_r}{\partial\alpha}\right|_{\alpha=0},$$

and using definitions previously given, this can be reexpressed as

$$\frac{\epsilon_o C V_o^2 L^4}{z_0^3}=\frac{2\sqrt{2}}{\left.\frac{\partial\Delta g}{\partial\alpha}\right|_{\alpha=0}}$$

If the torsion hinge compliance C is known, then the foregoing equation can be solved for V_o, the differential bias that just makes pixel **20** bistable. If C is unknown, then V_o can be expressed as a percentage of the collapse voltage V_c for operation of pixel in the analog mode and determined experimentally.

To make a bistable pixel **20** addressable, a preferred direction for rotation must be established. If both address electrodes **42** and **46** are grounded, then small perturbations about $\alpha=0$ will cause beam **30** to randomly rotate and collapse to one of the landing electrodes upon application of the differential bias ($V_B>V_o$) to beam **30** and landing electrodes **40** and **41**. However, if prior to application of the differential bias, address electrode **46** is set to a potential of $\phi_+=-\gamma V_B$ where γ is a positive number much less than 1, then application of the differential bias V_B to beam **30** and landing electrodes **40** and **41** (see FIG. **15**) will produce a net torque to rotate beam **30** towards landing electrode **41**. This is illustrated by the τ_α curve in FIG. **16**. In effect, torsion beam has been "triggered" into the $\alpha=+1$ stable state by ϕ_+ of the opposite sign of V_B. Note that the opposite signs of ϕ_+ and V_B implies the attraction to address electrode **46** is greater than the attraction to address electrode **42** once the differential bias is applied even if beam **30** is still undeflected; also the small size of γ means that prior to application of V_B beam **30** need rotate a small distance to reach a stable equilibrium point analogous to point "P" in FIG. **5**. Symmetrically, applying the triggering potential ϕ_- to address electrode **42** will rotate beam **30** to landing electrode **40** upon application of the differential bias. Also, if the triggering potential $\phi_\pm$ is of the same sign as V_B, then this is approximately equivalent to applying a triggering potential of the opposite sign to the opposite address electrode once the differential bias is applied.

As long as V_B is maintained, beam **30** in a stable state ($\alpha=\pm1$) will remain in that stable state even if a triggering potential $\phi_\pm=-\gamma V_B$ is removed and the address electrodes returned to ground. In order to trigger beam **30** from one stable state to the other stable state, the differential bias must be momentarily turned off. When the differential bias is turned back on, the potentials of the two address electrodes are "sampled" and beam **30** is triggered into the appropriate stable state. FIG. **17** is a timing diagram for beam **30** alternately switched between $\alpha=1$ and $\alpha=-1$ with a negative V_B.

The magnitude of γ is just the ratio of the address voltage to the differential bias; and the smaller γ can be made, the lower the voltage of operation of pixel **20**. Analysis of γ begins with consideration of the attractive torque produced by electrode **46** with potential $\phi_+=\gamma|V_B|$ when the differential bias $-|V_B|$ is applied to beam **30** and landing electrodes **40** and **41** and electrode **42** is grounded. (A positive address voltage and a negative differential bias will be presumed.) Because the potential difference is $\phi_+ + |V_B|$,

$$\tau_+ = \frac{\frac{1}{2}\epsilon_o(V_B+\gamma V_B)^2 L^3}{z_0^2}g(\alpha,\beta) = (1+\gamma)^2\tau_0 g(\alpha,\beta)$$

The attractive torque produced by electrode **42** at ground is the same as previously derived:

$$\tau_- = -\tau_0 g(-\alpha,\beta)$$

Thus the net attractive torque is

$$\tau_\alpha = \tau_0[(1+\gamma)^2 g(\alpha,\beta) - g(-\alpha,\beta)]$$

FIG. **19** illustrates τ_α for $\gamma=0$ and $\gamma=0.1$, and shows that for $\gamma=0$ pixel **20** is bistable with no preferred direction of rotation at $\alpha=0$. Contrarily, for $\gamma=0.1$ the net torque is zero at the point labelled "P", and for $\alpha > -|\alpha_p|$ beam **30** rotates towards landing electrode **41** and for $\alpha < -|\alpha_p|$ beam **30** rotates towards landing electrode **40**. Now γ also relates to the torque gain at $\alpha=0$ by use of differential bias; this gain is defined as the ratio of the net attractive torque at $\alpha=0$ with an applied address voltage of $\phi_+ = -\gamma V_B$ plus an applied differential bias of V_B to the net attractive torque at $\alpha=0$ with an applied address voltage of $\phi_+ = -\gamma V_B$ but no applied differential bias. Thus

$$\begin{aligned} G &= \frac{\tau_\alpha(0,\beta)V_B}{\tau_\alpha(0,\beta)_0} \\ &= \frac{(V_B + \gamma V_B)^2 g(0,\beta) - V_B^2 g(0,\beta)}{(\gamma V_B)^2 g(0,\beta)} \\ &= \frac{(1+\gamma)^2 - 1}{\gamma^2} \\ &= 1 + \frac{2}{\gamma} \end{aligned}$$

For example, if $V_B = -50$ volts and $\gamma=0.1$ (so the address voltage $\phi_+ = +5$ volts), then G=21. This means that the torque at $\alpha=0$ is twenty-one times greater when the 5 volt address voltage is combined with a 50 volt differential bias than when the 5 volt address voltage is used alone. This concept of torque gain helps illustrate the feature of differential bias of providing a gain in the torque produced by a smaller address voltage without also producing a net torque when acting alone.

A feature of the use of address electrodes with $\beta<1$ in pixel **20** is the soft landing that beam **30** makes when it hits landing electrode **40** or **41** as compared to the landing that beam **130** of pixel **120** makes when it hits electrode **142** or **146** under similar operating conditions. First consider pixel **120**. FIG. **20** illustrates the attracting and restoring torques for pixel **120** with the collapse voltage applied to address electrode **146** but with electrode **146** decreased in width to β times the half-width of beam **130** (this is the same β as in pixel **20** and is needed to avoid the unbounded nature of the attractive torque if beam **130** hits electrode **146**). The landing torque is just the difference between the attracting and restoring torques at the landing deflection ($\alpha=1$); and the landing torque normalized to the restoring torque is this difference divided by the restoring torque at the landing deflection:

$$\begin{aligned} \tau_L &= \frac{\tau_\alpha(1,\beta) - \tau_r(1,\beta)}{\tau_r(1,\beta)} \\ &= \frac{g(1,\beta)}{g(\alpha_c,\beta)} \frac{\alpha_c}{1} - 1 \end{aligned}$$

where the geometry of FIG. **20** was used to substitute $\tau_r(1,\beta) = \tau_0 g(\alpha_c,\beta)/\alpha_c$. Thus if β can be chosen to make the collapse deflection (α_c) approximately equal to 1, then τ_L approaches zero. For $\beta=0.5$ the collapse deflection $\alpha_c=0.9$ and τ_L computes to 0.011 so the landing torque is only 1% of the restoring torque at landing.

Applying a thin dielectric layer over electrode **146** will permit use of $\beta=1$ width electrodes **146** because this will prevent beam **130** from hitting electrode **146** and destructing (in effect, α is limited to a value slightly less than 1.0). Thus the landing deflection α_L may be less than 1, and the product $\alpha_L\beta$ approaching 1 is the logarithmic singularity in $g(\alpha,\beta)$. And the normalized landing torque for $\beta=1$ and $\alpha_L=0.987$ (which corresponds to pixel **120** with polysilicon electrode **146** covered 2,000 Å of silicon dioxide and a spacer layer of 4 micron thickness and operation in air) computes to about 3.06, and the collapse deflection $\alpha_c=0.54$. The ratio of the normalized landing torque with $\beta=1$ to the normalized landing $\beta=0.5$ is thus about 278; this indicates the large effect of β on normalized landing torque.

There are two effects to be considered in determining the utility of soft landing. The first effect is the kinetic effect which deals with the mechanical damage produced by the impact of the moving beam hitting the electrode (either a landing electrode or the dielectric on an address electrode). The second effect is the static effect which deals with cold welding effects produced between the beam and the electrode caused by a sustained landing torque. The static effect is reduced by lowering the landing torque as has just been considered, and the kinetic effect is reduced by lowering the kinetic energy (speed) at landing.

The kinetic energy at landing can be computed in two extreme cases, depending on the degree of mechanical damping. Damping is caused by the displacement of the air in the gap between the beam and the electrode as the beam quickly rotates (≈ 1 μsec) to hit the electrode; and the two extreme cases are overdamping and no damping.

In the overdamped case the speed of the beam is quickly brought to zero in the absence of a sustained attractive torque. Thus for the case of β selected to reduce the normalized landing torque the speed is reduced to near zero upon landing.

In the undamped case the kinetic energy continually increases until the beam hits the electrode and may be computed by integrating $\tau_\alpha - \tau_r$ from $\alpha=0$ to $\alpha=1$. The ratio of this integration for $\beta=0.5$ to this integration for $\beta=1.0$ is even smaller than the ratio of normalized landing torques considered previously. Thus the soft landing is effective in reducing both static and kinetic landing effects for pixel **120**.

The soft landing analysis for pixel **20** with the differential bias at a level to just make pixel **20** bistable ($V_B = V_o$) is as follows. FIG. **21** shows τ_α for $\gamma=0$ (curve no. **1**) and for $\gamma=0.1$ (curve no. **2**). Now the condition $V_B = V_o$ implies the tangency of the attractive and restoring torque curves at $\alpha=0$:

$$\tau_0 \frac{\partial}{\partial\alpha}(g(\alpha,\beta) - g(-\alpha,\beta))_{\alpha=0} = \tau_r$$

and the normalized landing torque for the bistable pixel **20** is

$$\tau_L = \frac{\tau_\alpha(1,\beta) - \tau_r(1,\beta)}{\tau_r(1,\beta)}$$

$$= \frac{(1+\gamma)^2 g(1,\beta) - G(-1,\beta)}{\frac{\partial}{\partial\alpha}(g(\alpha,\beta) - g(-\alpha,\beta))_{\alpha=0}}$$

For $\beta=0.5$ and $\gamma=0.1$ the normalized landing torque is 0.74; that is, the landing torque is 74% of the restoring torque. Contrarily, for $\beta=1.0, \alpha=0.987, \gamma=0.1$, the normalized landing torque is 15.8, so the ratio of landing torques is 21.4.

The normalized landing torque can be experimentally determined by measuring the holding voltage V_H as shown in FIG. **22**. The upper τ_α curve represent the attracting torque for the minimal differential bias V_o making pixel **20** bistable and a address voltage $\phi_\alpha=-\gamma V_B$, and the beam lands with a landing torque τ_L. Now presume that γ is fixed and V_B is slowly decreased in magnitude below V_o. At $V_B=V_H$, $\tau_\alpha(1)$ has decreased in magnitude to $\tau_r(1)$, and the landing torque has decreased to zero. For smaller $|V_B|$ the net torque is in a direction to restore beam **30** to the analog equilibrium position labelled "P" in FIG. **22**. Therefore, as V_B is slowly decreased and becomes slightly less than V_H in magnitude, beam **30** suddendly releases from its landed position and returns to the much smaller deflected analog equilibrium.

The operation of pixel **20** in the bistable mode can thus be described in terms of a hystersis curve as in FIG. **23** which is a graph of α as a function of differential bias V_B for a fixed γ. At point (**0**) $V_B=0$ so $\phi_\alpha=-\gamma V_B$ is also zero and beam **30** is undeflected ($\alpha=0$). From point (**0**) to point (**1**) pixel **20** is in the analog mode and the address voltage ($\phi_\alpha=-\gamma V_B$) applied to address electrode **46** with address electrode **42** grounded results in a beam **30** deflection to the stable equilibrium $\alpha(V_B)$ which is less than 1. As V_B increases, α increases until bistable operation at $V_B=V_o$ is reached at point (**1**) with a deflection of α_c, and beam **30** collapses to landing electrode **41** at point (**2**). Now beam **30** stays on landing electrode **41** as the magnitude of V_B is decreased until $V_B=V_H$ is reached at point (**3**) and beam **30** releases from electrode **41**. Released beam **30** returns to the deflection corresponding to V_H in the analog mode; see point (**4**) in FIG. **23**.

As with any digital device, pixel **20** operating in the bistable mode will not switch into proper stable states if certain pixel parameters deviate from the intended operating point by more than a specified amount. The amount of allowed deviation is called the noise margin; if any pixel parameter varies by more than the noise margin, then the pixel will switch into the wrong state. Moreover, any noise or deviation of one parameter from the intended operating point, reduces the noise margin of the other parameters for the pixel.

The two most significant pixel **20** parameter deviations that can lead to faulty bistable operation are (i) torsion beam **30** deviation from flatness and (ii) address electrode **42** and **46** misalignment with respect to torsion hinges **34** and **36** and beam **30**. First consider the margin for beam **30** deviation from flatness, denoted $\Delta\alpha$. FIG. **24** shows the attracting torque τ_α for pixel **20** addressed at electrode **46** (to deflect beam **30** to $\alpha=+1$ at landing electrode **41**), and also the restoring torque τ_r for three different deviations of beam **30** from flatness (the dashed lines labelled (**1**), (**2**), and (**3**)). For line (**1**) beam **30** is flat and the net torque rotates beam **30** towards $\alpha=+1$. For line (**2**) beam **30** has a built-in initial deflection of $-|\alpha_m|$ (towards landing electrode **40**) and the application of the differential bias plus addressing voltage to address electrode **46** and ground to address electrode **42** produces zero net torque because of the in-built initial deflection. For line (**3**) the built-in initial deflection is so large that application of the differential bias plus addressing voltage on electrode **46** and ground **42** produces a net torque rotating beam **30** towards $\alpha=-1$; that is, the wrong stable state results. Thus $|\alpha_m|$ is the maximum tolerable deviation from beam flatness and is called the margin for angular deviation. $|\alpha_m|$ is computed by simply finding the solution of

$$\tau_\alpha(\alpha)=\tau_0[(1+\gamma)^2 g(\alpha,\beta)-g(-\alpha,\beta)]=0$$

For $|\alpha_m| << 1$ the function g is easily approximated and the solution is

$$\alpha_m \approx -\frac{1/2 - 1/3\beta}{2/3\beta - 1/2\beta^2}\,\frac{(1+\gamma)^2 - 1}{1 + (\gamma)^2 + 1}$$

Of course, the angular margin in the direction of landing electrode **46** is the same by symmetry.

For $\beta=0.5$ and $\gamma << 1$, the expression for α_m reduces to

$$\alpha_m = \pm 1.6\gamma$$

The angular deviation margin increases with γ, as expected, and as flatness degrades proper operation requires larger addressing voltage relative to the differential bias. For example, with $\gamma=0.1$ and a landing angle of 10 degrees, $|\alpha_m|=0.16$ and this corresponds to 1.6 degrees of angular deviation from flatness (recall α is the normalized deflection). A flatness of 0.5 degree has been routinely achieved in practice.

One type of address electrode **42** and **46** misalignment with respect to beam **30** and torsion hinges **34** and **36** is illustrated in plan view in FIG. **25**; namely, the electrodes are misaligned along the diagonal by a distance ϵ in the direction of landing electrode **40** and away from landing electrode **41** but all other alignments are correct. For simplicity, only this misalignment will be analyzed. First, as shown in FIG. **25** the misalignment defines the shaded areas of difference between beam **30** and electrodes **42** and **46**; these areas lead to changes in the torque produced by the differential bias and addressing voltages. The torque changes from area $\pm\Delta A_2$ will be ignored due to their small moment arms, and assume electrode **46** has the addressing voltage $\phi_\alpha=\gamma V_B$ and electrode **42** is grounded. Thus area $-\Delta A_1$ diminishes the positive torque τ_{30} and area ΔA_1 increases the negative torque τ_{31}. FIG. **26** illustrates this effect on the attractive torque for three misalignments. For curve (**1**) the misalignment ϵ is zero and the net torque is positive so beam **30** rotates to the correct landing electrode. For curve (**2**) the misalignment equals ϵ_m and the attractive torque about $\alpha=0$ approximates the restoring torque and the net torque is zero, so fluctuations of beam **30** determine to which of the landing electrodes **40** or **41** beam **30** will rotate. With the larger misalignment $\epsilon>\epsilon_m$ of curve (**3**), the net torque at $\alpha=0$ is negative and beam **30** rotates to landing electrode **40** instead of landing electrode **41**; that is, the wrong stable state results. To determine the margin ϵ_m, simply compute the effect of the misalignment ϵ on τ_+

and τ_- and solve for the ϵ that makes τ_α zero at $\alpha=0$. Of course, ϵ misalignment is just the same as a different width electrode, so

$$\tau_+(\alpha) = \tau_0(1+\gamma)^2 g(\alpha,\beta - \epsilon\sqrt{2}/L)$$

$$\tau_-(\alpha) = -\tau_0 g(-\alpha,\beta + \epsilon\sqrt{2}/L)$$

and the asymptotic form for $g(\alpha,\beta)$ for α very small is easily derived from the definition of g:

$$g(\alpha,\beta) \approx \frac{\beta^2(3-2\beta)}{6\sqrt{2}} + O(\alpha)$$

For small ϵ the condition τ_α vanishes at $\alpha=0$ is just

$$(1+\gamma)^2(\beta - \epsilon\sqrt{2}/L)^2 - (\beta + \epsilon\sqrt{2}/L)^2 = 0$$

$$\frac{\epsilon_m}{L} \approx \frac{\beta\gamma}{2\sqrt{2}}$$

For example, with $\gamma=0.1$ and $\beta=0.5$, the misalignment margin is $\epsilon_m=0.02L$; for pixel **20** with L=12.5 microns this is $\epsilon_m=0.25$ microns, which exceeds typical current stepper misalignment. Of course, increasing γ increases ϵ_m.

Address electrode misalignment can also be compensated for by use of balance electrodes as illustrated schematically in cross sectional elevation view of preferred embodiment pixel **220** in FIG. **27**. Pixel **220** has address electrodes **242** and **246**, landing electrodes **240** and **241**, plus balance electrodes **243** and **245** interposed between the address electrodes and the landing electrodes. If there is no misalignment, then the balance electrodes would be biased at the differential bias voltage; whereas, if there is misalignment of the address electrodes in the direction of landing electrode **240** (as in the previous discussion), then balance electrode would be biased towards ground to supply additional torque (increase τ_+) to counteract the misalignment. If the misalignment is in the other direction, then balance electrode **243** is biased towards ground.

The noise margins computed above are not independent, and the effects interact to lower the margins. For example, FIG. **28** illustrates the attractive torques for the two bistable address conditions (addressing the +electrode **46** or the −electrode **42**) with zero misalignment and with misalignment equal to one half of the margin ($\epsilon=\frac{1}{2}\epsilon_m$). The margin for angular deviation α_m is shown for both the aligned and misaligned cases, and clearly the misaligned case has a margin for angular deviation of one half of the aligned case margin with respect to the +electrode and a 50% greater margin with respect to the −electrode. Of course, the argument is symmetric and nonflatness within the angular deviation margin will lower the misalignment margin. Increase of γ will expand the margins.

Despite the fact that beam **30** and landing electrodes **40** and **41** are electrically connected and the fact that beam **30** soft lands on landing electrodes **40** and **41** during operation, beam **30** may stick to landing electrode **40** or **41**. Thus the following electrical reset methods may be used with pixel **20** to augment the restoring torque provided by the torsion hinges **34** and **36** to pull beam **30** off of one of the landing electrodes **40** or **41** and reset beam **30** to an undeflected position. The first method uses address electrode **42** as a reset electrode and address electrode **46** for addressing; pixel **20** is operated in the monostable or tristable mode and with rotation in one direction (to landing electrode **41**) only. The reset method includes a high voltage pulse (90 volts for 1 μsec) applied to reset electrode **42** during the time that both the differential bias and the addressing voltage are at ground: See FIG. **29** for a timing diagram which shows the differential bias ϕ_B applied to beam **30** and landing electrodes **40** and **41**, the reset pulses ϕ_R applied to electrode **42** during times that ϕ_B vanishes, the addressing voltage ϕ_A for a sequence of deflect, not deflect, deflect applied to electrode **46**, and the resultant beam deflection α. If beam **30** were stuck on landing electrode **41**, then the pulse on reset electrode **42** provides a short duration torque to help the restoring torque of torsion hinges **34** and **36** pull beam **30** off of landing electrode **41**. If beam **30**, however, were not stuck on landing electrode **41** but rather were undeflected, then the pulse on reset electrode **41** would rotate beam **30** towards landing electrode **40**. But the short duration of the pulse (1 μsec) is less than the time constant of beam **30** (about 12 μsec) and beam **30** will not reach landing electrode **40** and the restoring torque of torsion hinges **34** and **36** will return beam **30** to the undeflected state. This short-duration fluctuation in the direction of landing electrode **40** is indicated by the dip to negative α values in FIG. **29**. Also, if beam **30** does not stick, then the restoring force of torsion hinges **34** and **36** brings beam **30** back to $\alpha=0$ as indicated by the dashed line in the α plot in FIG. **29**. All of the reset electrodes **40** of an array of pixels **20** on a single integrated circuit chip could be tied together on-chip and a single off-chip high voltage pulse driver would supply the reset pulses.

A second reset method is illustrated in FIGS. **30A–B** and uses a nonrotational bending of torsion hinges **34** and **36** to help pull a stuck beam **30** off of landing electrodes **40** or **41**. In this method the reset pulse is applied to the landing electrodes **40** and **41** and beam **30** while address electrodes **42** and **46** are grounded. In an array of pixels **20** a differential bias bus may be used to connect together all of the landing electrodes and this bus is connected to the reflecting layer **26–28** which includes the torsion beams **30**, so the reset pulse would just be applied to the differential bias bus. In contrast to the first reset method, with the second reset method pixel **20** may be operated in any mode. The reset pulse (typically 60 volts for 1 μsec) applied to beam **30** with the address electrodes grounded deflects beam **30** towards substrate **22** whether beam **30** is undeflected or stuck to one of the landing electrodes; the nonrotational bending of torsion hinges **34** and **36** stores the potential energy of this deflection. See FIG. **30A** for a timing diagram and FIG. **30B** for illustration of the deflection. In FIG. **30A** the beam and landing electrode bias ϕ_B has a reset pulse $(+|V_R|)$ of opposite polarity to the differential bias $(-|V_B|)$, although the reset pulse could have the same polarity; the addressing voltages ($\phi_A(+)$ for electrode **46** and $\phi_A(-)$ for electrode **42**) are for a sequence of deflections of beam **30** first to landing electrode **41**, then landing electrode **40**, and lastly back to landing electrode **41**. At the end of the reset pulse this stored potential energy is released and provides an impulse pulling beam **30** straight up. Thus an undeflected beam **30** will just exhibit vertical damped oscillation about the unde-

flected state, wheres a stuck beam **30** is pulled off of the landing electrode and the restoring torque returns it to the undeflected state plus also exhibiting vertical damped oscillations. Because this second reset method resets a beam no matter what its landing direction, any inadvertent collapse and sticking of beams on account of electrostatic discharge due to handling is automatically corrected as soon as a reset pulse is applied. See FIG. **30B** for illustration of the vertically deflected beam **30** in cross sectional elevation view along the torsion hinge axis which is between the address electrods **42** and **46**.

FIG. **31** is a plan view of a portion of a linear array **310** of second preferred embodiment pixels **320**, **320'**, **320''**, . . . with each of the pixels similar to pixel **20**. For pixel **320** the beam **330**, torsion hinges **334** and **336**, landing electrodes **340** and **341**, and address electrodes **342** and **346** are shown; similarly for pixel **320'**. Note that the landing electrodes all connect to a central metal line **343**. Linear array **310** could be used for electrophotographic printing as illustrated schematically in FIGS. **32A–C**. FIG. **32A** is a perspective view and FIGS. **32B–C** are elevation and plan views showing system **350** which includes light source and optics **352**, array **310**, imaging lens **354**, and photoconductive drum **356**; the light from source **352** is in the form of a sheet **358** and illuminates linear array **310** with the light reflected from the area between beams **330**, **330'**, **330''**, . . . forming sheet **360**, the light reflected from negatively deflected beams within sheet **361**, and the light reflected from positively deflected beams passing through imaging lens **354** within sheet **362** and focussed on drum **356** within line **364** as a series of dots, one for each deflected beam. Because linear array **310** is actually two rows of pixels, the image on drum **356** are dots within two lines and electronic delay of addressing one of the rows of pixels together with the drum rotation bring the image dots back into one line **364**. Thus a page of text or a frame of graphics information which has been digitized and is in raster-scanned format can be printed by feeding the information a line at a time to array **310** to form dots a line **364** at a time on drum **356** as drum **356** rotates; these dot images are transferred to paper by standard techniques such as xerography. If θ is the deflection angle of beam **330** when on landing electrodes **341**, then sheet **362** is normal to linear array **310** when the angle of incidence of sheet **358** is 2θ from the normal to linear array **310**. This geometry is illustrated in FIG. **32B** and permits imaging lens **354** to be oriented normal to linear array **310**. Each positively deflected beam produces an image **355** of light source **352** on imaging lens **354** as schematically shown in FIG. **32C** for three beams.

Linear array **310** with the pixels operating in bistable mode has advantages over linear arrays of cantilever beam pixels because (i) the bistable pixel operates at a larger deflection angle, so the angular subtense of the light source can be increased to yield a brighter dot at the drum; (ii) the turn-off pixels have the torsion beams deflected in the opposite direction rather than just undeflected as in the cantilever case, this doubles the reflection angle from turned-off pixels and lessens the optical contrast degradation due to beam curvature and eliminates the influence of anguar deviation for zero applied voltage; and (iii) brightness uniformity is improved because the deflection angle is a linear function of the spacer thickness and not dependent upon a non-linear region of operation where the deflection uniformity is very sensitive to spacer thickness and hinge compliance as with the cantilever beam.

The addressing of individual pixels in linear array **310** is illustrated in a simplified version in FIGS. **33** and **34**; FIG. **33** is a cross sectional view of a single pixel **420** along address electrode **446** showing an input and enable gate **450** and FIG. **34** is a plan view showing pixels **420** and **420'** and addressing circuitry. Ti:Si:Al electrode **446** is insulated from p type silicon substrate **422** by silicon dioxide **444**, and the voltage to deflect beam **430** is applied to electrode **446**, with metal layers **426–428** a common bias for all pixels and substrate **422** grounded. The landing electrodes **441** and **440** (shared as landing electrode **441'** in pixel **420'**) are connected to metal layers **426–428** and thus beam **430**. Enable gate **450** is polysilicon and insulated from substrate **422** by gate oxide **454**, and n^+ doped regions **452**, **456**, **452'**, **456'**, . . . and **462**, **466**, **462'**, **466'**, . . . form the drains and sources, respectively, for MOSFETs with enable gate **450** as a common gate. Inputs for address electrodes **442** and **446** are applied to the MOSFET drains **452** and **456** and connected to the address electrodes when the MOSFETs are turned on by enable gate **450**.

The steps of a first preferred embodiment method of fabrication of pixel **320**, including addressing electrode **346** on substrate **322**, are illustrated in cross sectional elevation view in FIGS. **35A–E** as follows.

(a) First, 2,000 Å of thermal oxide **344** is grown on (**100**) silicon substrate **322**. Next, 3,000 Å of Ti:Si:Al (0.2% Ti and 1% Si) is sputter deposited on oxide **344**, and patterned and plasma etched to define electrodes **346**. See FIG. **35A**.

(b) Positive photoresist is spun on and baked in three applications to a total thickness of four microns to form spacer **324**; three applications of resist are used to build up the thickness in order to avoid resist surface waves which can occur when spinning on a single very thick layer. A bake of approximately 180° C. is required after each application of resist to prevent the previous layers from dissolving in the resist solvent and to drive out excess solvent from the spacer; the last bake avoids the formation of solvent bubbles under the hinge metal during the photoresist bake for the beam pattern photolithography. Note that the photoresist planarizes over any circuitry that has been formed on the surface of substrate **322**. The positive photoresist is preferably chosen to be insoluble in chlorobenzene, for example, novalac based resists. Then 800 Å of Ti:Si:Al (0.2% Ti and 1% Si) to form hinge layer **326** is sputter deposited at a substrate temperature as near to room temperature as possible to minimize thermal expansion mismatch between organic spacer **324** and metal layer **326**. Also, this alloy of aluminum minimizes the hillocking arising in deposition of pure aluminum. Next, 1,500 Å of silicon dioxide is deposited by PEVCD; the oxide is then patterned and etched to form torsion hinge etch stops **348** (in plan view etch stops **348** occupy the areas to become torsion hinges **334** and **336** plus a small extension at each hinge end) and the photoresist used in the patterning and etching is plasma stripped. See FIG. **35B**.

(c) 3,600 Å of Ti:Si:Al (0.2% Ti and 1% Si) to form beam layer **328** is sputter deposited, again near room temperature, and photoresist **50** is spun on. The deposition of the metal is under the same conditions as for the deposition of hinge layer **326** so that no stresses between the metal layers are developed. Photoresist **50** is patterned to define plasma etch access holes **332** and plasma etch access gap **338** plus hinges **334** and **336**.

Patterned photoresist **50** is then used as the mask for plasma etching the metal layers **326** and **328** with hinge etch stops **348** preventing the etching of the portion of hinge layer **326** that becomes hinges **334** and **336**. The plasma etch of the aluminum alloy may be with a chlorine/boron trichloride/carbon tetrachloride etch gas mixture. An alternative would be to use silicon dioxide masking as in step (b) with 2,000 Å of silicon dioxide patterned in place of photoresist **50**; in this alternative the aluminum alloy etch could be reactive ion etching with silicon tetrachloride. Note that the hinge thickness is determined by the thickness of layer **326**, the hinge width is determined by the width of etch stops **348**; thus the compliance of hinges **334** and **336** may be adjusted by three different process parameters. See FIG. **35C**.

(d) A thin layer of positive photoresist is spun on to act as an adhesion layer, and then 1.5 microns of PMMA (polymethyl methacrylate) **52** is spun on as a protective layer during subsequent steps, and substrate **322** is diced into chips (each chip to become a spatial light modulator). The dicing debris is illustrated sitting on PMMA **52** in FIG. **35D**.

(e) PMMA **52** is dissolved by spraying with chlorobenzene and immediately centrifuging; note that resist (or oxide) **50** and spacer **24** do not dissolve in chlorobenzene. Thus the dicing debris is removed without beam **330** being diretly exposed to the debris. Lastly, resist **50** and spacer **324** are isotropically plasma etched in oxygen, with a few percent fluorine (such as from CF_4 or NF_3) to remove the exposed portion of etch stops **348**; this etching is at low temperature and monitored to remove just enough of spacer **324** to form the well below beam **330**. See FIG. **35E** which is analogous to FIG. **1B** but along a different cross section. Note that FIG. **35E** shows the remnants **349** of the etch stops **348** which are omitted from FIGS. **1A** and **1C** because the second preferred embodiment method of fabrication (described infra) avoids the remnants and for clarity in FIGS. **1A** and **1C**. FIGS. **36A–C** illustrate in plan view and FIGS. **37A–C** in cross sectional view the stages of the etch of spacer **324**.

FIG. **38** illustrates in plan view a portion of linear array **510** of third preferred embodiment pixels including pixels **520**, **520'**, **520''**. Beams **530**, **530'**, **530''** are octagonal with plasma etch access holes **532**, **532'**, **532''** and plasma etch access gaps **538**, **538'**, **538''**, respectively; note that plasma etch access gaps **538** and **538'** have a common portion between beams **530** and **530'**, as do the other gaps between abutting pixels. The wells in spacer **524** beneath beams **530**, **530'**, **530''**, . . . all connect together and form one long well as indicated by the dotted lines in FIG. **38**. The address electrodes **542**, **546**, **542'**, **546'**, . . . and landing electrodes **540**, **541**, **540'**, **541'**, . . . are shown in FIG. **38** by dashed lines; note that abutting landing electrodes are shared, for example, **541** and **540'**. For clarity in FIG. **38** torsion hinges **534**, **536**, . . . were shown as made from the same layer as beams **530**, **530'**, **530''**, ...

FIGS. **39A–D** illustrate in plan views alternative beam geometries. In particular, FIG. **39A** shows a cantilever beam **570** with cantilever hinge **572**, plasma etch access hole **574**, plasma etch access gap **576**, address electrode **578**, and landing electrode **579**. A cantilever beam only deflects in one direction and has torque curves similar to the curves of FIG. **5** but bounded, so only monostable and bistable (one stable deflection point plus collapsed to landing electrode **579**) operation is available.

FIG. **39B** shows torsion beam **580** with torsion hinges **581** and **582**, plasma etch access holes **584**, plasma etch access gap **586**, address electrode **588**, and landing electrode **589**. Beam **580** deflects in only one direction and has operation similar to beam **570**.

FIG. **39C** shows a linear array of cantilever beams **590**, **590'**, **590''**, . . . arranged as abutting inverted cloverleaves of groups of four beams. As with linear array **510**, the wells under beams **590**, **590'**, **590''**, . . . join to form a single elongated well as indicated by the dotted lines. Cantilever hinges **592**, **592'**, **592''**, . . . are shown as made of the same layer as the beams and the address and landing electrodes are not shown for clarity.

FIG. **39D** illustrates a portion of an area array of cantilever beams **560**, **560'**, **560''**, . . . grouped in fours and supported on posts **561**, **561'**, **561''**, . . . by cantilever hinges **562**, **562'**, **562''**, ... Landing electrodes for the beams may be connected in rows such as electrode **563**, and the beams are connected through the conductive posts to row electrodes **564**. The address electrodes **565**, **565'**, **565''**, . . . are addressed through circuitry not shown and fabricated in layers beneath the electrodes. Some of the electrodes are omitted for clarity.

A second preferred embodiment buried hinge fabrication method is shown in cross section (FIGS. **40A–E**) and in plan (FIGS. **41A–C**) views for a hinge located on a flat side of a torsion beam rather that at a corner. The cross section is taken in a transverse direction to the axis of the hinge (Section AA in FIG. **41C**). The second preferred embodiment process relies on metal liftoff to define the thin hinge metal region, rather than a buried SiO_2 etch stop. As with the first preferred embodiment process, only one plasma etch is required to etch both the hinge and beam metalization layers.

The process begins with a sputter deposition of thin aluminum hinge layer **180** over spacer **182** (FIG. **40A**). A trilayer resist process is used to delineate what will later become the thin metal region into which the hinge pattern is finally etched. The trilayer resist process chosen is a modification of the Sestertious process of Y. C. Lin, et al, J. Vac. Sci. Technol., B1(4), 1215 (1983).

The modified Sestertious process begins by spinning a spacer layer **184** of PMMA onto hinge metal **180**. The thickness (approximately 5000 Å) is chosen to be slightly greater than the thickness of the beam metal. PMMA **184** is baked at a reduced temperature compared to the standard process in order to maintain a reasonably high solubility rate in its developer during the subsequent undercut of the photoresist capping layer. Next, an antireflection coating (ARC) **186** is spun onto PMMA **184** and baked. ARC **186** coating serves to prevent an interfacial layer from forming between photoresist **188** and PMMA **184**. It also reduces the amount of reflected light from hinge metal **180** during the subsequent photolithography exposure.

ARC **186** is then coated with a positive photoresist **188**. Photoresist **188** is exposed and developed in the desired hinge liftoff pattern and finally deep UV hardened and baked. ARC **180** is developed at the same time as photoresist **188**. Next PMMA **184** is deep UV flood exposed so that regions of PMMA **184** not coated with photoresist **188** are reduced in their average molecular weight and become more soluble in chlorobenzene. A chlorobenzene develop of PMMA **184** quickly dissolves the exposed portion of PMMA **184** and an overdevelop produces approximately a one micron undercut of the photoresist capping layer as shown in FIG. **40A**. An ash serves to remove filaments of softened PMMA which

are thrown out during the spin dry following PMMA **184** develop. A hardbake then reduces the volatile components still contained in photoresist **188** and PMMA **184**. These volatile components are caused by chlorobenzene absorption during the PMMA develop.

After the trilayer resist pattern (photoresist **188**, ARC **186**, and PMMA **184**) is formed, beam metal **190** is sputter deposited. The overhanging photoresist cap on PMMA **184** causes sputtered beam metal **190** to break into two layers as shown in FIG. **40B**. Beam metal **190** is then lifted off by soaking and dissolving the trilayer resist pattern in either chlorobenzene or 1-methyl-2-pyrrolidinone. The result (shown in cross sectional elevation view in FIG. **40C** and in plan view in FIG. **41A**) is a thin metal region **180** surrounded by a thick metal region **190**, with thick metal **190** being tapered at its patterned edge **192**.

Next a pattern corresponding to the hinge and beam is photolithographically defined as shown in FIG. **40D** (cross sectional elevation) and FIG. **41B** (plan view). The opening in the photoresist is denoted **194** in the Figures, and the exposed metal is only hinge metal **180** for the two short horizontal portions of opening **194** in FIG. **41B** and beam metal **190** elsewhere. Note that this pattern contains both the hinge and beam geometries, unlike the first preferred embodiment process. For this reason, the second preferred embodiment process is self-aligned. The exposed portion of hinge metal **180** and beam metal **190** is then plasma etched to simultaneously form both the hinge and beam geometries. After the photoresist has been ashed away the process is complete and the beam appears as in FIG. **40E** (cross section) and FIG. **41C** (plan view).

FIG. **42A** is a plan view of a portion of array **610** of fourth preferred embodiment pixels **620**, each pixel **620** includes torsion beam **630** supported by torsion hinges **634** and **636** which are in turn connected to posts **624**, **624'**, **624''**, . . . ; the addressing circuitry for array **610** is not shown in FIG. **42A** but the overall addressing for the array is schematically illustrated in FIG. **42B**. Each pixel is represented as two variable capacitors (one for each address electrode) and two MOSFETs controlling access to the capacitors; the MOSFET gates are common for all pixels in a row, and the MOSFET drains are common for all pixels in a column. Array **610** is line addressed; that is, data is fed to the array one row of pixels at a time by the gate decoder selecting the wordline (gates) and the data is applied on the bitlines (drains) which then charge the floating sources and appropriately deflect the beams. As shown in FIG. **42B**, the data may be entered in serial format and then converted to parallel format by a serial-to-parallel converter ("S/P Converter") and held in a storage register ("Register") until applied to the bitlines; the gate decoder sequentially selects the rows of the array.

FIGS. **43A-D** are plan views illustrating successive levels in a pixel, and FIGS. **44A-C** are cross sectional elevation views along lines A—A, B—B, and C—C in FIGS. **42A** and **43A-D**. In particular, FIG. **43A** shows n^+ diffused regions **660**, **661**, **662**, **666**, **660'**, . . . and p^+ channel stops **670**, **672**, **670'**, . . . in p^- silicon substrate **622**. Diffused lines **660** and **661** are bitlines and the drains for the MOSFETs, and regions **662** and **666** are the floating sources for the MOSFETs in pixel **620**. Note that other devices could be fabricated on the same chip as array **610**, and that array **610** could be formed in a p well of a CMOS chip. FIG. **43B** is the gate level and shows polysilicon wordlines **680** and **680'** with attached gates **682**, **686**, **682'**, **686'**, ... FIG. **43C** illustrates the electrode level with only the wordlines and gates and floating sources indicated for clarity. Address electrodes **642** and **646** vertically connected to floating sources **662** and **666** through vias **663** and **667**, respectively; whereas, landing electrodes **640** and **641** are shared with abutting pixels and interconnected through the beams and hinges in the reflecting layer. FIG. **43D** is the spacer level and shows that metal posts **624**, **624'**, **624''**, . . . have taken the place of spacer **24** in pixel **20** to support reflecting layers **626** and **628** in which beams **630**, **630'**, **630''**, . . . are formed. Metal posts **624**, **624'**, **624''**, . . . electrically connect beams **630**, **630'**, **630''**, . . . to landing electrodes **642**, **646**, . . . in contrast to pixel **20** in which the spacer **24** insulates the beams from both the address and landing electrodes. Of course, FIG. **42A** is the reflecting layer level plan view.

FIGS. **44A-C** are cross sectional elevation views of pixel **620** along lines A—A, B—B and C—C of FIG. **42A** and illustrate posts **624**, **624'**, **624''**, . . . supporting the reflecting layer (hinge metal **626** plus beam metal **628**) and which are fabricated from the hinge and beam metal depositions. Insulating silicon dioxide (oxide) **644** is about 8,000 Å thick but has been reflowed to slope the sidewalls of the openings down to floating sources **662**, **666**, **662'**, . . . to help the step coverage during deposition of the metal electrodes **642**, **646**, **642'**, ... Gate oxide **643** is about 800 Å thick and preserved during the etching of deposited polysilicon to form wordlines and gates **682**, **686**, **682'**, ...

Array **610** may be fabricated by a method analogous to the first and second preferred embodiment methods described except the spacer layer (**324** of the first method and **182** of the second method) is patterned to form openings for posts **624**, **624'**, **624''**, . . . prior to deposition of hinge and beam metal. Then the deposition of hinge and beam metal forms the posts, and the spacer is totally etched away about the pixels. The circuitry beneath the electrodes is fabricated by standard silicon processing.

MODIFICATIONS AND ADVANTAGES

Various modifications of the preferred embodiment devices and methods may be made while retaining the separation of addressing and landing electrodes which leads to soft landing in the preferred embodiments. Further, the effectively symmetric beams may use differential bias. For example, the address electrodes could be moved outside of the landing electrodes although this would require a more careful analysis of the attractive torque than that presented because the fringing fields would be the basis for the attraction. Further, the dimensions and shapes can be varied such as the hinge length, width, and thickness (even hinges made of beam metal), the size of the beams and their thickness, the thickness of the spacer, and so forth. Even the geometry of the beams and hinges can be varied as shown in FIG. **39**. In fact, patterns of thick and thin portions could be fabricated in the beams, and three or more layers of metal with etch stops in each layer could yield various beam structures. Also, the materials can be varied such as Cu:Al, Ti:W, chromium, etc. for the metal, differing resists or insulators such as polyimide for the spacer or composite spacers including conductive sublayers, radiation hardening of the spacer, other semiconductors for the substrate and the electrodes or metal electrodes, and so forth. The buried hinge etch stop could be a different material, such as tungsten; and processing could result

in no etch stop remnants between the hinge metal and the beam metal. The landing electrodes could be covered with a thin layer of silicon dioxide or other material to prevent the sticking of the beams on the landing electrodes; or the landing electrodes could be made of a material different from the beams and thereby deter cold welding of the beam to the landing electrode; or the landing electrodes could be contoured to contact the beam away from the beam tip or edge. Various addressing circuitry may be formed beneath the electrodes, including vias to the backside of a substrate.

The advantages of the landing electrode include the uniform, large-angle and soft-landed deflection of the beams.

What is claimed is:

1. A spatial light modulator, comprising:
(a) a plurality of pixels, each of said pixels including a deflectable beam, an address electrode adjacent said beam, and a landing electrode adjacent said beam;
(b) wherein a voltage applied between said beam and said address electrode deflects said beam toward said address electrode, and said landing electrode is located to contact said beam deflected toward said address electrode and prevent said deflected beam from contacting said address electrode.

2. The spatial light modulator of claim 1, wherein:
(a) said deflectable beams are formed in a reflecting layer supported away from said address electrodes and landing electrodes, said deflectable beams connected to said reflecting layer by hinges formed in said reflecting layer.

3. The spatial light modulator of claim 2, wherein:
(a) said reflecting layer is supported away from said address electrodes and landing electrodes by a spacer layer with wells between said deflectable beams and said electrodes.

4. The spatial light modulator of claim 3, wherein:
(a) each of said deflectable beams is connected to said reflecting layer by two torsion hinges; and
(b) each of said pixels has two address electrodes and two landing electrodes.

5. The spatial light modulator of claim 4, wherein:
(a) said deflectable beams and landing electrodes are connected to a voltage source.

6. The spatial light modulator of claim 2, wherein:
(a) said reflecting layer is supported away from said address electrodes and landing electrodes by a plurality of posts.

7. The spatial light modulator of claim 6, wherein:
(a) each of said deflectable beams is connected to said reflecting layer by two torsion hinges; and
(b) each of said pixels has two address electrodes and two landing electrodes.

8. The spatial light modulator of claim 7, wherein:
(a) said deflectable beams and landing electrodes are connected to a voltage source.

9. A spatial light modulator, comprising:
(a) a plurality of pixels formed in a layered structure;
(b) said layered structure including an insulated substrate, a spacer layer on said substrate, a conductive reflecting layer on said spacer layer, and a plurality of addressing and landing electrodes;
(c) each of said pixels including
i. a deflectable element formed in said reflecting layer and connected to the remainder of said reflecting layer by at least one hinge formed from said reflecting layer,
ii. a well formed in said spacer layer and extending from said deflectable element to said substrate,
iii. a first addressing electrode on said substrate at the bottom of said well and located to deflect said deflectable element by electrostatic attraction, and
iv. a first landing electrode on said substrate at the bottom of said well, said first landing electrode located both to contact said deflectable element when said deflectable element is deflected by attraction by said first addressing electrode to said substrate and to prevent said deflectable element from contacting said addressing electrode.

10. The spatial light modulator of claim 9, wherein:
(a) said deflectable element and said first landing electrode are electrically connected.

11. The spatial light modulator of claim 9, wherein:
(a) said deflectable element is connected to the remainder of said reflecting layer by two hinges formed from said reflecting layer, said deflectable element deflectable by rotation about the axis defined by said two hinges.

12. The spatial light modulator of claim 11, wherein said each pixel further includes:
(a) a second addressing electrode on said substrate at the bottom of said well and located to deflect said element by electrostatic attraction in a direction of rotation opposite the direction of rotation due to attraction by said first addressing electrode; and
(b) a second landing electrode on said substrate at the bottom of said well, said second landing electrode located to contact said deflectable element when said deflectable element is deflected by attraction by said second addressing electrode to said substrate.

13. The spatial light modulator of claim 12, wherein said each pixel further includes:
(a) a voltage supply connected between said deflectable element plus said landing electrodes and said substrate.

14. The spatial light modulator of claim 9, wherein:
(a) said reflecting layer is made of first and second sublayers, each of said sublayers a metal; and
(b) said at least one hinge is formed from only said first sublayer.

15. A spatial light modulator, comprising:
(a) a plurality of pixels formed in a layered structure;
(b) said layered structure including a bottom layer, a plurality of electrodes on said bottom layer, a planarizing spacer layer on said electrodes and bottom layer, and a conductive reflecting layer on said spacer layer;
(c) each of said pixels including:
i. a deflectable element formed in said reflecting layer;
ii. first and second of said electrodes, said first and second electrodes both extending beneath said deflectable element, said first electrode an addressing electrode and said second electrode a landing electrode; and
iii. a well formed in said spacer layer, said well extending from said deflectable element to said first and second electrodes and of width greater than the width of said deflectable element.

16. The spatial light modulator of claim 15, wherein:
(a) said deflectable element is a portion of said reflecting layer connected to the remainder of said re-

flecting layer by two hinges formed from said reflecting layer.

17. The spatial light modulator of claim 16, wherein:

(a) said portion of said reflecting layer is of square shape and said hinges are located at diagonally opposite corners of said portion.

18. The spatial light modulator of claim 15, wherein:

(a) said well is characterized by a plasma etching of said spacer layer after said reflecting layer is on said spacer layer and said spacer layer is on said electrodes and said bottom layer and said deflectable element has been formed in said reflecting layer.

19. The spatial light modulator of claim 15, wherein said each pixel further includes:

(a) third and fourth of said electrodes extending beneath said deflectable element, said third electrode an addressing electrode and said fourth electrode a landing electrode.

20. A deflectable beam light modulator, comprising:

(a) an air gap capacitor with a first capacitor plate being a light-reflecting deflectable and conductive beam and a second capacitor plate being an addressing electrode; and

(b) a conductive landing electrode of a selected potential different from the potential of said addressing electrode located to stop the deflection of said beam at a predetermined position away from maid addressing electrode.

21. The light modulator of claim 20, wherein said:

(a) said beam is conductive; and

(b) said deflection stop is a conductive landing electrode has the same electrical potential as said beam.

22. The light modulator of claim 20, wherein:

(a) said beam is metal;

(b) said landing electrode is a metal landing electrode adjacent said addressing electrode; and

(c) said addressing electrode is metal.

23. The light modulator of claim 20, wherein:

(a) said landing electrode is insulated.

24. A deflectable beam light modulator, comprising:

(a) an air gap capacitor with a first capacitor plate being a light reflecting deflectable beam and a second capacitor plate being an addressing electrode; and

(b) an insulated landing electrode located to stop the deflection of said beam at a predetermined position away from said addressing electrode.

25. A deflectable beam light modulator, comprising:

(a) an air gap capacitor with a first capacitor plate being a light-reflecting deflectable beam having a deflection axis and a second capacitor plate being an addressing electrode; and

(b) a deflection stop located outwardly of said deflection axis and said addressing electrode, said deflection stop to stop the deflection of said beam when said beam comes in contact with said deflection stop at a predetermined position away from said addressing electrode.

26. The light modulator of claim 25, wherein:

(a) said beam is conductive; and

(b) said deflection stop is a conductive landing electrode at a selected electrical potential different from that of said addressing electrode.

27. The light modulator of claim 26, wherein:

(a) said beam is metal;

(b) said deflection stop is a metal landing electrode adjacent said addressing electrode; and

(c) said addressing electrode is metal.

28. The light modulator of claim 25, wherein:

(a) said deflection stop is an insulated landing electrode.

* * * * *